LIBRARY
CALIFORNIA AIR RESOURCES BOARD
P.O. BOX 2815
SACRAMENTO, CA 95812

SoRI-85-438

FINE PARTICLE HANDBOOK

Prepared for the
California Air Resources Board
Sacramento, California 95812

CARB Contract No. A3-092-32 SoRI Project No. 5598-1

Southern Research Institute

Table S-1. Typical flue gas sample conditions.

	RANGE	TYPICAL VALUE
Temperature:	170 to 450°C	150°C
Absolute Pressure:	490 to 850 mm Hg	750 mm Hg
Pressure Differential to Ambient	±75 mm Hg	-25 mm Hg
Moisture (Volume Percentage)	1 - 20%	10%
CO_2 (Volume Percentage)	8 - 15%	12%
SO_2 (Volume Percentage)	0 - 5%	0.2%
SO_3/H_2SO_4 (Volume Percentage)	0 - 0.25%	0.0005%
Particulate Mass Concentrations	≤ 20 g/m^3	Uncontrolled 5 g/m^3 Controlled 0.02 g/m^3
Concentration by Number of Particles Larger than 0.01 μm	$\leq 3 \times 10^7$/cm^3	Uncontrolled 2×10^7/cm^3 Controlled 2×10^5/cm^3

4879-111

LIBRARY
CALIFORNIA AIR RESOURCES BOARD
P.O. BOX 2815
SACRAMENTO, CA 95812

Table S-2. Particle sizing device applications.

DEVICE	PRINCIPLE OF OPERATION	MODE OF OPERATION	SAMPLING LOCATION	SIZING RANGE, μm	INLET CONC. RANGE, g/m^3	OPERATIONAL STATUS
Impactor	Inertial	In situ	I/O	0.3 to 20	0.001 to 10.0	Routine use by skilled operator
Impactor-Low Pressure	Inertial	In situ	I/O	0.03 to 20	0.001 to 10.0	Prototype
Cyclone	Inertial	In situ/Extractive	I/O	0.3 to 20	0.01 to 100	Routine use by skilled operator
Optical counter	Light scattering	In situ	O	0.2 to 20	0.6 to 60 mg/m^3	Some commercial instruments in use
Optical counter	Light scattering	Extractive	I/O	0.3 to 10	10 $\mu g/m^3$ to 40 mg/m^3	Non-routine use by skilled operator
Diffusion battery	Brownian diffusion	Extractive	I/O	0.003 to 1.0	$\leq$ 0.5	Non-routine use by skilled operator
Mobility analyzer	Electrical mobility	Extractive	I/O	0.003 to 1.0	$\leq$ 1.0 mg/m^3	Non-routine use by skilled operator
Centrifugal classifier	Inertial	Off-line	n. a.	1 to 500	n. a.	Routine lab use
Cell counters	Electrical resistance	Off-line	n. a.	0.5 to 200	n. a.	Routine lab use
Optical microscope	Visual	Off-line	n. a.	$\geq$ 0.2	n. a.	Routine lab use
Transmission electron microscope	Electron beam attenuation	Off-line	n. a.	0.001 to 20	n. a.	Routine lab use
Scanning electron microscope	Electron beam scattering	Off-line	n. a.	0.02 to 20	n. a.	Routine lab use

4879-118

n. a. = not applicable, I = Control device inlet, O = Control device outlet

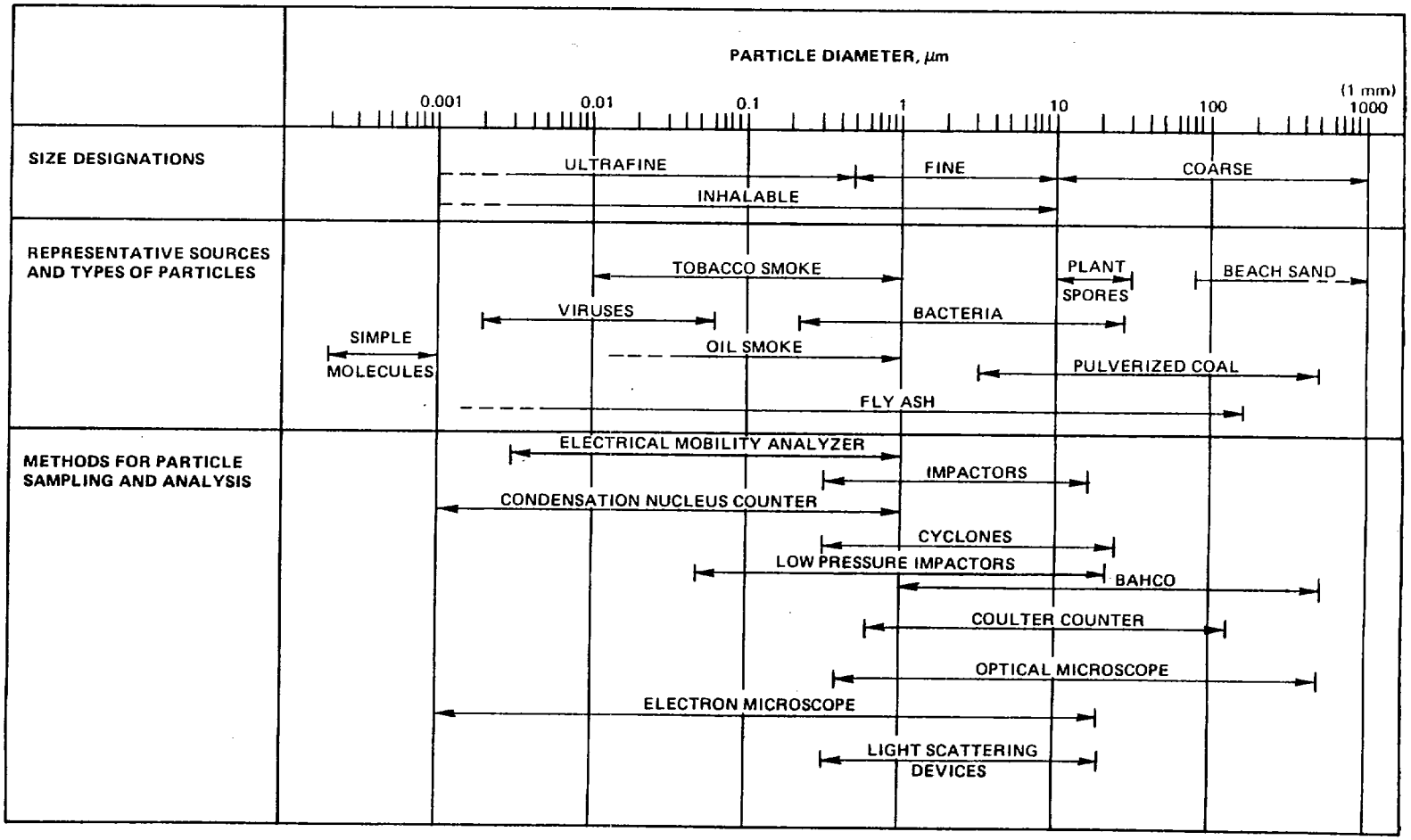

Figure S-1. Size definitions and characteristics of fine and ultrafine particulate matter. (Source: Adapted from a diagram by C. E. Lapple, Stanford Research Institute)

4266-102

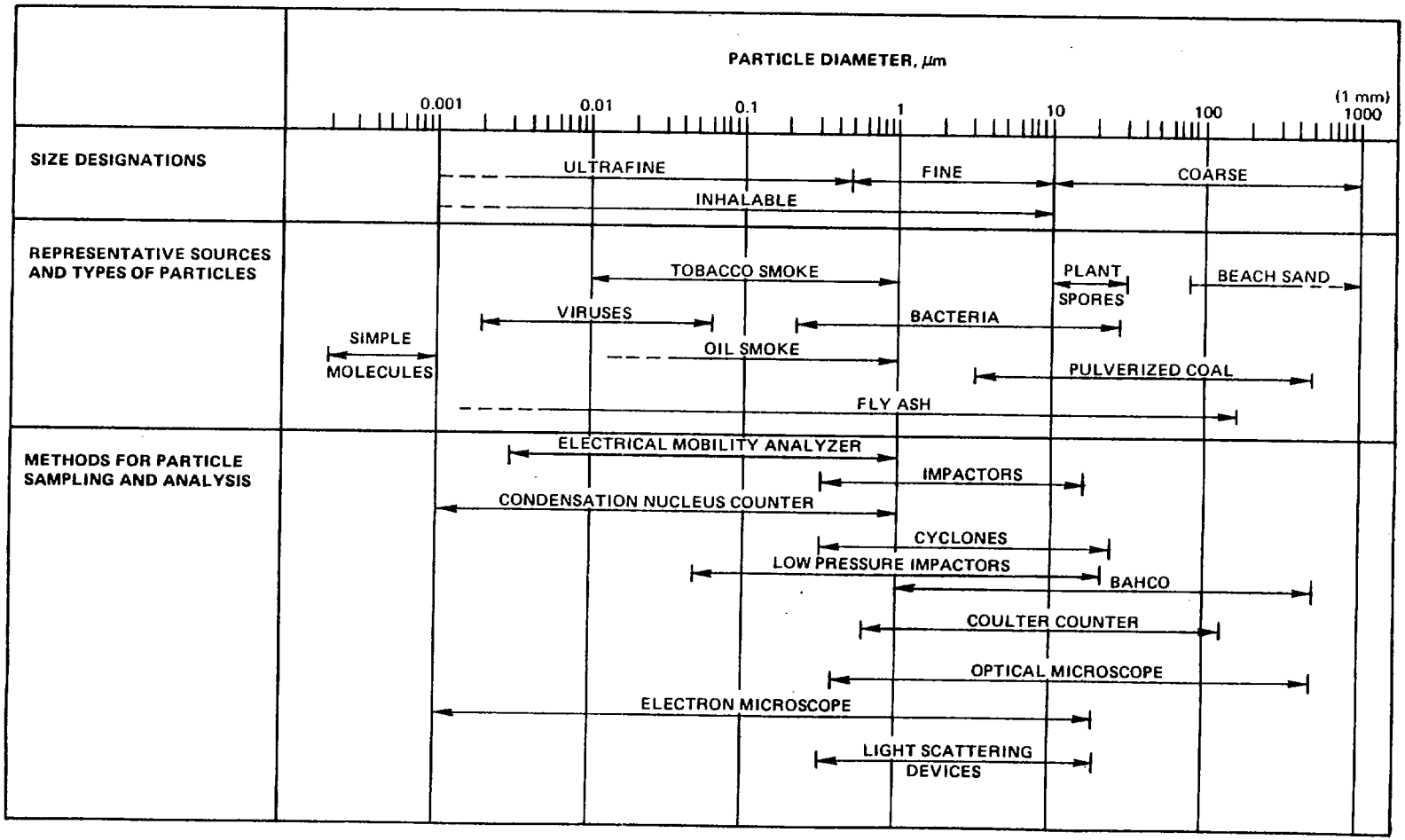

Figure 1-1. Size definitions and characteristics of fine and ultrafine particulate matter. (Source: Adapted from a diagram by C. E. Lapple, Stanford Research Institute)

4266-102

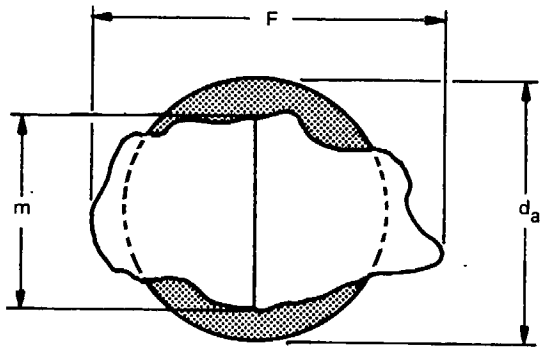

F - Feret's diameter, the distance between two tangents on opposite sides of the particle, parallel to a fixed direction.

M - Martin's diameter, the length of the line which bisects the image of the particle, parallel to a fixed direction.

d_a - Diameter of a circle having the same projected area as the particle in the plane of the surface on which it rests.

3540-070

Figure 2-1. Three diameters used to estimate particle size in microscopic analyses.[131]

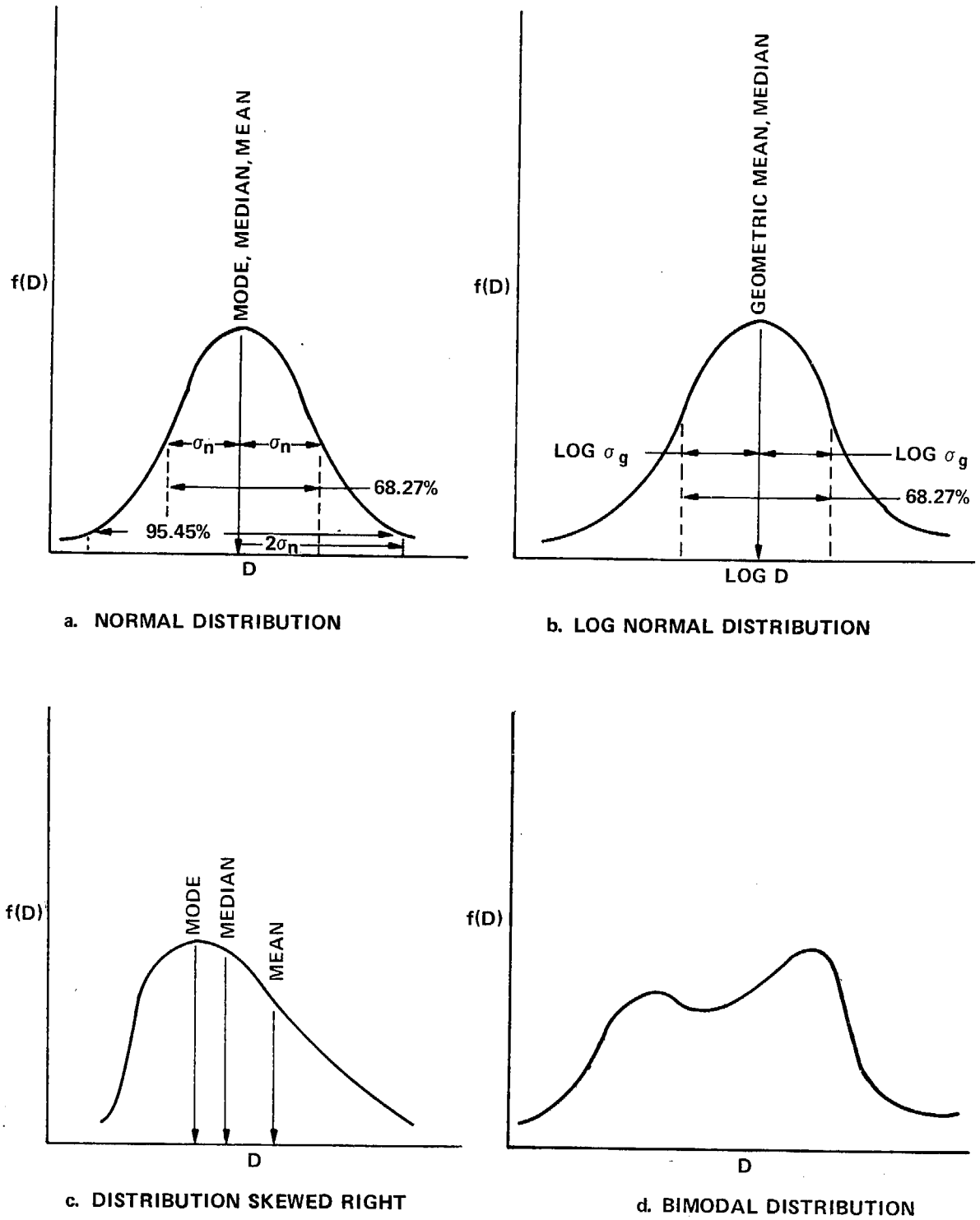

3540-38A

Figure 2-2. Examples of frequency or particle size distributions. D is the particle diameter.

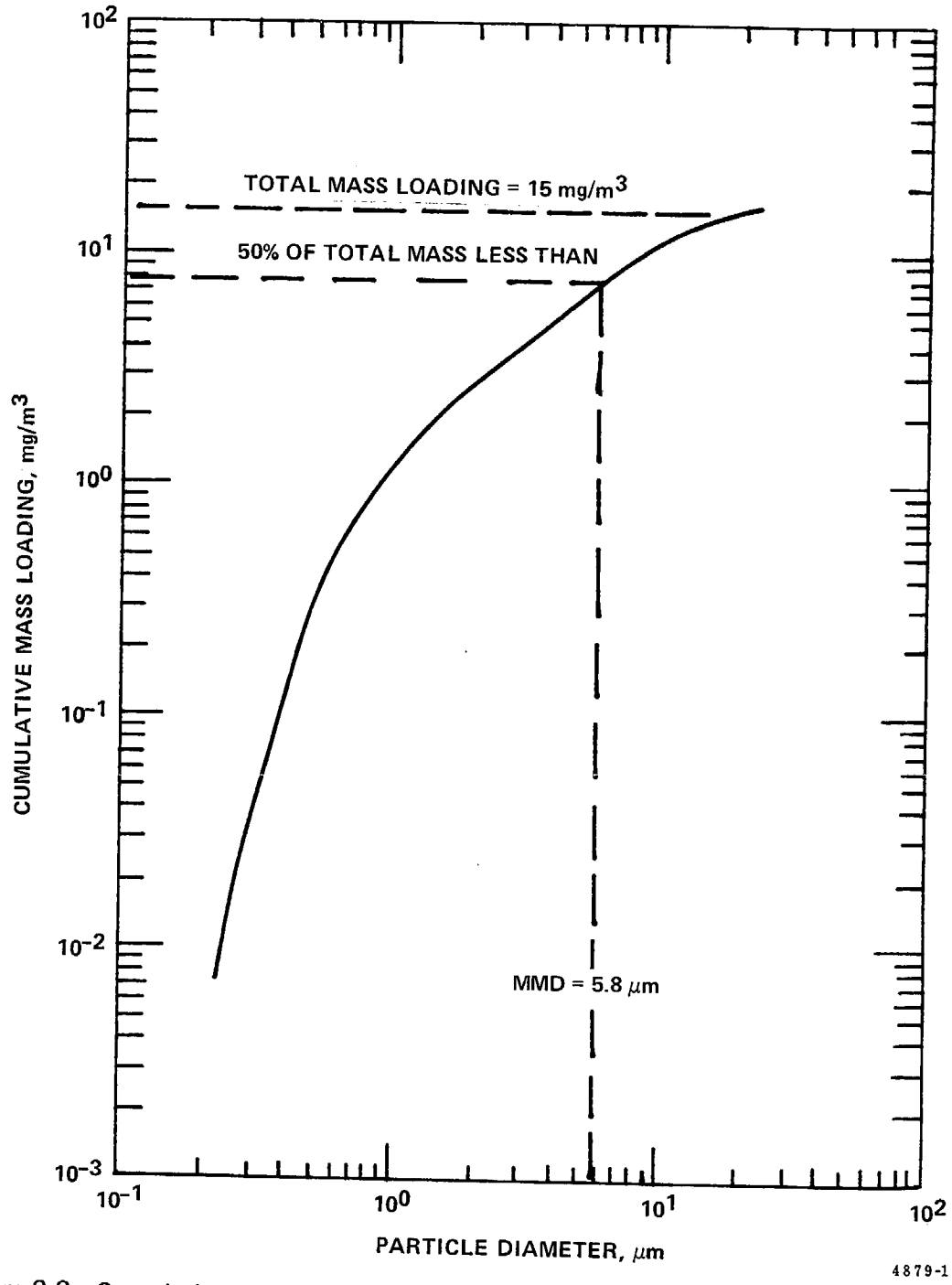

Figure 2-3. Cumulative mass concentration versus particle diameter (Stokes, aerodynamic, or aerodynamic impaction basis).

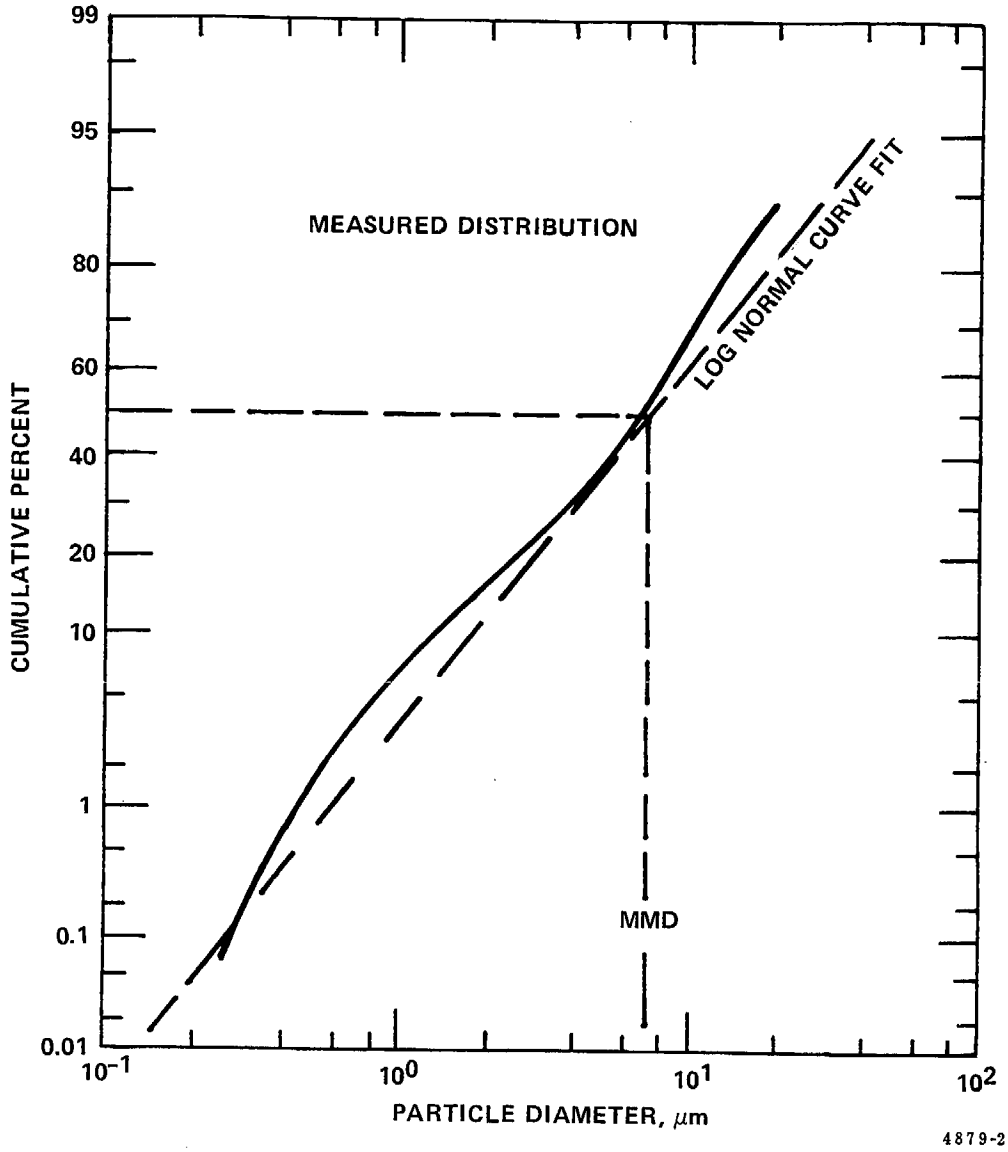

Figure 2-4. Percent of mass concentration (cumulative percent) versus particle diameter (Stokes, aerodynamic, or aerodynamic impaction basis).

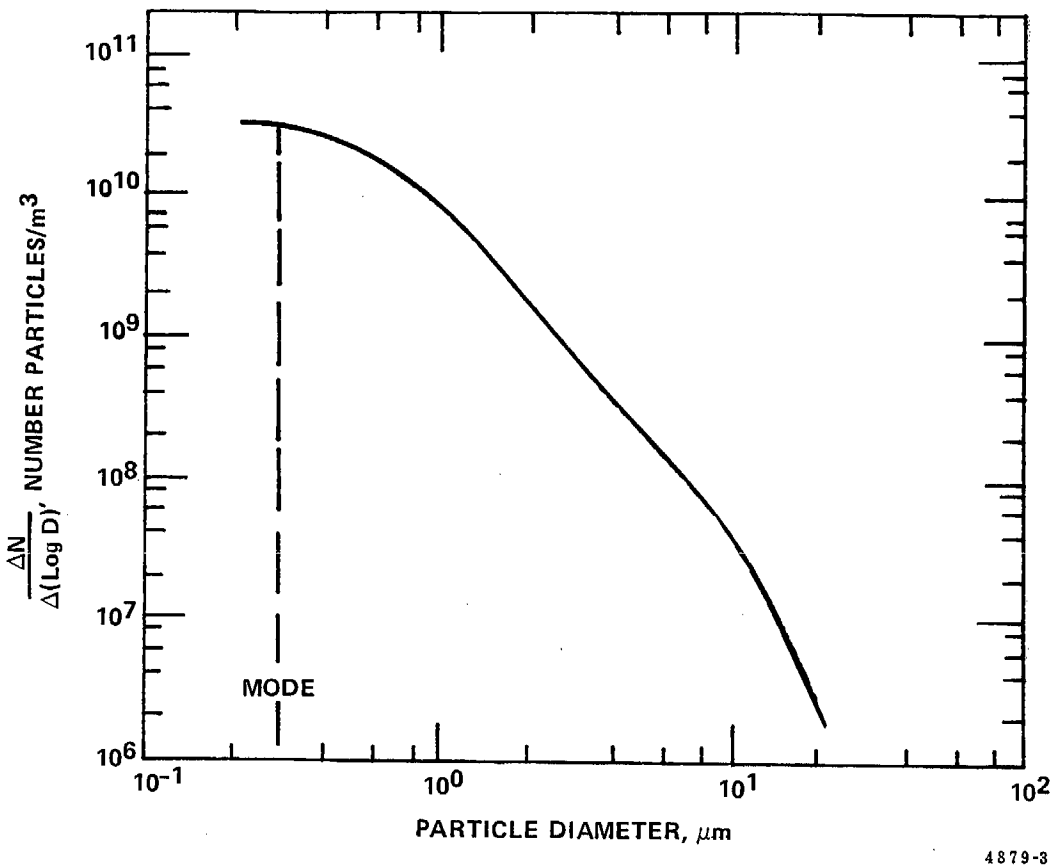

Figure 2-5. Differential number concentration (dN/dlog D) versus particle diameter (Stokes, aerodynamic, or aerodynamic impaction basis).

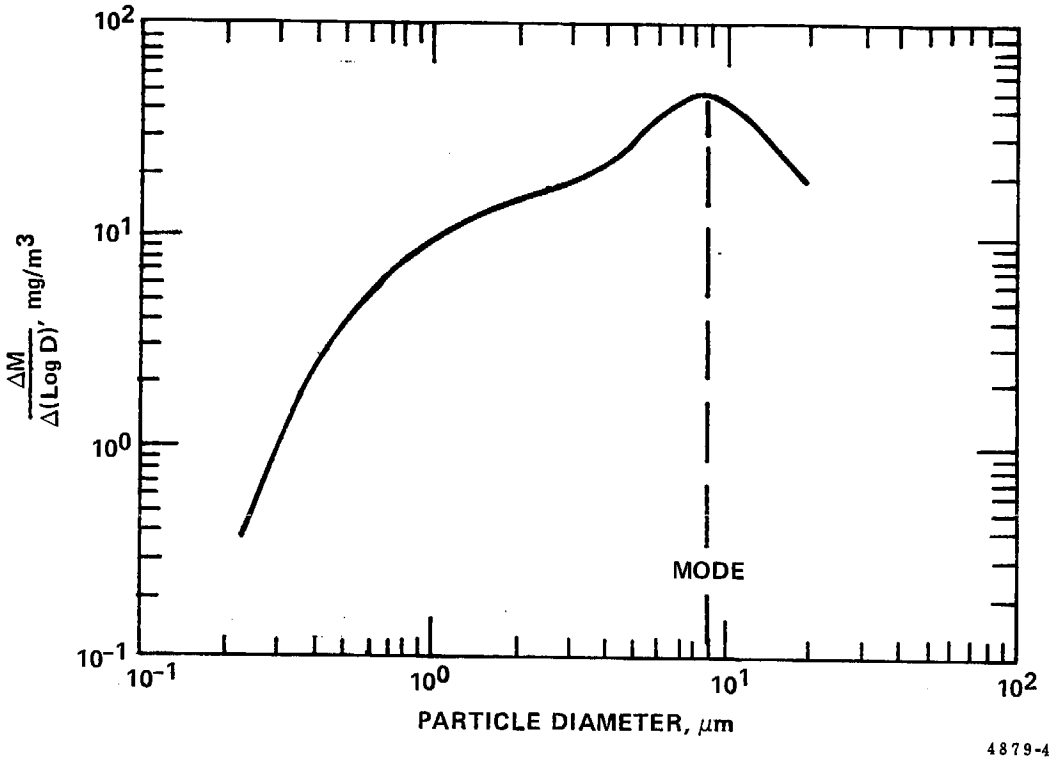

Figure 2-6. Differential mass concentration (dM/dlog D) versus particle diameter (Stokes, aerodynamic, or aerodynamic impaction basis).

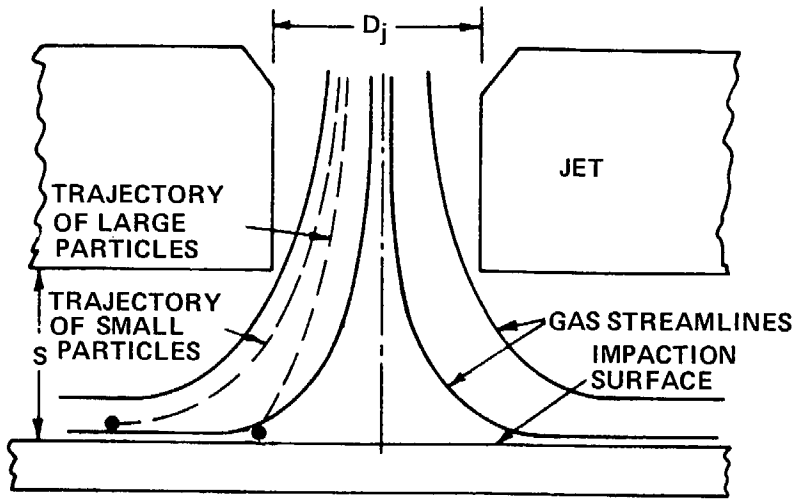

A TYPICAL IMPACTOR JET AND COLLECTION PLATE

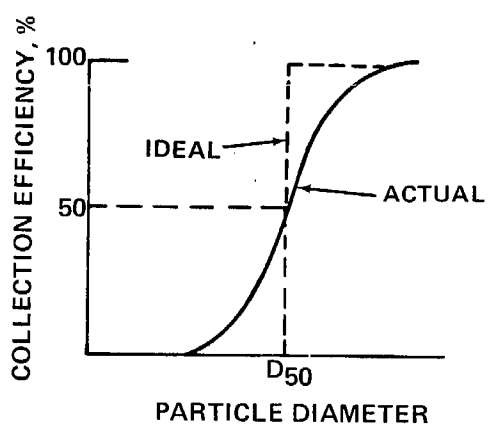

B GENERALIZED STAGE COLLECTION EFFICIENCY CURVE

4879-5

Figure 3-1. Operating principle and typical performance for a cascade impactor.

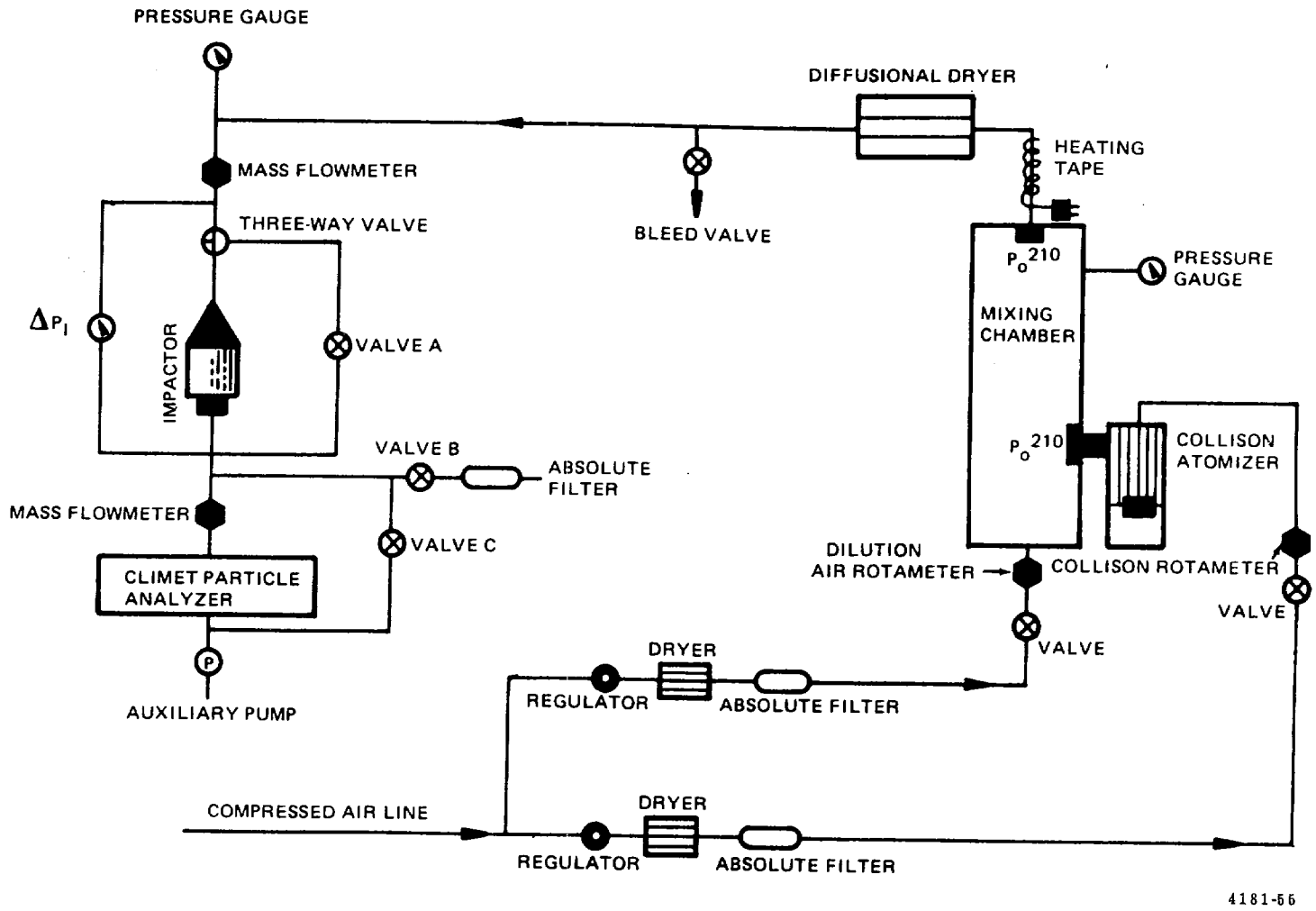

Figure 3-2. PSL calibration system for high and low flowrate impactor.

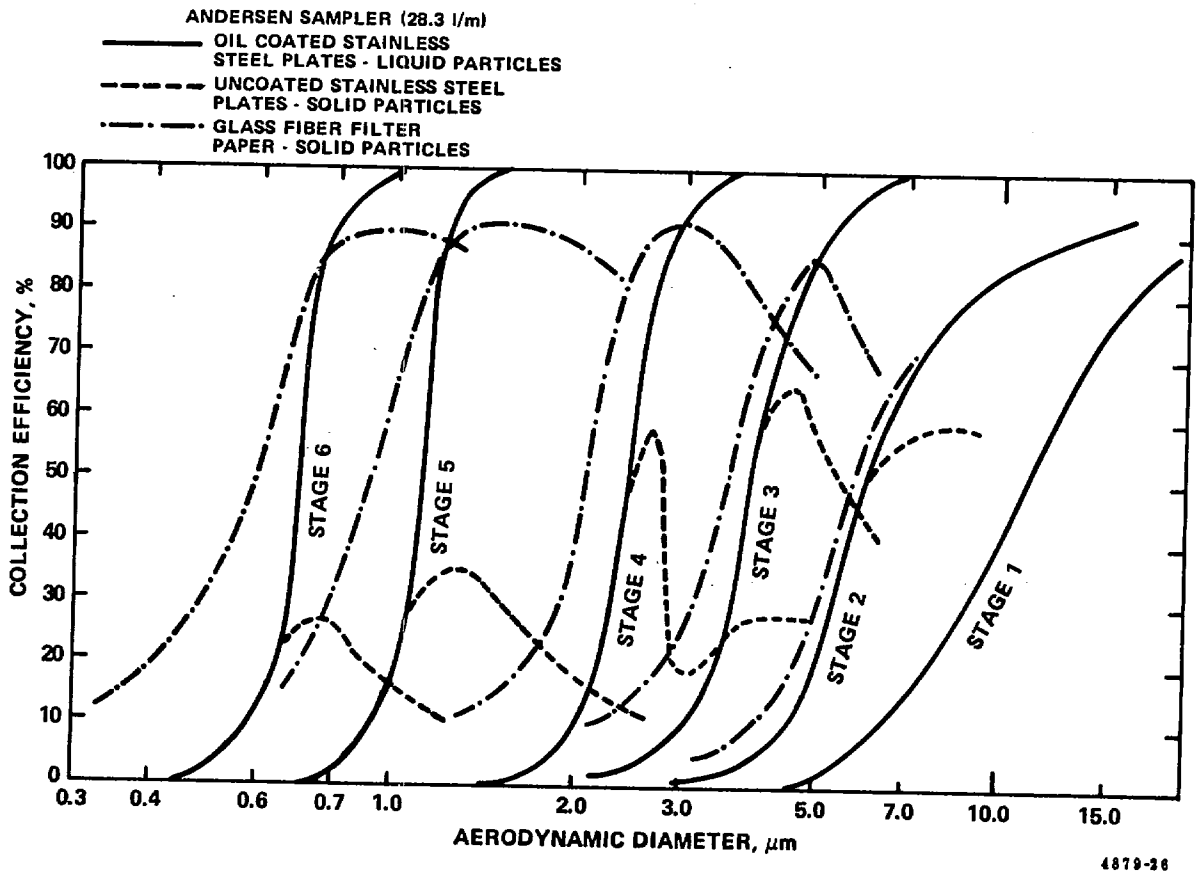

Figure 3-3. Collection characteristics of the Andersen sampler. (Source: Reference 20)

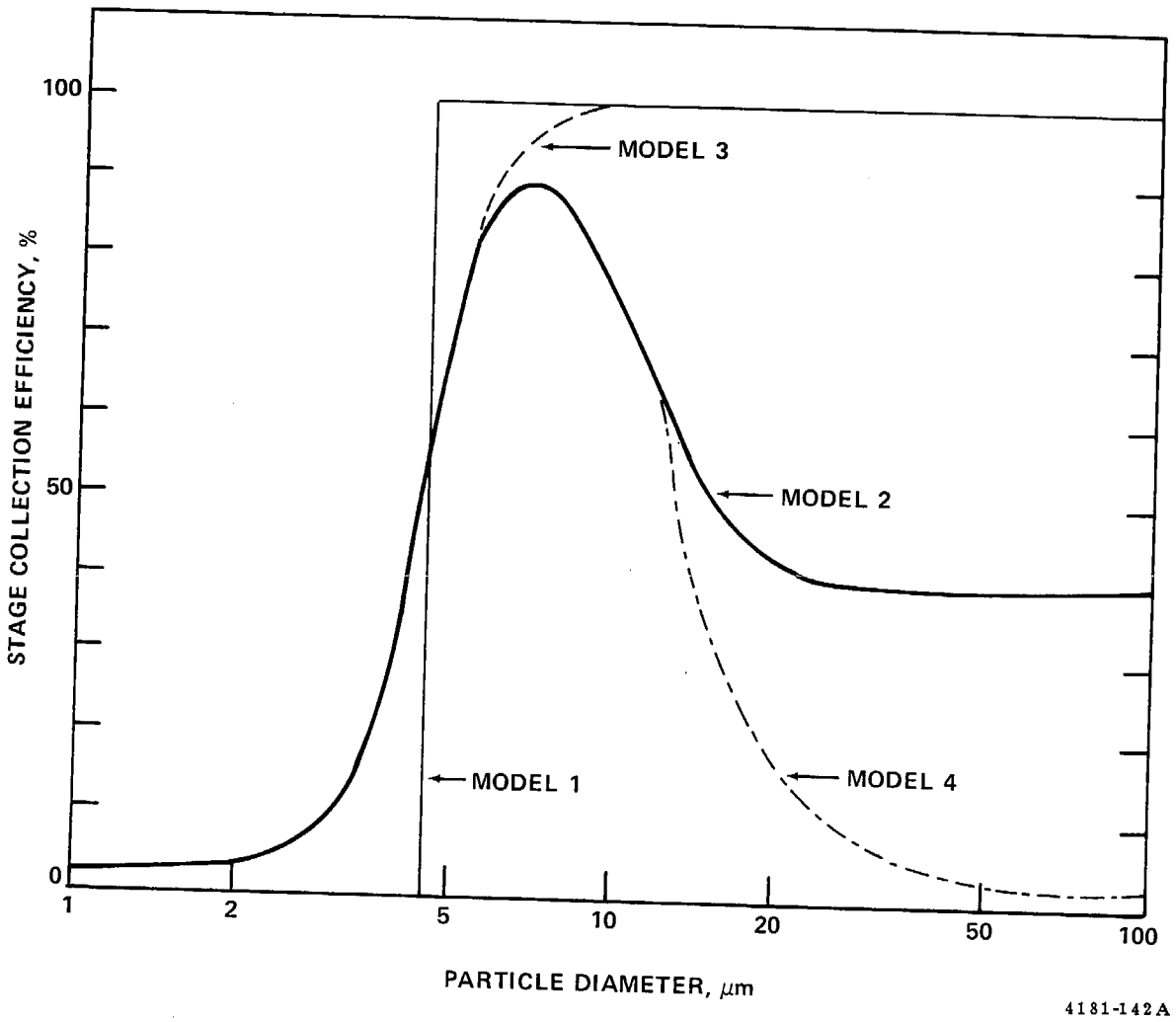

Figure 3-4. An illustration of the four modeled stage collection efficiency curves of a typical stage of the Andersen impactor. Model 1 is the ideal behavior model, model 2 is the normal bounce model, model 3 is the no bounce model, and model 4 is the extreme bounce model.

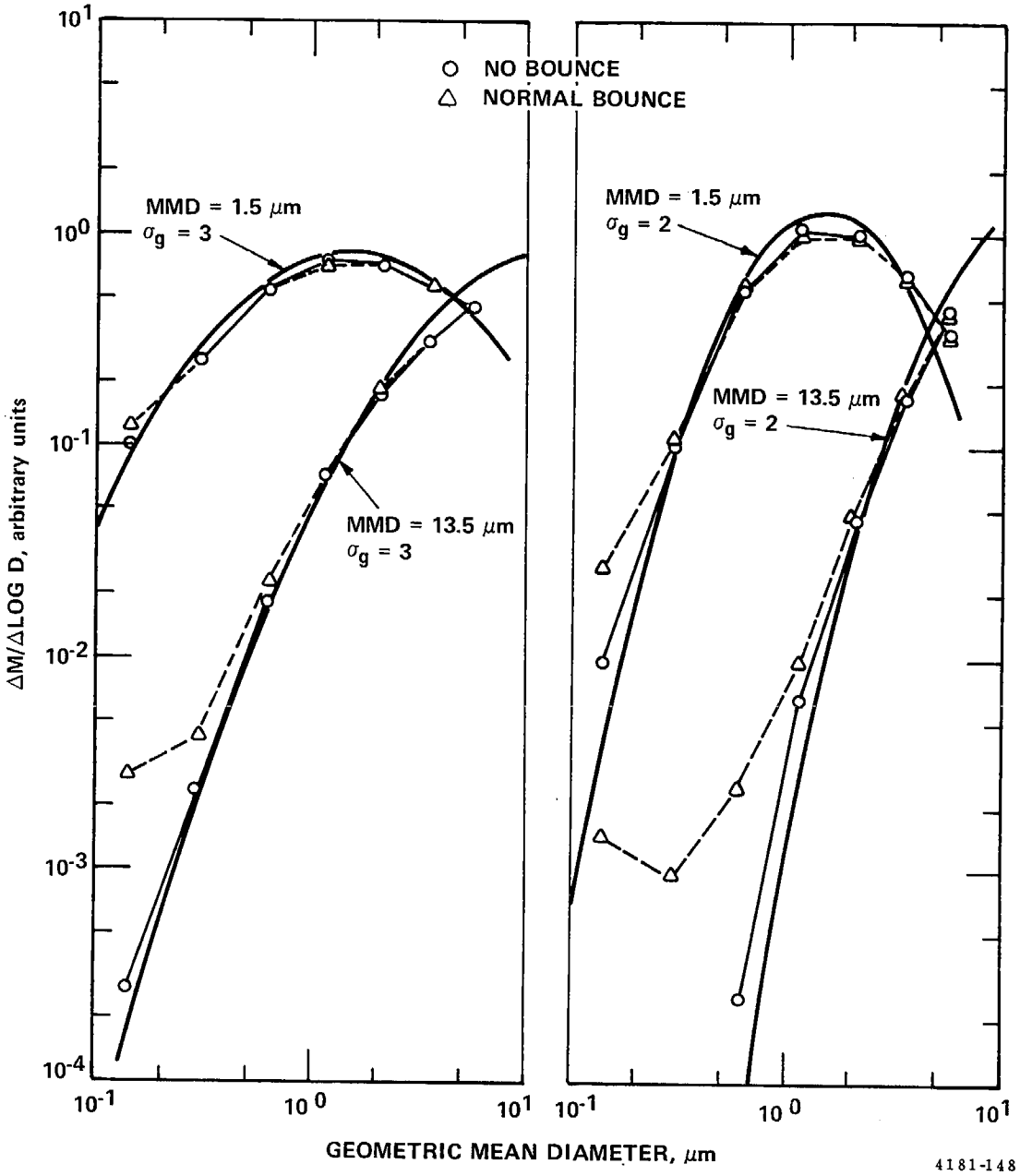

Figure 3-5. Recovered size distributions on a differential basis from the Andersen impactor models for MMD's of 1.5 and 13.5 μm and σ_g's of 2 and 3. The bold curves represent the input distributions.

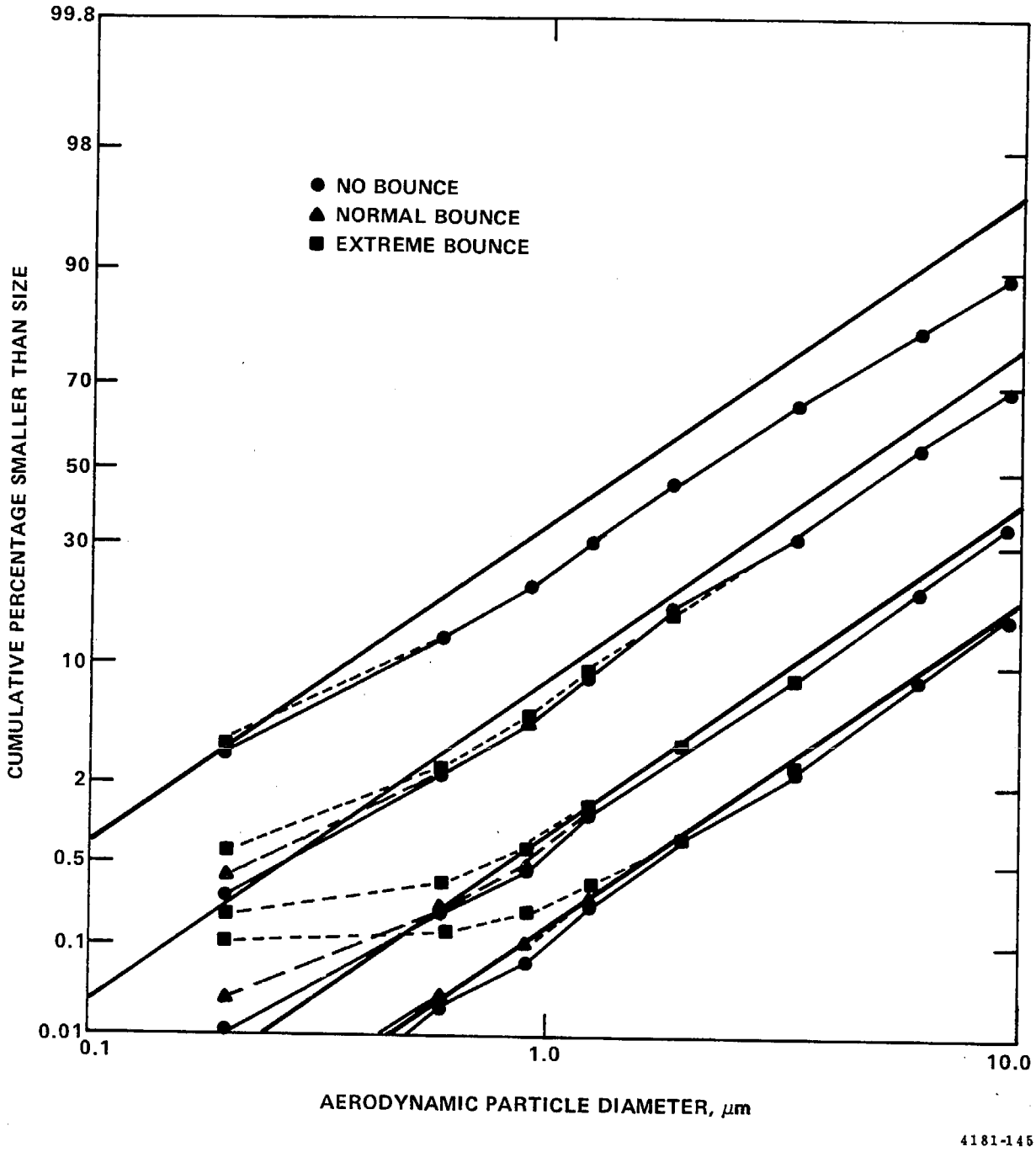

Figure 3-6. Recovered size distributions on a cumulative percentage basis from the Brink impactor models for σ_g = 3.0 and MMD's of 1.5, 4.5, 13.5 and 27 μm (backup filter included in the analysis). The bold lines represent the input distributions.

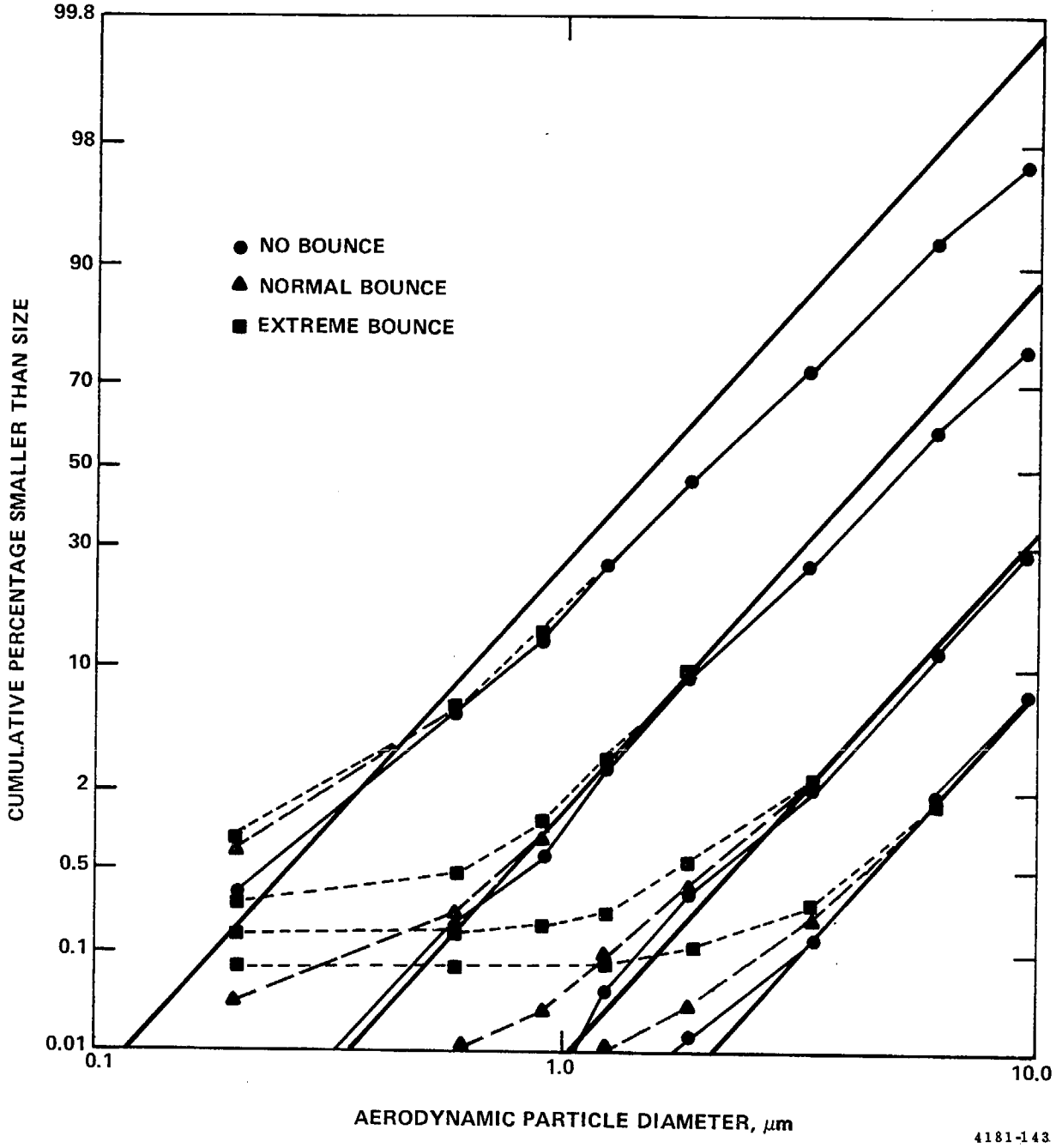

Figure 3-7. Recovered size distributions on a cumulative percent basis from the Brink impactor models for σ_g = 2.0 and MMD's of 1.5, 4.5, 13.5, and 27 μm. The bold lines represent the input distributions.

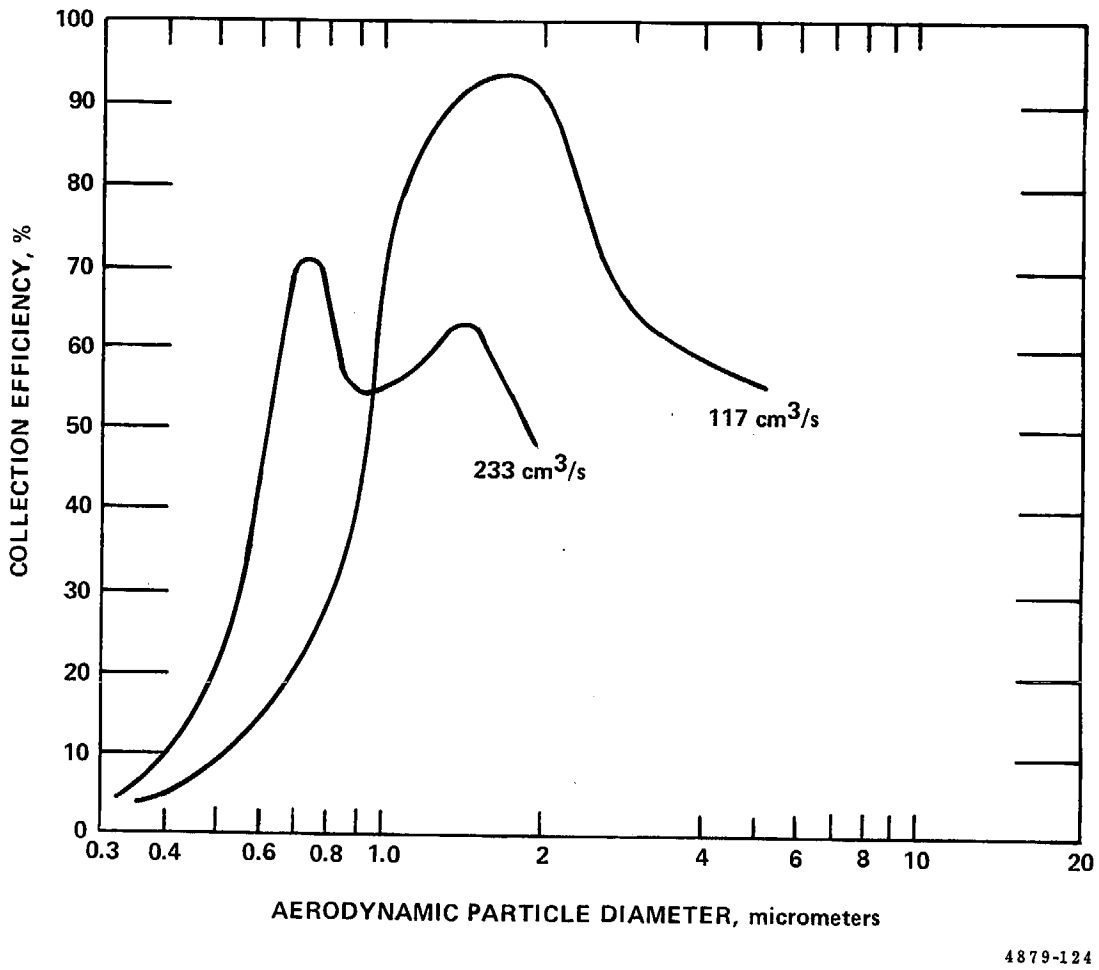

Figure 3-8. The effects of particle bounce and scouring on collection efficiencies of one stage of a cascade impactor. Glass fiber substrates, sampling flowrates of 117 cm^3/s and 233 cm^3/s.

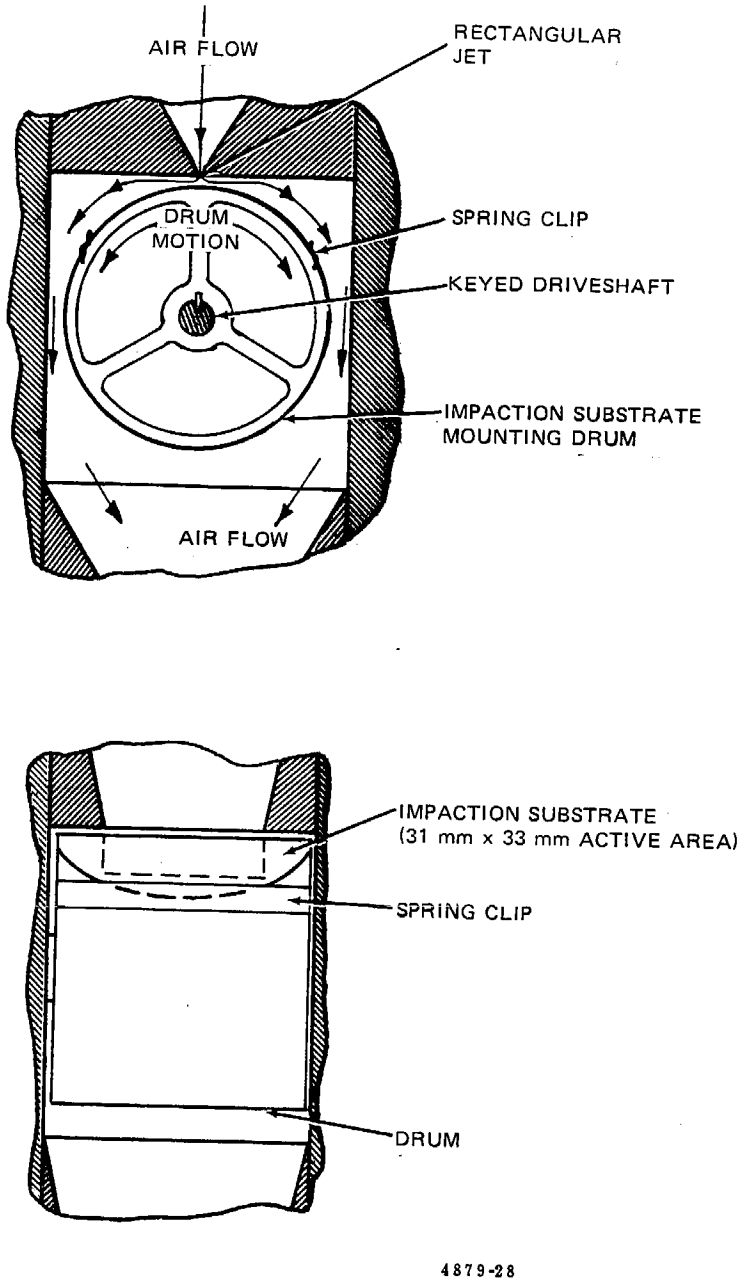

Figure 3-9. Preliminary design sketch of the drum and substrate arrangement for one stage of the EPA/SoRI impactor for elemental analysis. (Source: Adapted from Reference 38).

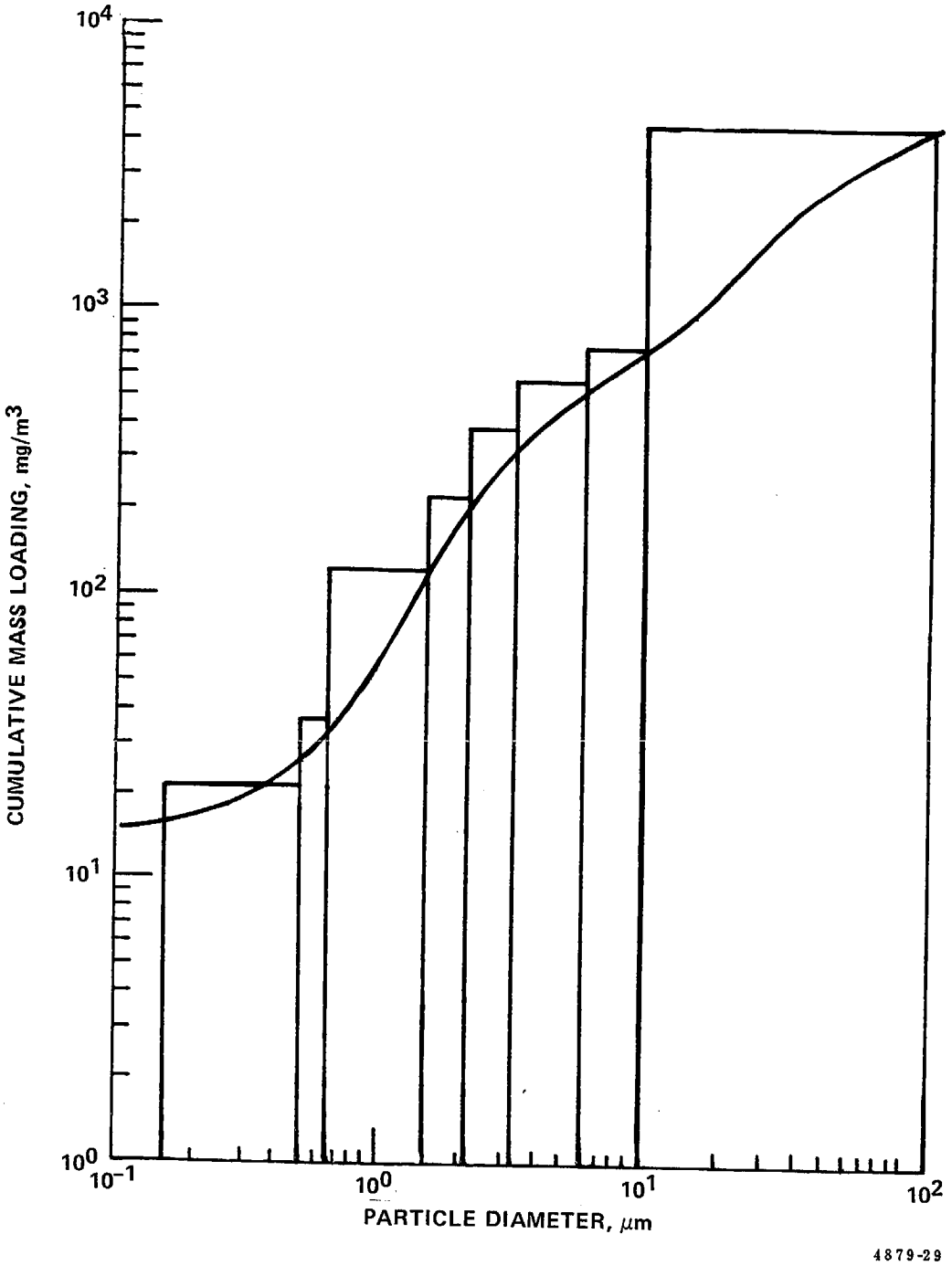

Figure 3-10. Typical cumulative mass loading of the emissions from a coal-fired power boiler.

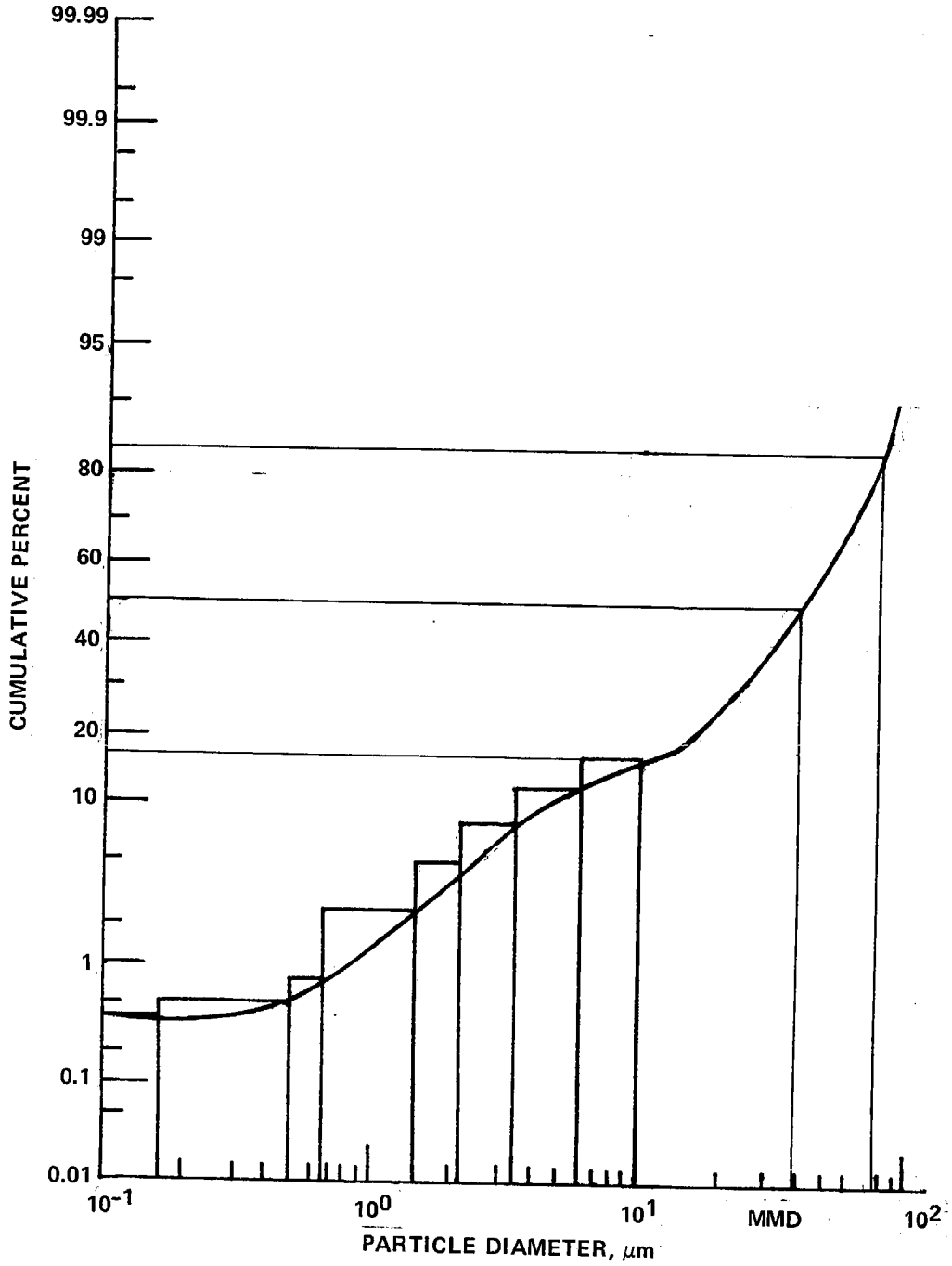

Figure 3-11. Same distribution as in the previous figure expressed in percent and plotted on a probability scale. Note that this format allows quick determination of the mass median diameter and σ_g.

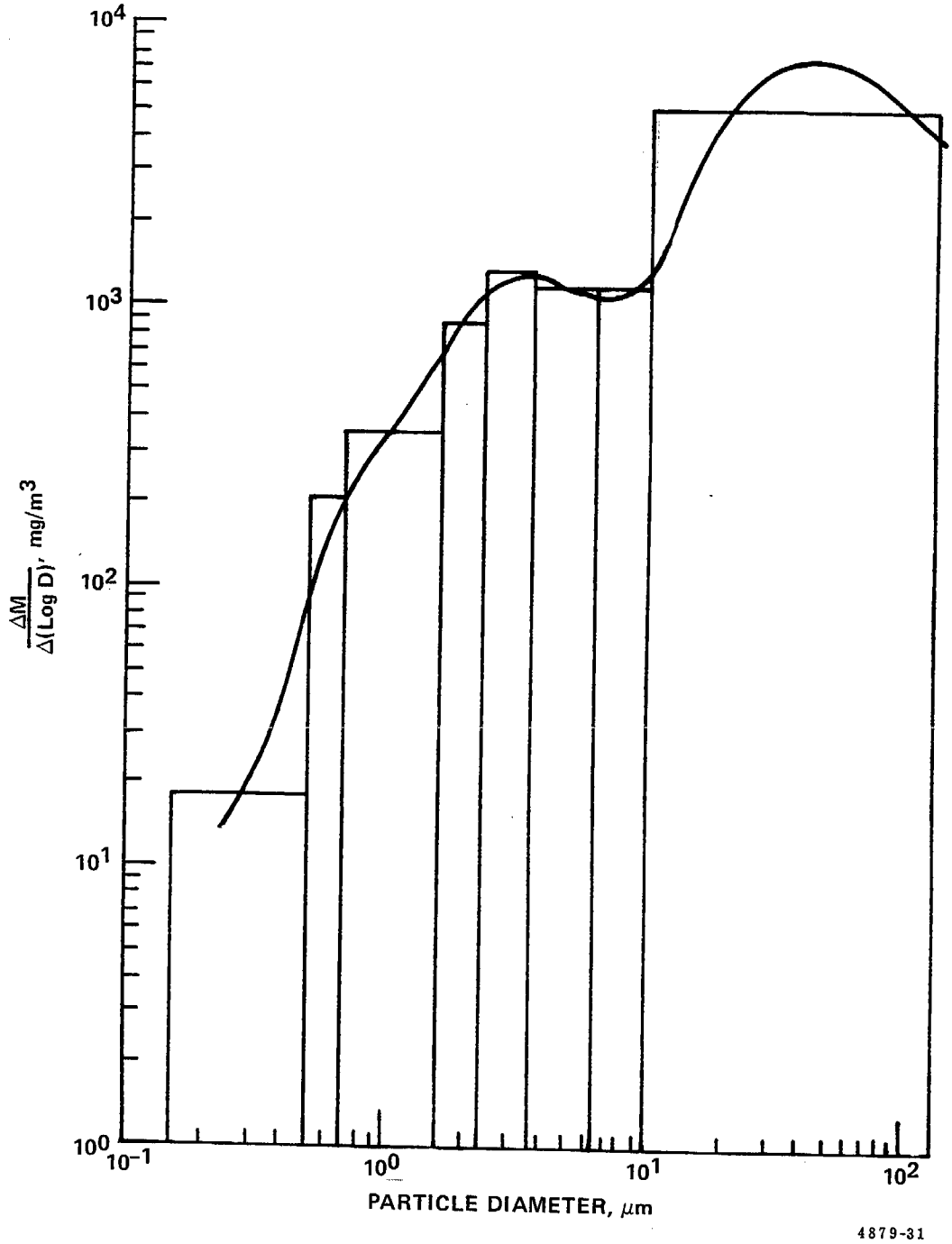

Figure 3-12. A differential particle-size distribution typical of emissions from a coal-fired utility boiler. The smooth curve represents interpolated dM/d(logD) results from the histogram data obtained from an actual cascade impactor run.

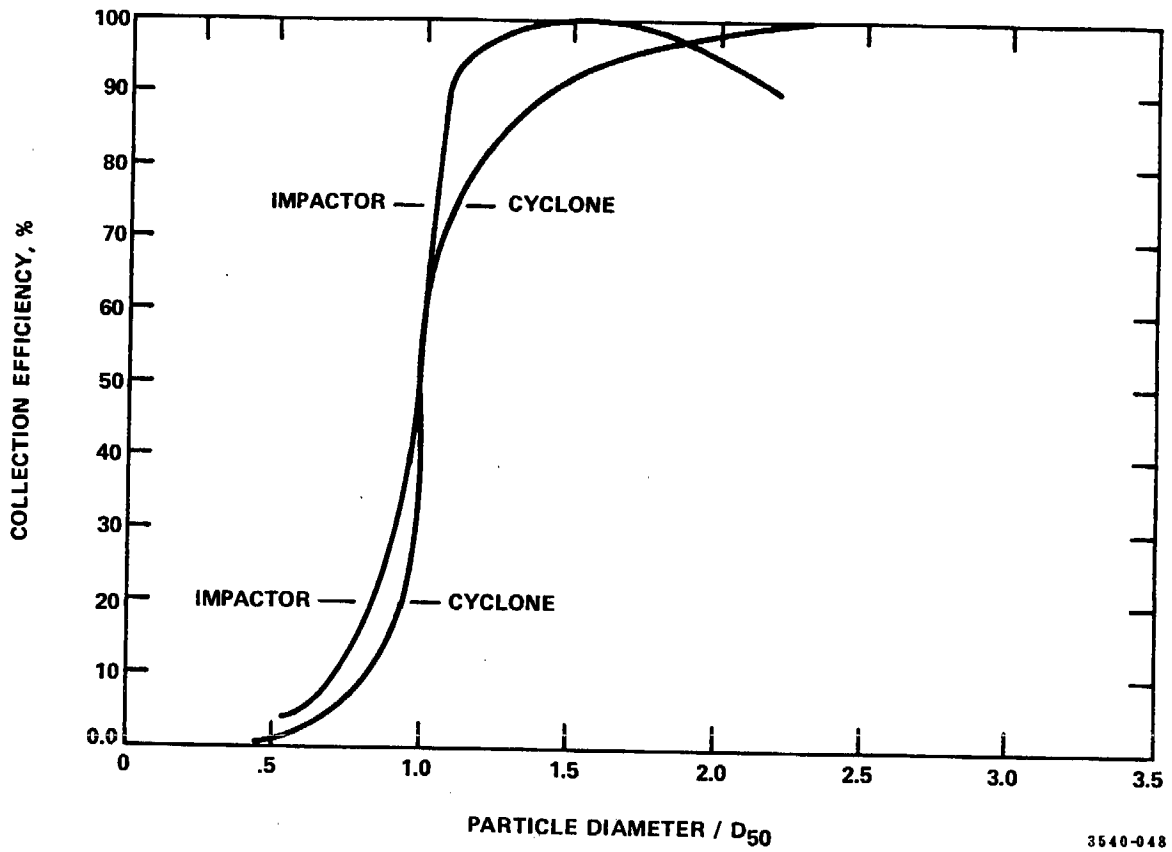

Figure 3-13. Comparison of cascade impactor stage with cyclone collection efficiency curve. (Source: Reference 39)

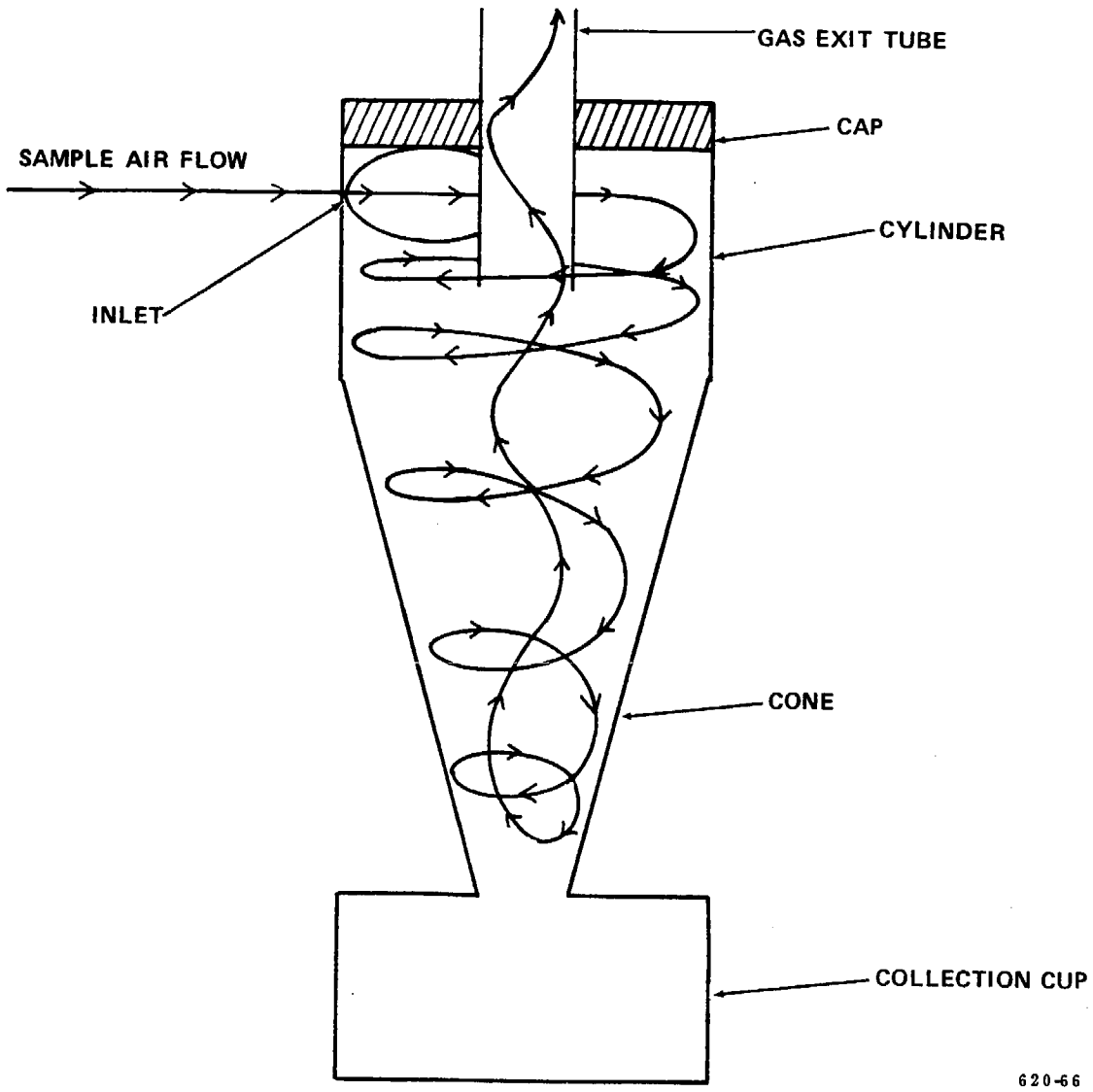

Figure 3-14. Hypothetical flow through a cyclone of conventional design.

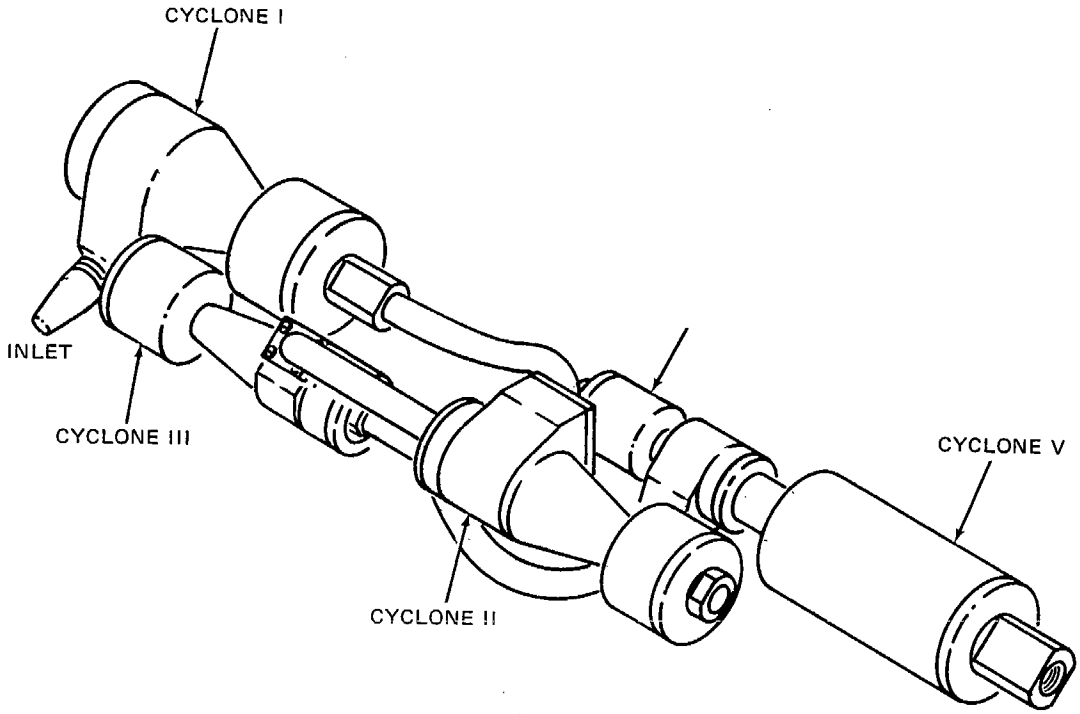

4546-1

Figure 3-15. The five-stage cyclone system. (Source: Adapted from Reference 46)

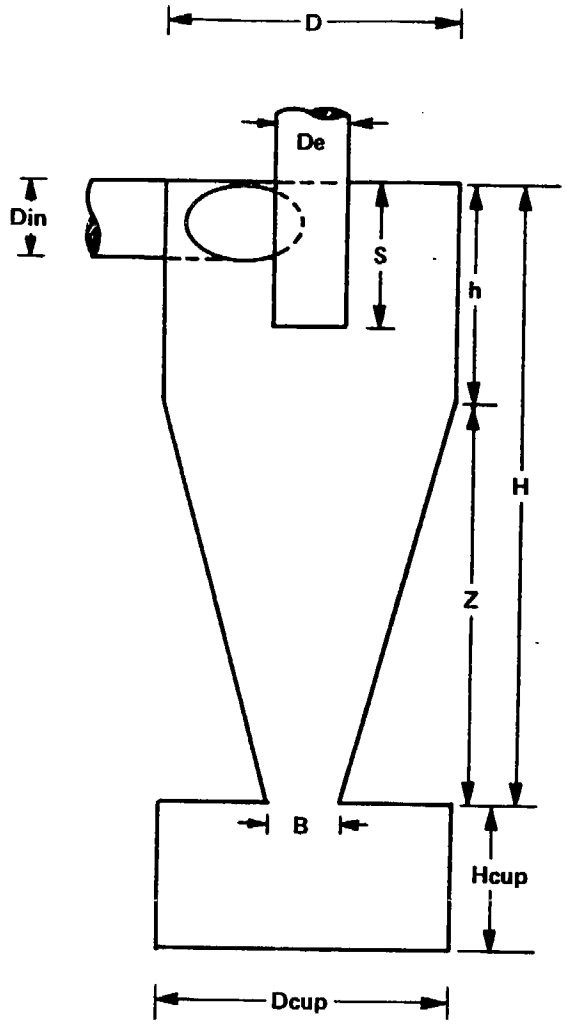

DIMENSIONS (CENTIMETERS)

CYCLONE	D	Din	De	B	H	h	Z	S	Hcup	Dcup
IX	5.12	1.53	1.81	2.43	7.06	2.35	4.71	2.00	2.26	5.12
I	4.47	1.27	1.50	1.88	6.95	2.24	4.71	1.57	2.25	4.45
II	3.66	1.01	1.05	1.29	6.82	2.11	4.71	1.57	2.22	3.73
III	3.11	.75	.83	.76	4.91	1.40	3.51	1.08	2.22	3.10
IV	2.54	.51	.59	.51	3.32	1.03	2.29	.58	2.22	2.62
V	1.52	.30	.36	.84	1.76	.47	1.29	.43	2.38	1.59

4181-379

Figure 3-16. Summary of cyclone dimensions. (Source: Reference 46)

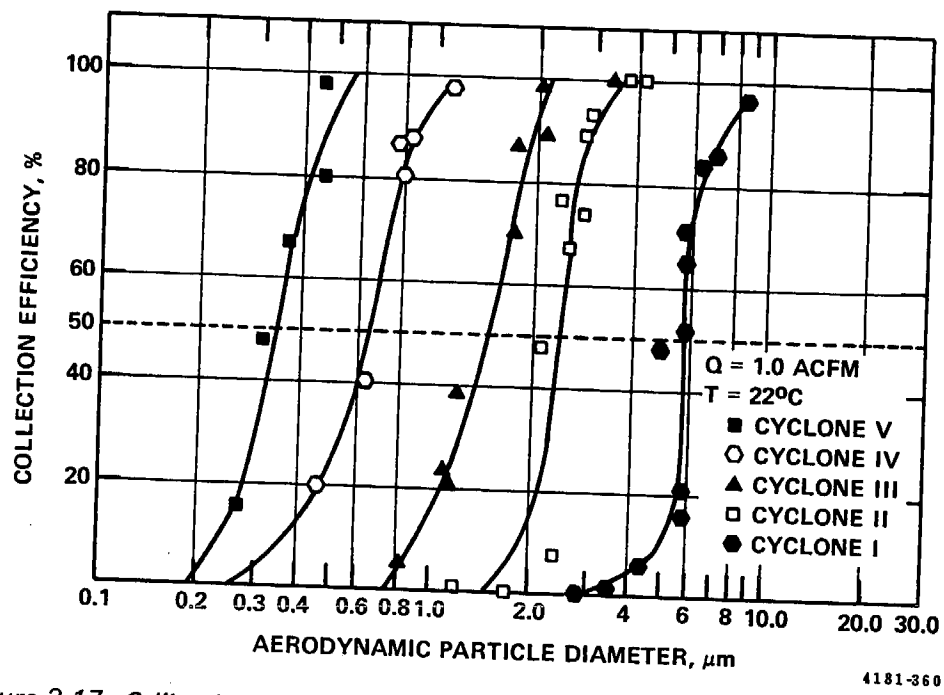

Figure 3-17. Calibration curves for the five-stage cyclone system. Flowrate 1.0 ft^3/min, temperature 22 °C. (Source: Adapted from Reference 45)

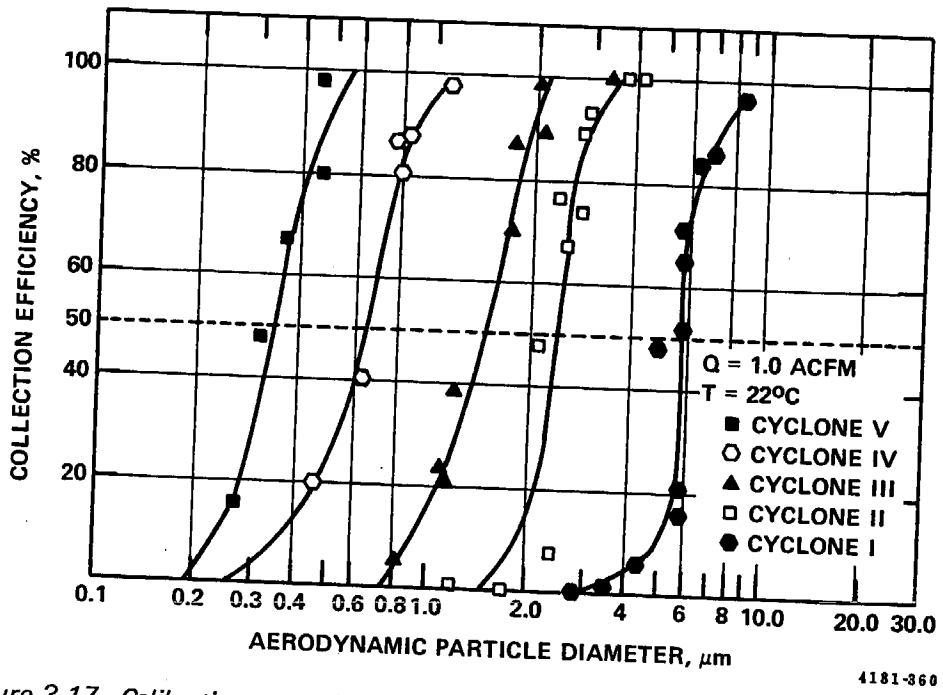

Figure 3-17. Calibration curves for the five-stage cyclone system. Flowrate 1.0 ft^3/min, temperature 22 °C. (Source: Adapted from Reference 45)

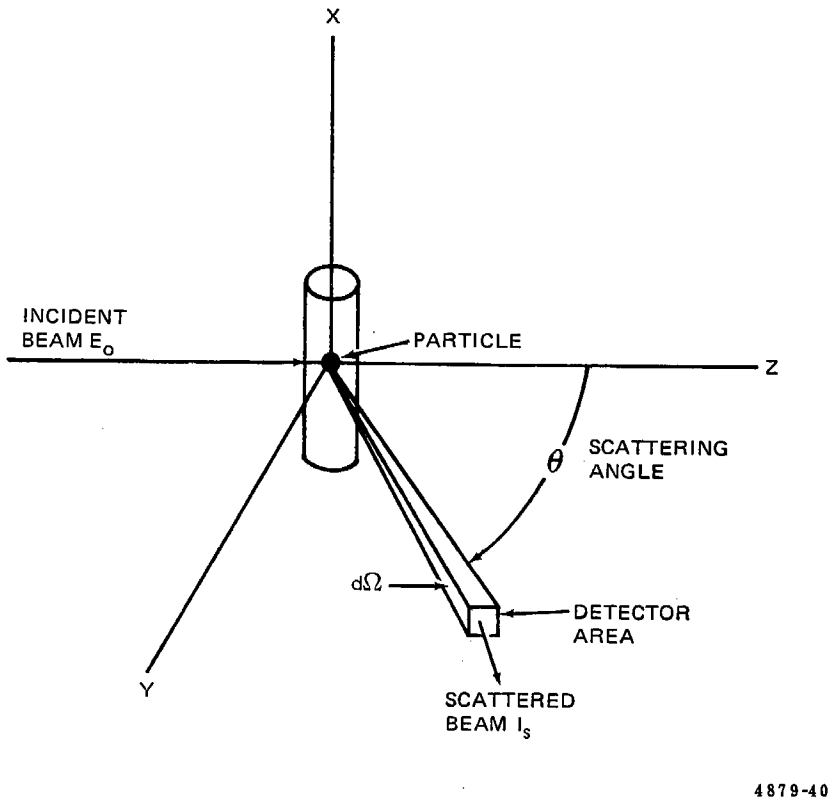

Figure 3-18. Typical photodetector-scatterer geometry for measuring the angular dependence of scattered light. An incident collimated beam of light E_o is scattered by the particle. For spherical or randomly oriented nonspherical cells, there is azimuthal symmetry about the z-axis and all measurements of the scattered beam I_s are made in the y-z or scattering plane. The detector subtends a solid angle $d\Omega = \sin\theta\, d\theta\, d\phi$ about the scatterer. (Source: Adapted from Reference 53)

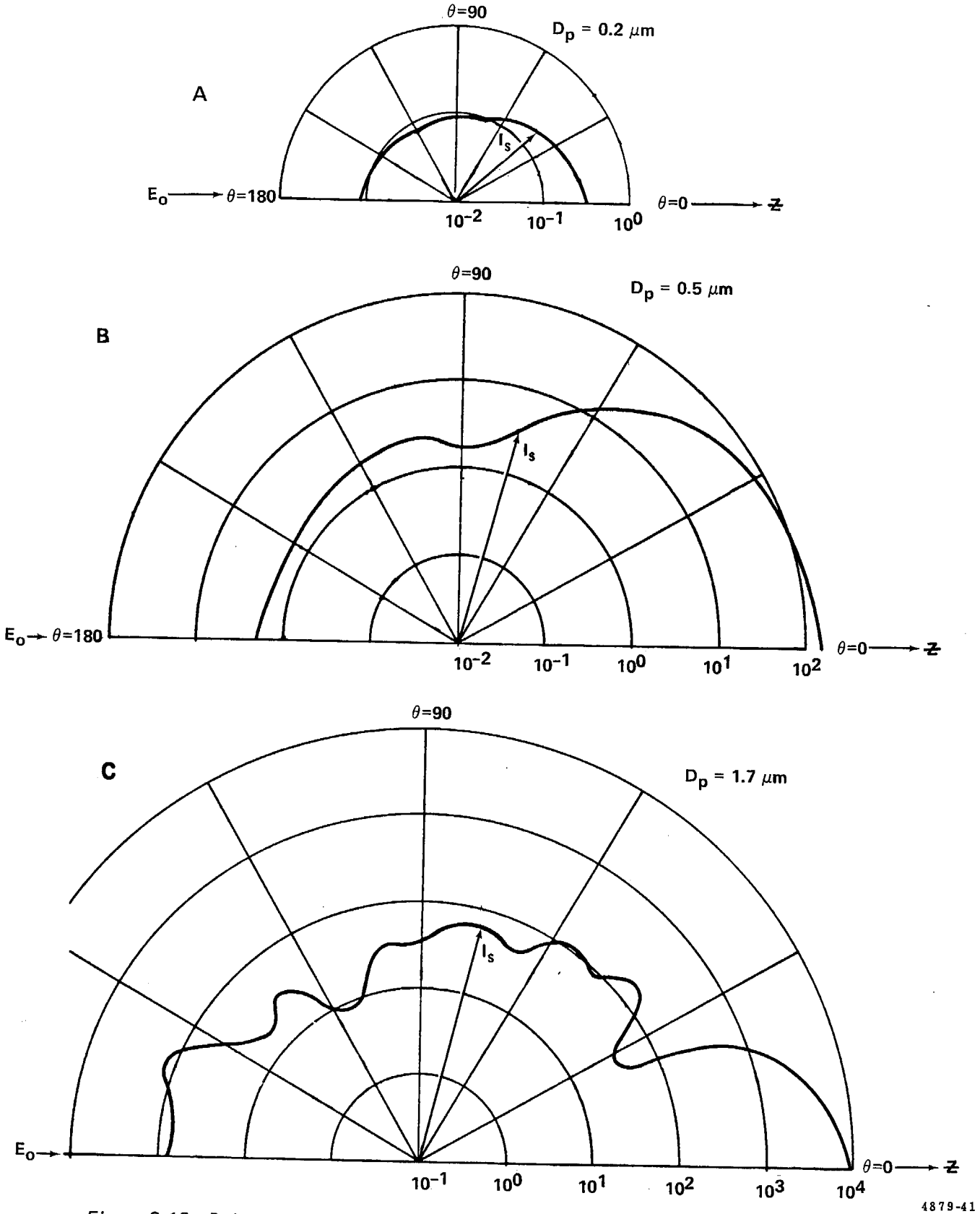

Figure 3-19. Polar plate of the scattered intensity for several sizes of spherical particles. (Source: Adapted from Reference 33)

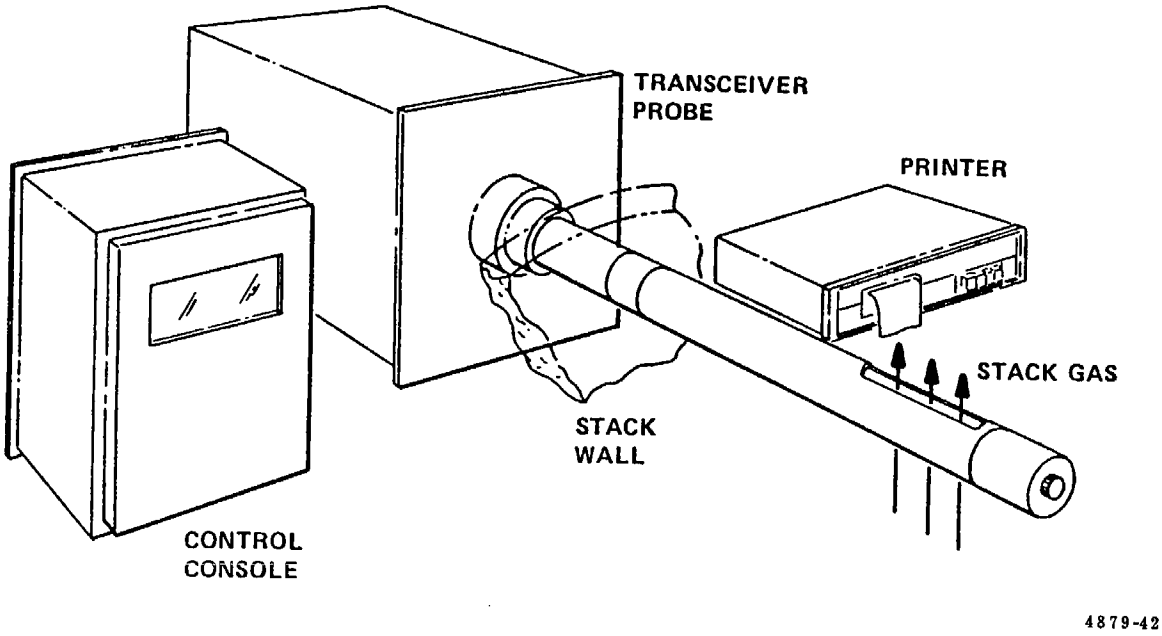

Figure 3-20: Leeds and Northrup Optical Stack Particulate Monitor. (Source: Leeds and Northrup)

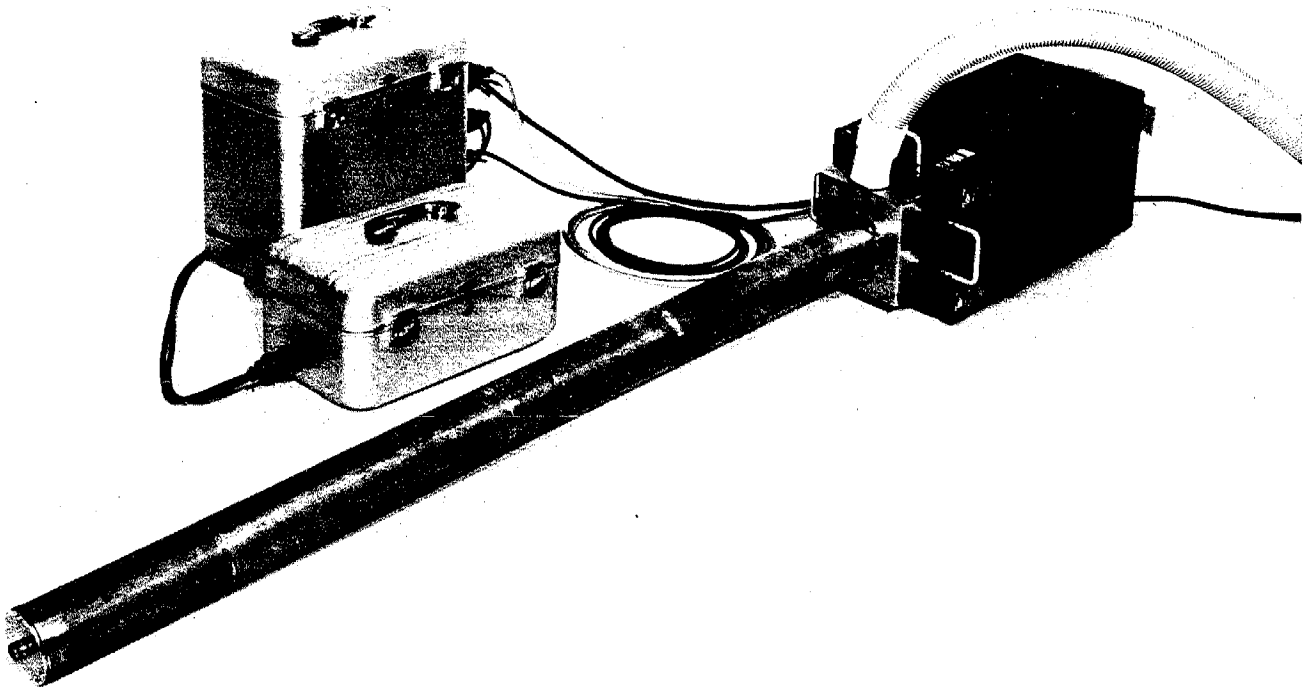

4879-43

Figure 3-21. The Stack Particulate Monitor. (Source: Leeds and Northrup)

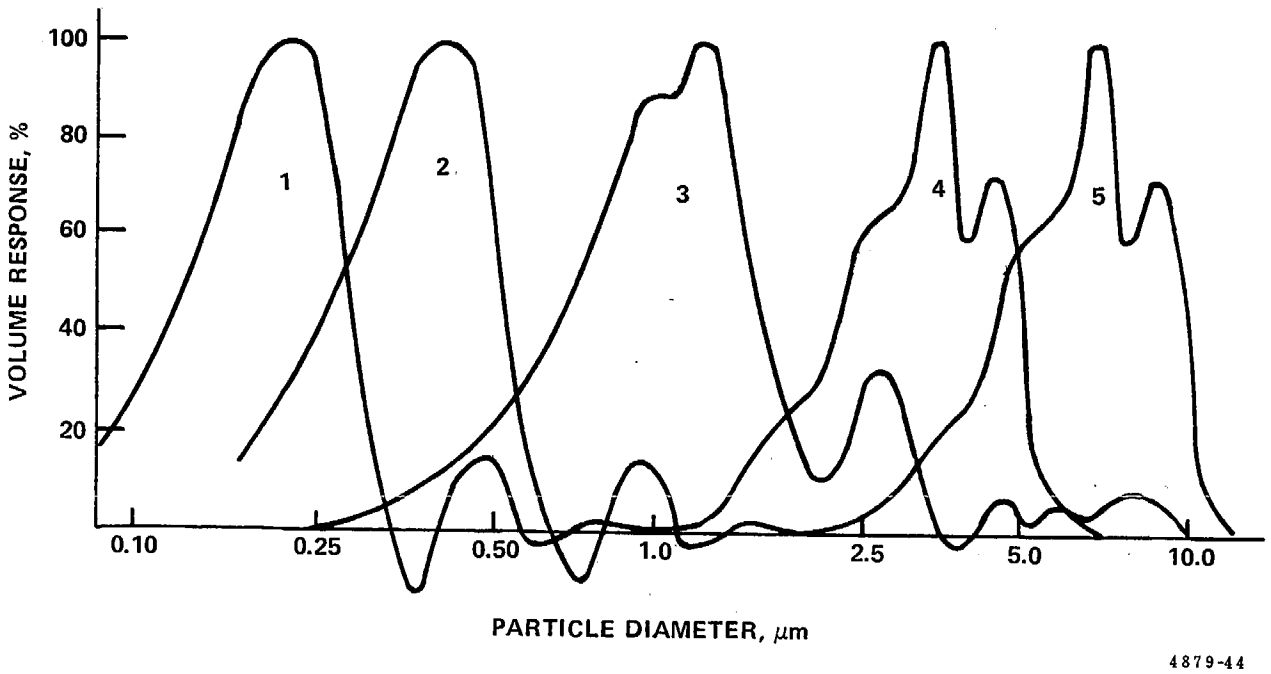

Figure 3-22. Volumetric response curves, as a function of particle diameter, for the five channels of the prototype. Curves 1 and 2 are obtained with 90° scattering, and curves 3, 4, and 5 from forward scattering. (Source: Reference 66)

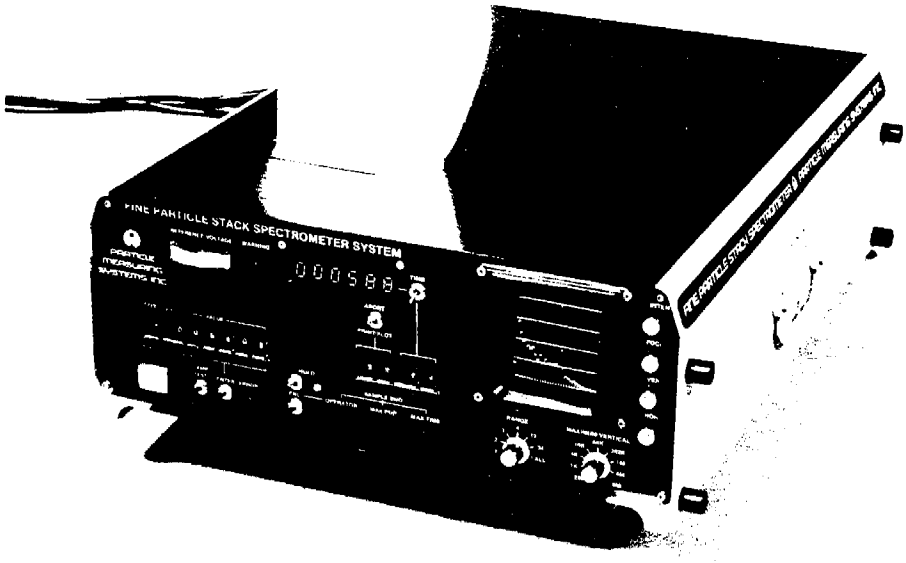

4879-45

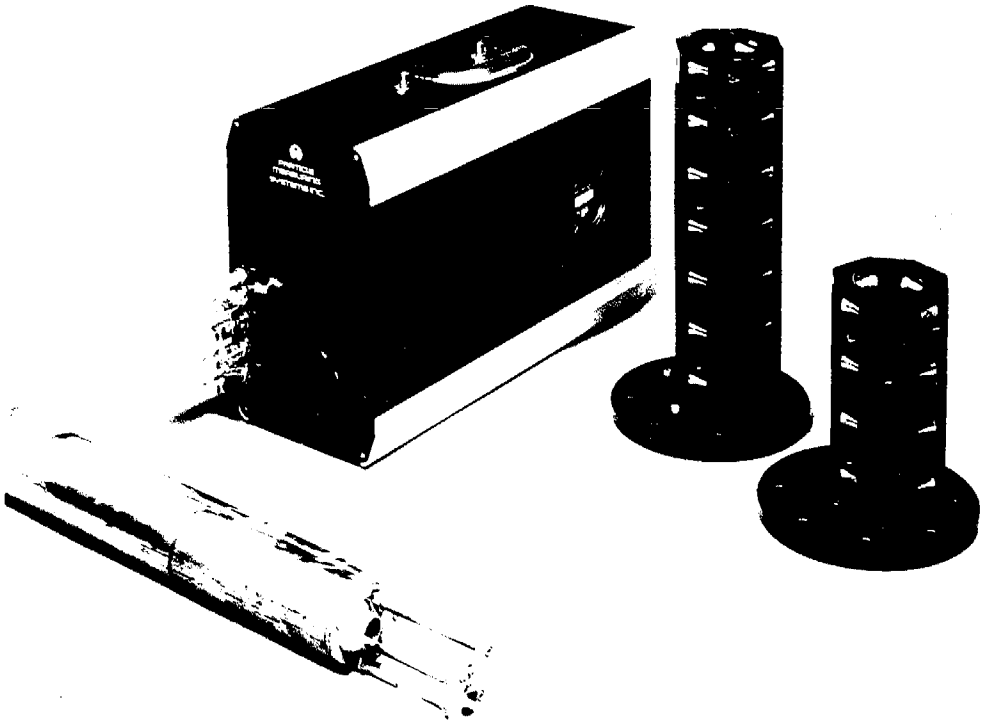

4879-46

Figure 3-23. The Fine Particle Stack Spectrometer System (FPSSS) probe and coolant pump. (Source: Particle Measuring Systems, Inc.)

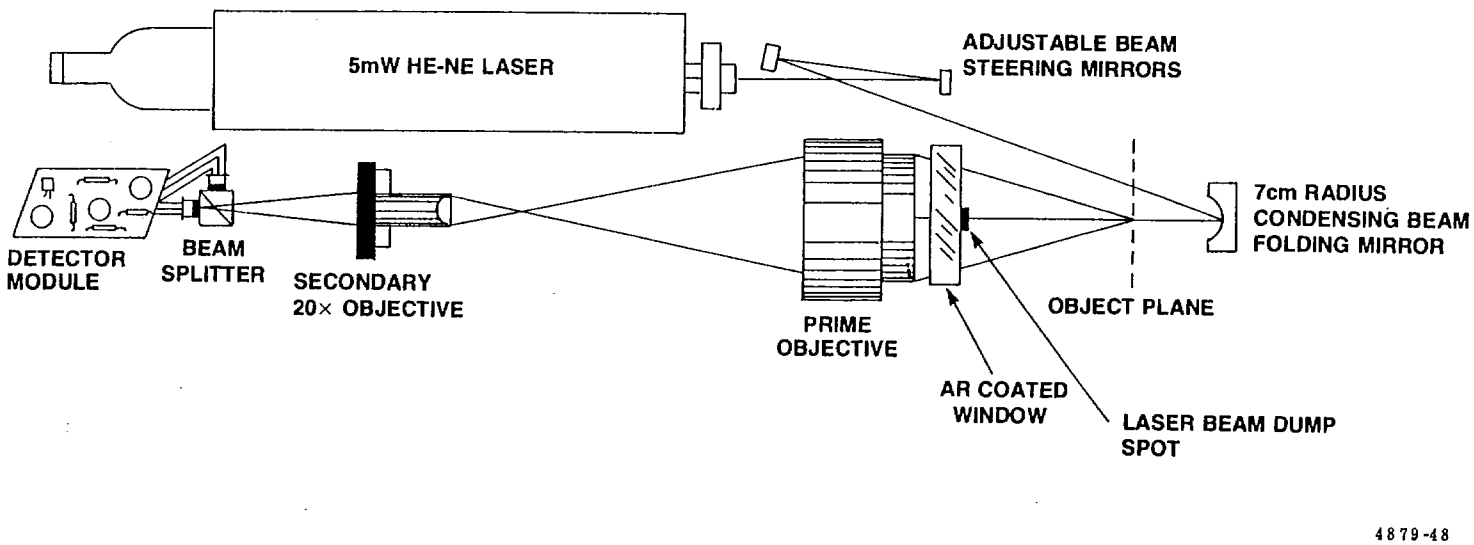

Figure 3-24. FPSSS Optical System diagram. (Source: Particle Measuring Systems, Inc.)

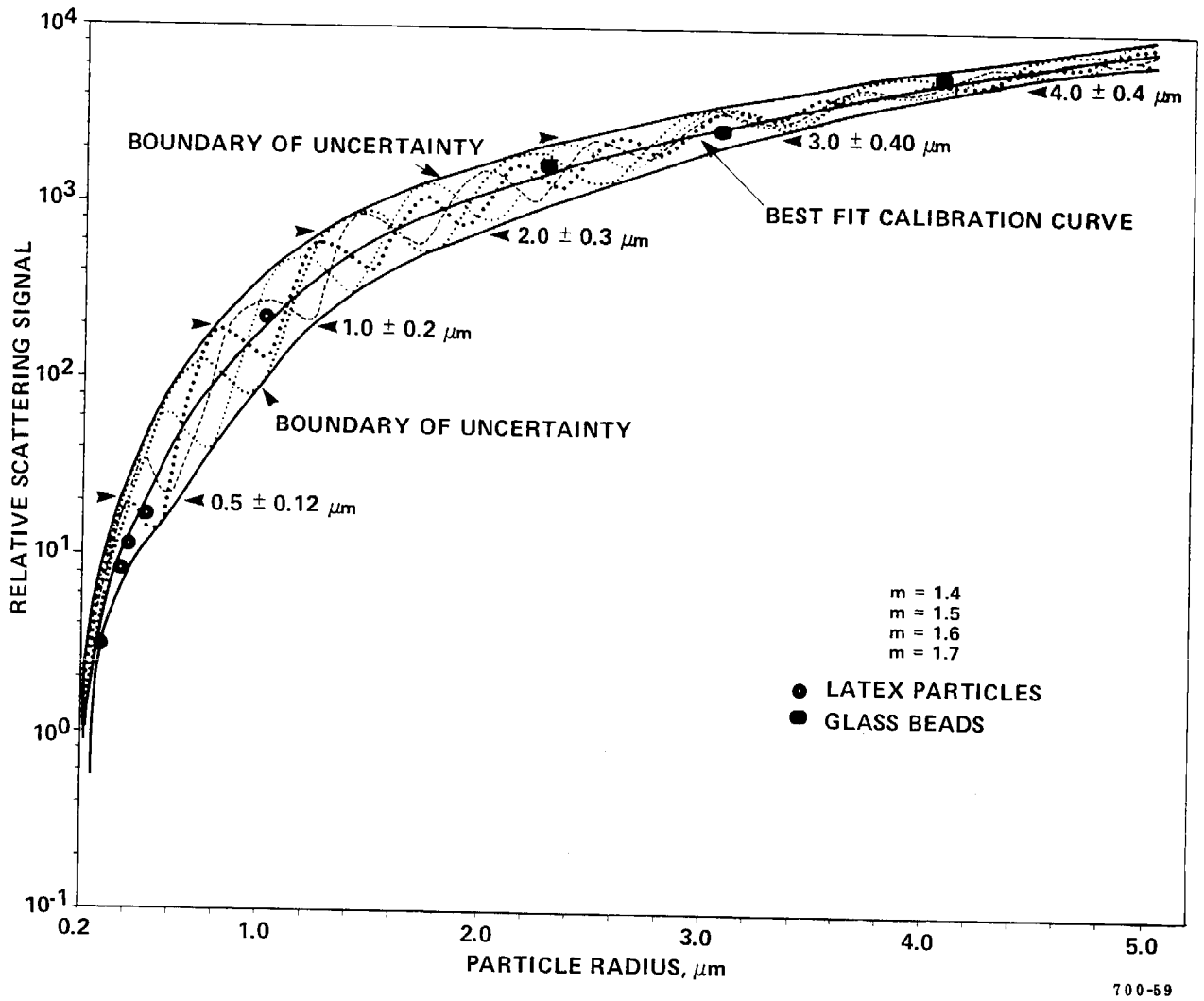

Figure 3-25. Theoretical Mie scattering for 2-11°, real refractive indices 1.4, 1.5, 1.6, and 1.7. (Source: Reference 60)

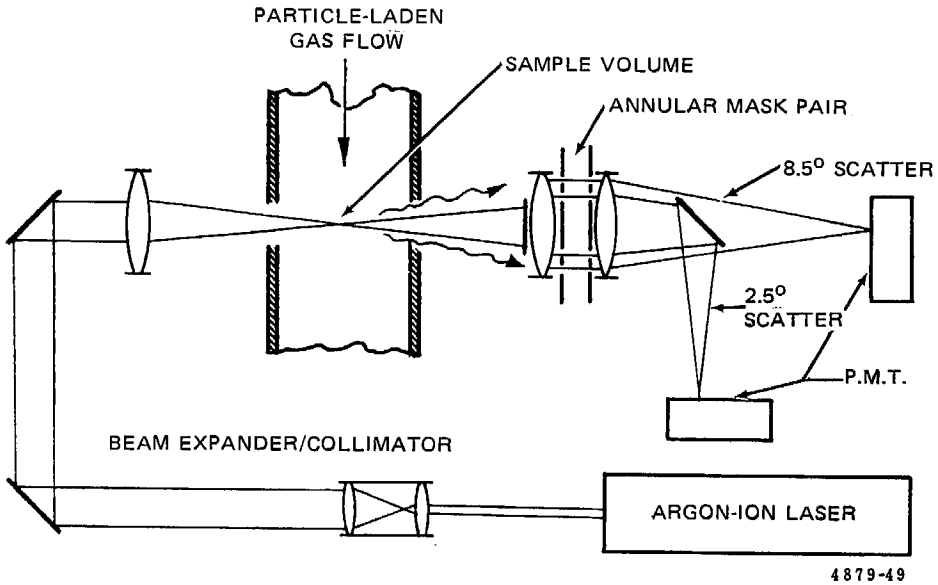

Figure 3-26. Schematic diagram of the PSI ratioing optics system. (Source: Reference 68)

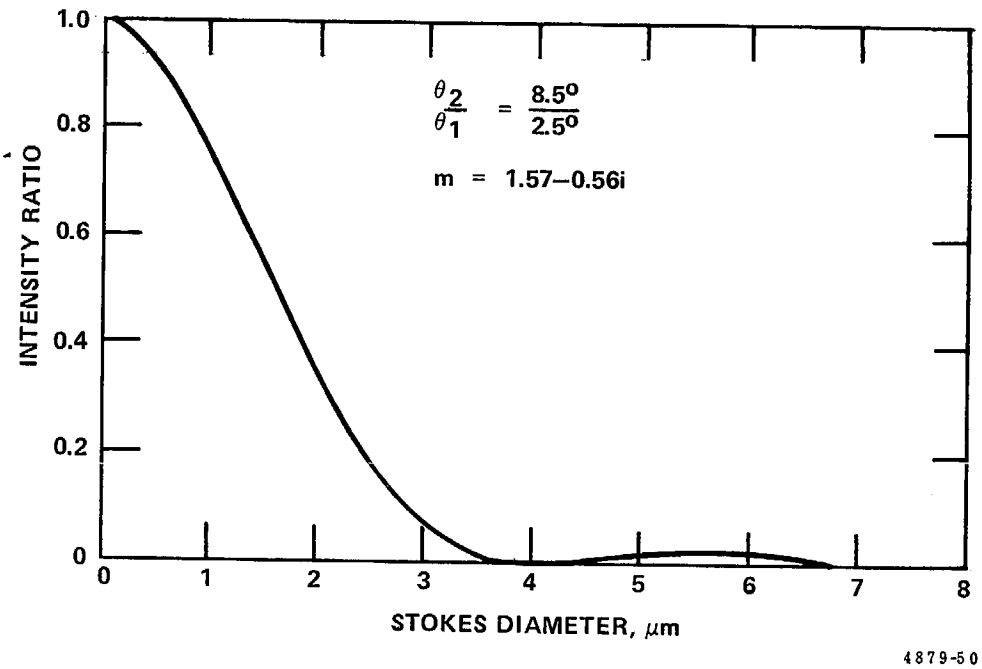

Figure 3-27. Scattering intensity ratio versus particle size for the PSI. (Source: Reference 68)

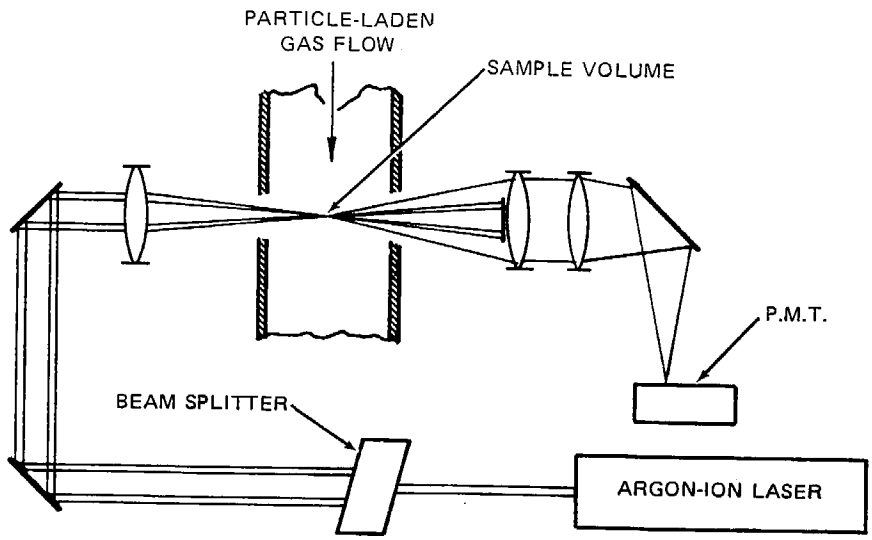

a. GENERALIZED COMPONENT ARRANGEMENT.

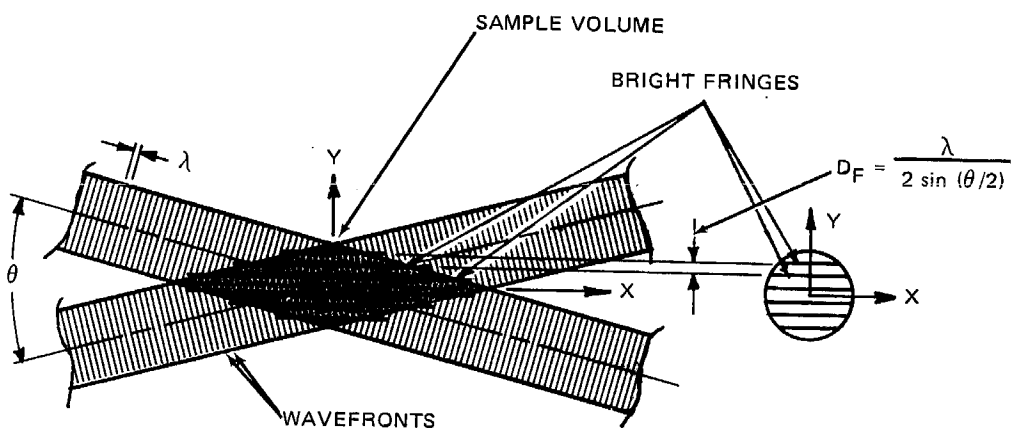

b. ENLARGED VIEW OF THE PROBE REGION.

4879-51

Figure 3-28. Schematical diagram of an interferometric particle sizing device. (Source: Adapted from Reference 68)

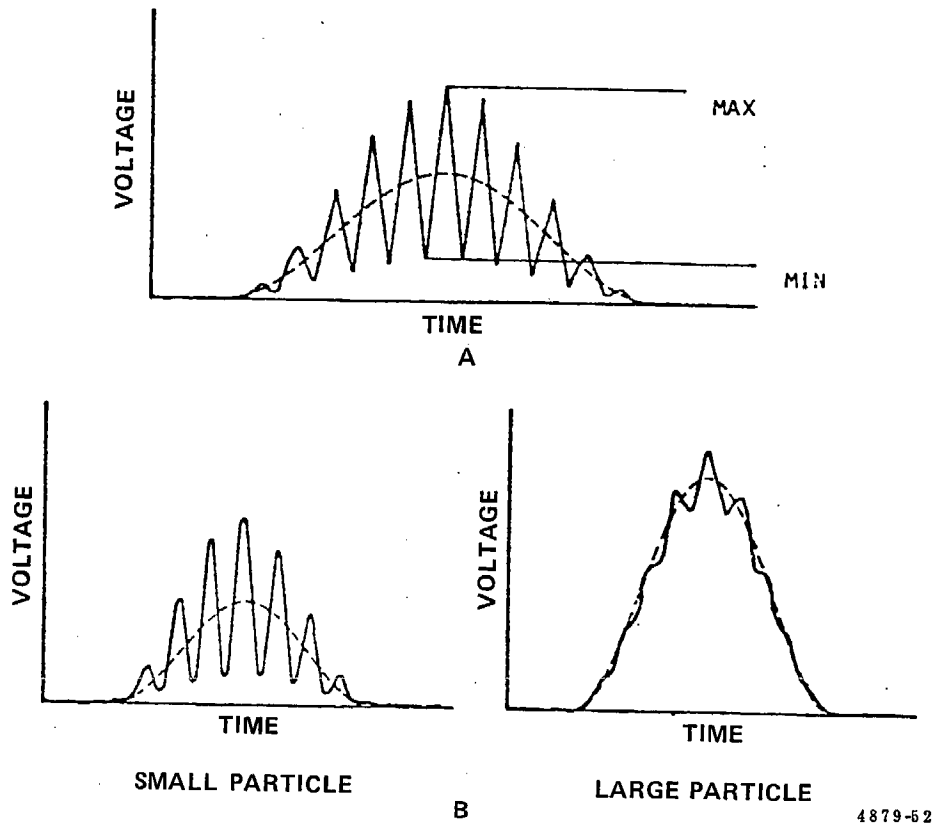

Figure 3-29. Output from the interferometric scattering detector. (Source: Spectron Development Labs., Inc.)

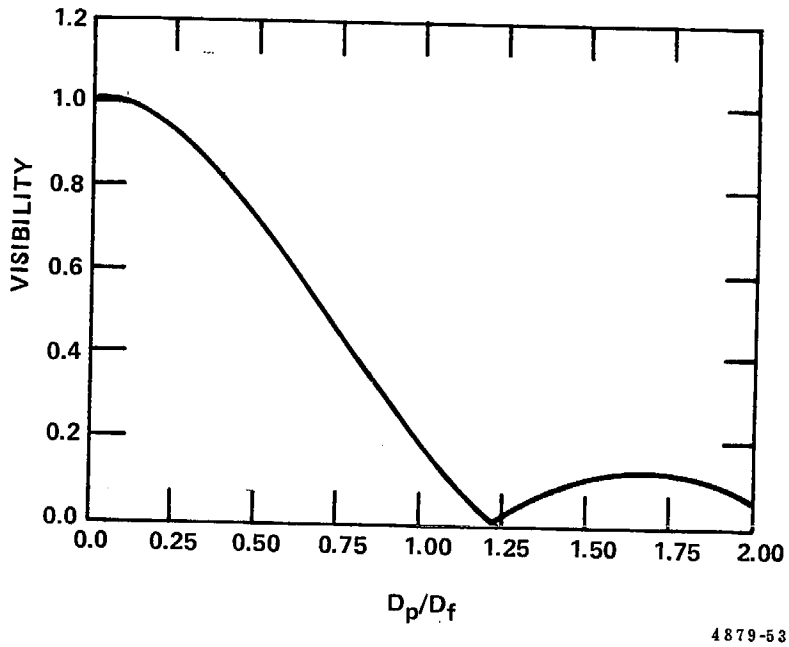

Figure 3-30. Simplified visibility relationship for particle sizing. (Source: Adapted from Reference 68)

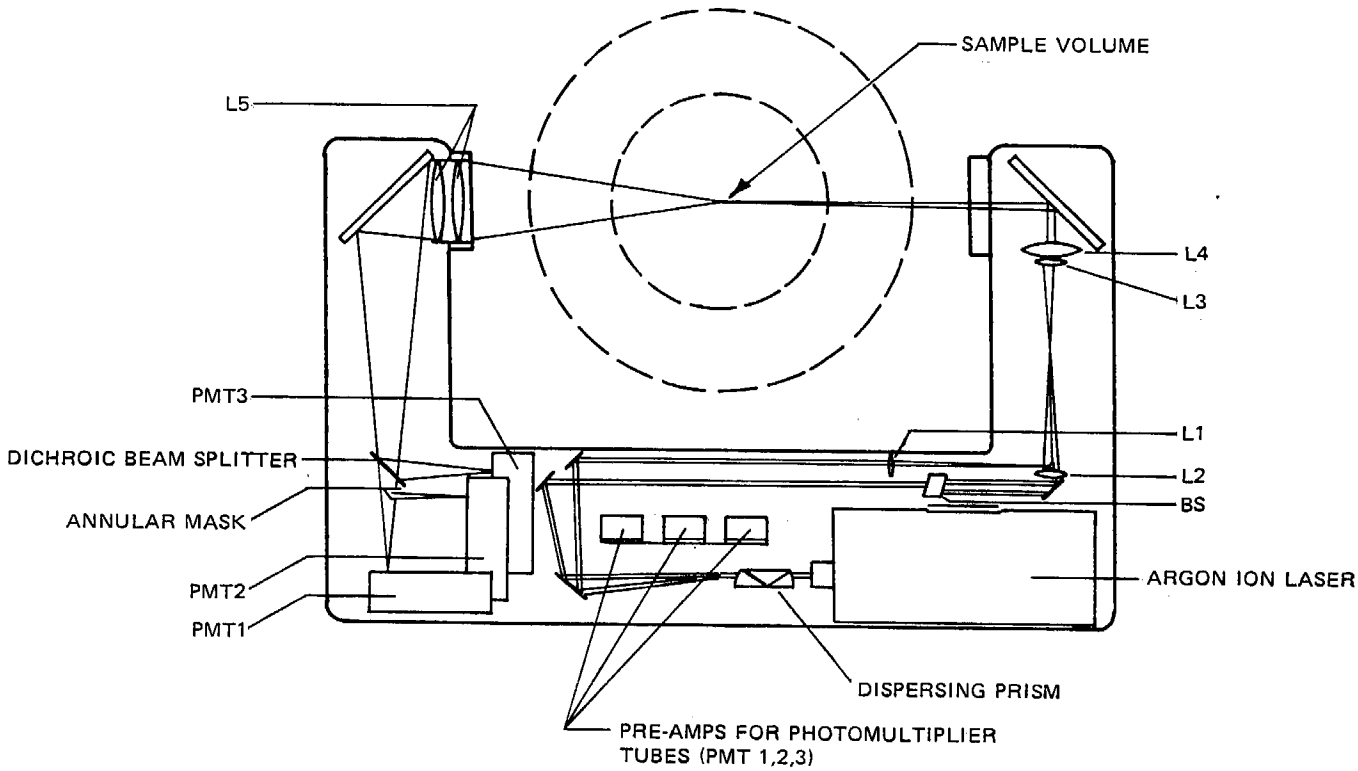

L1,L2,L3-BEAM EXPANSION—L4-TRANSMITTING LENS—L5-COLLECTING LENS
BS-BEAM SPLITTER

4879-54

Figure 3-31. Integrated particle sizing system combining particle sizing interferometry and scattering intensity ratioing. (Source: Reference 68)

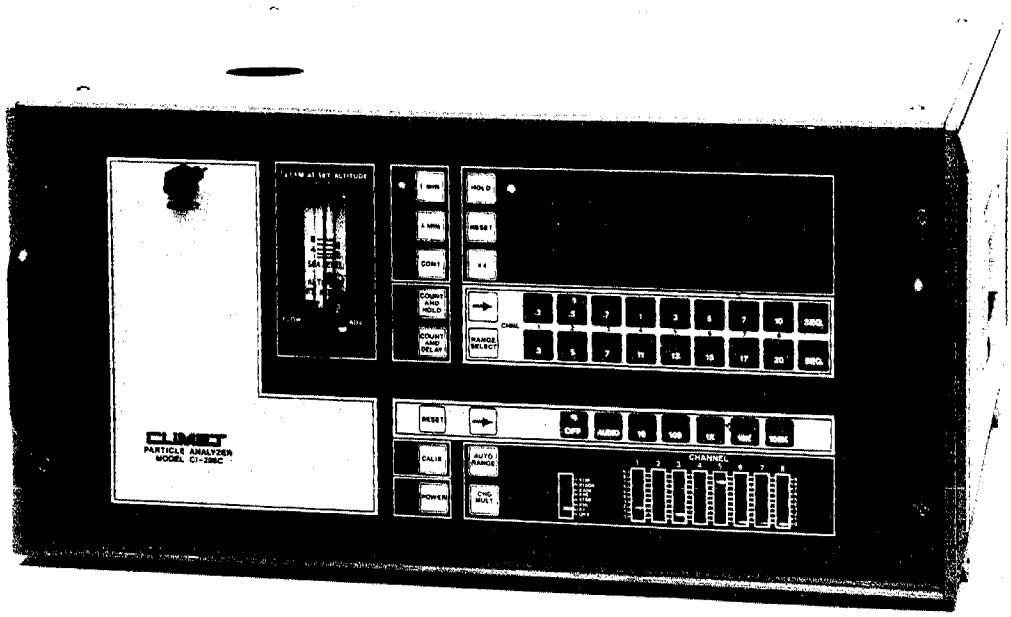

4879-55

Figure 3-32. The Climet Optical Particle Analyzer, Model CI-208C. (Source: Climet Instruments)

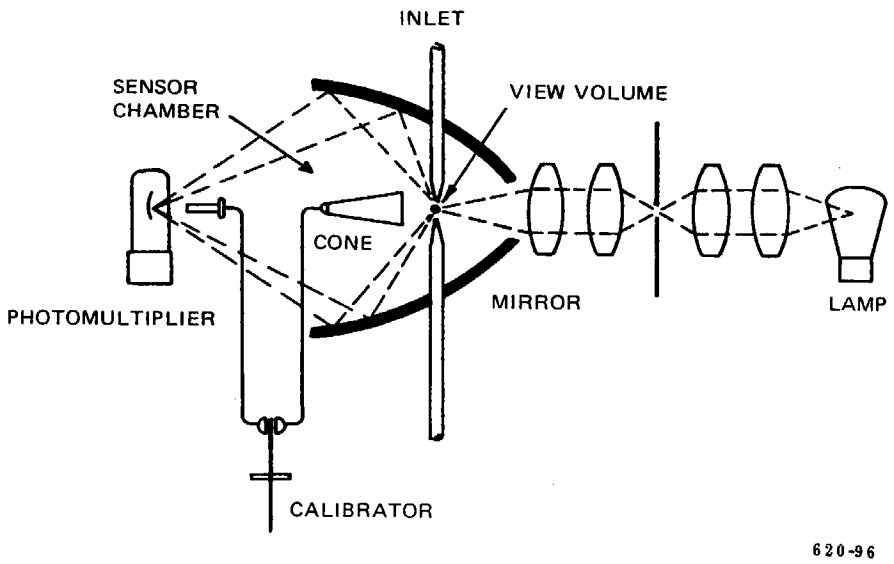

Figure 3-33. Operating principle of an optical particle counter. Courtesy of Climet Instruments Company.

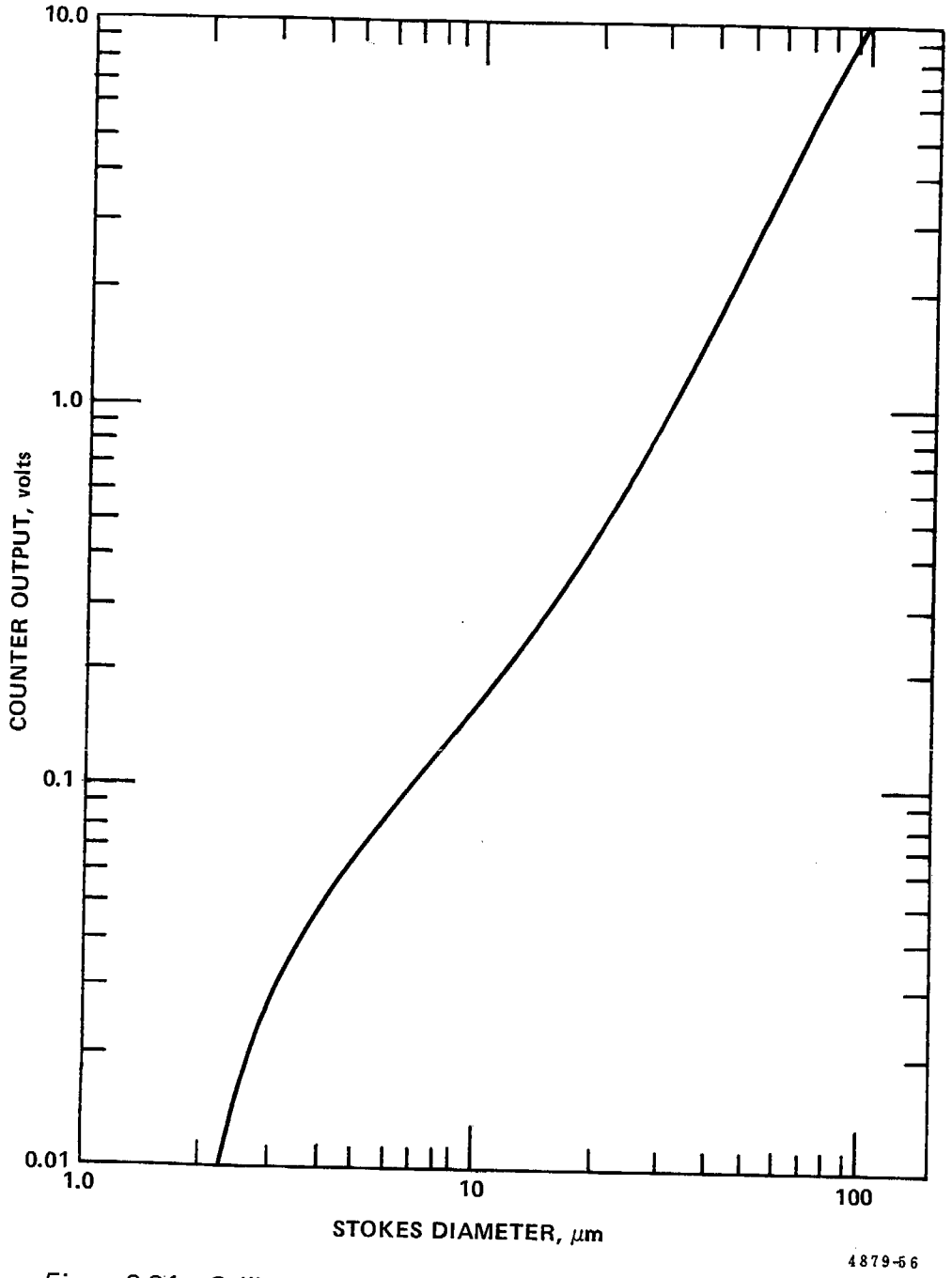

Figure 3-34. Calibration curve for the Climet Optical Particle Analyzer. (Source: Climet Instruments)

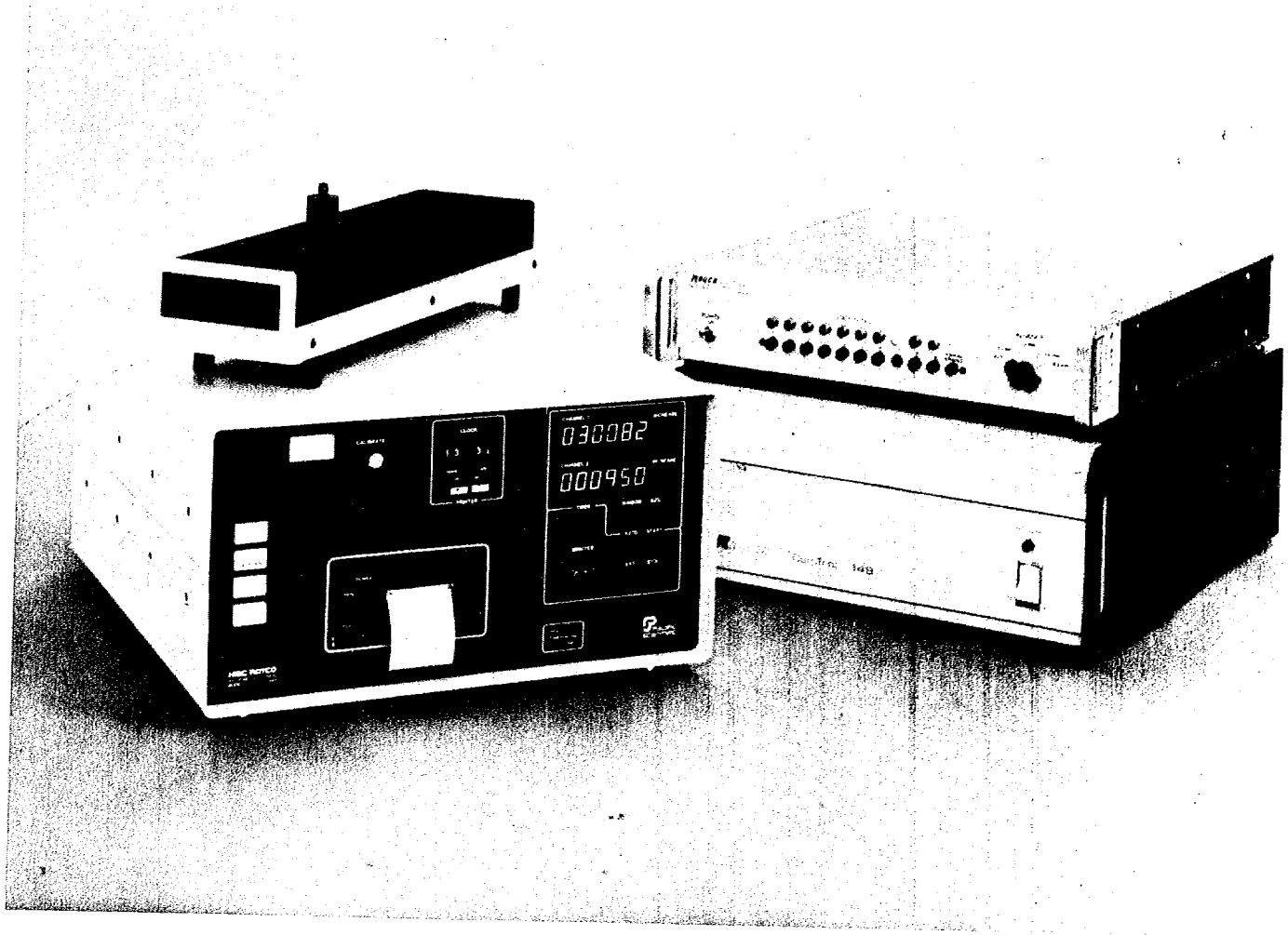

4879-57

Figure 3-35. The Royco Optical Particle Counter Model 247 and associated components. (Source: Royco Instruments, Inc.)

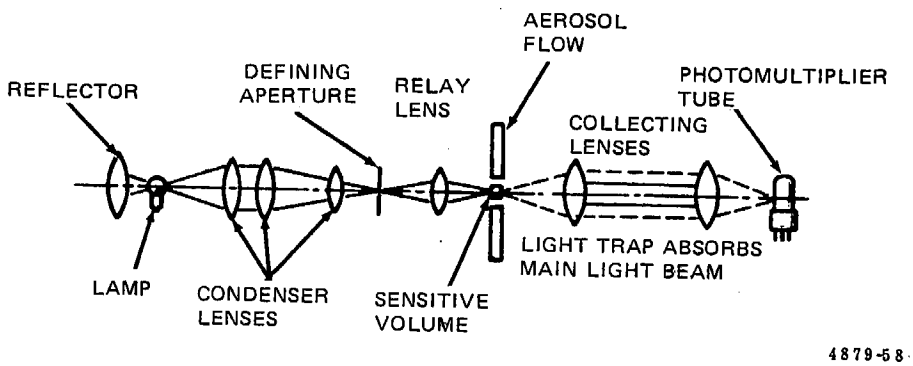

Figure 3-36. Schematic diatram of the Royco Optical Particle Analyzer. (Source: Royco Instruments)

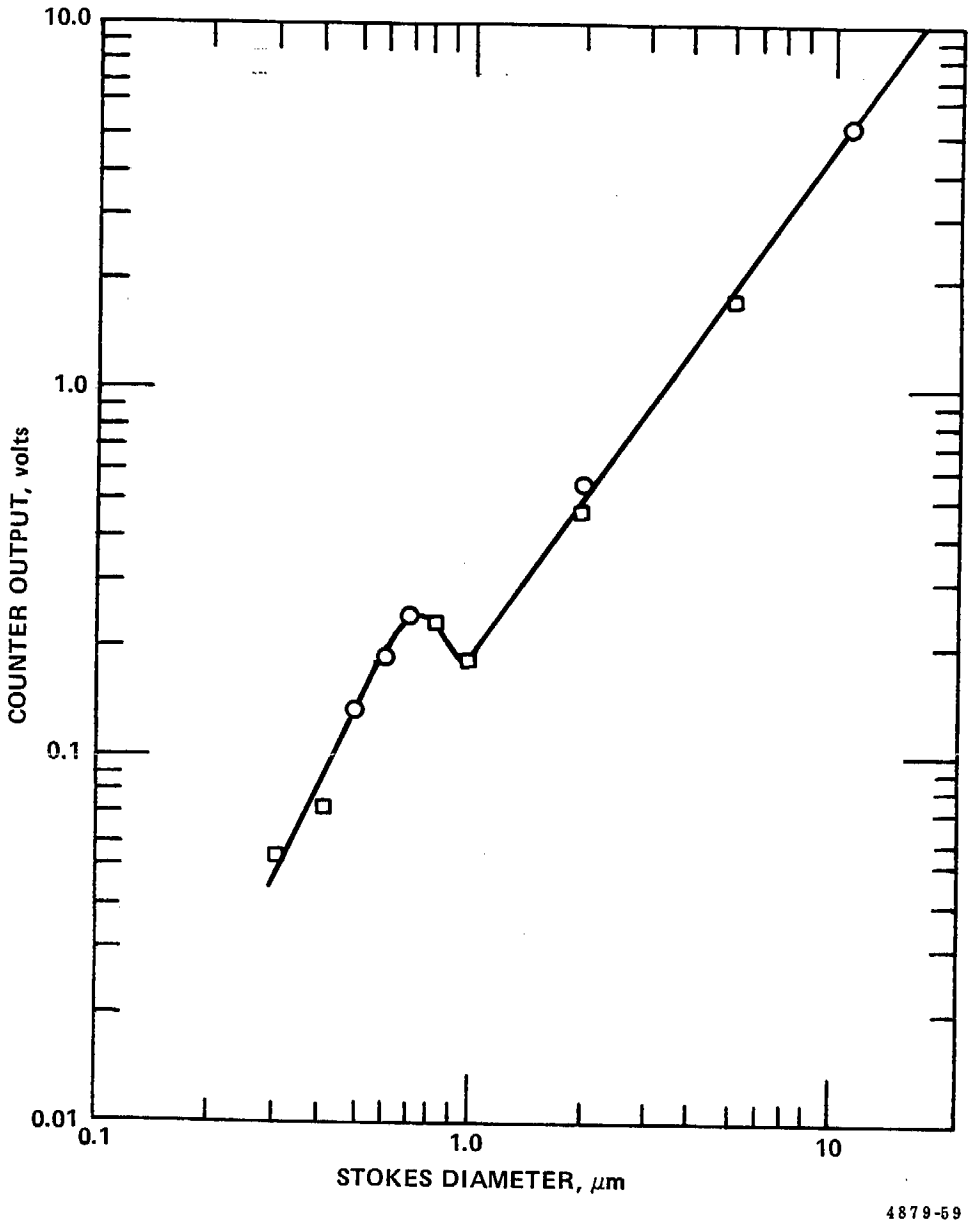

Figure 3-37. Calibration curve for the Royco Optical Particle Analyzer. (Source: Reference 70)

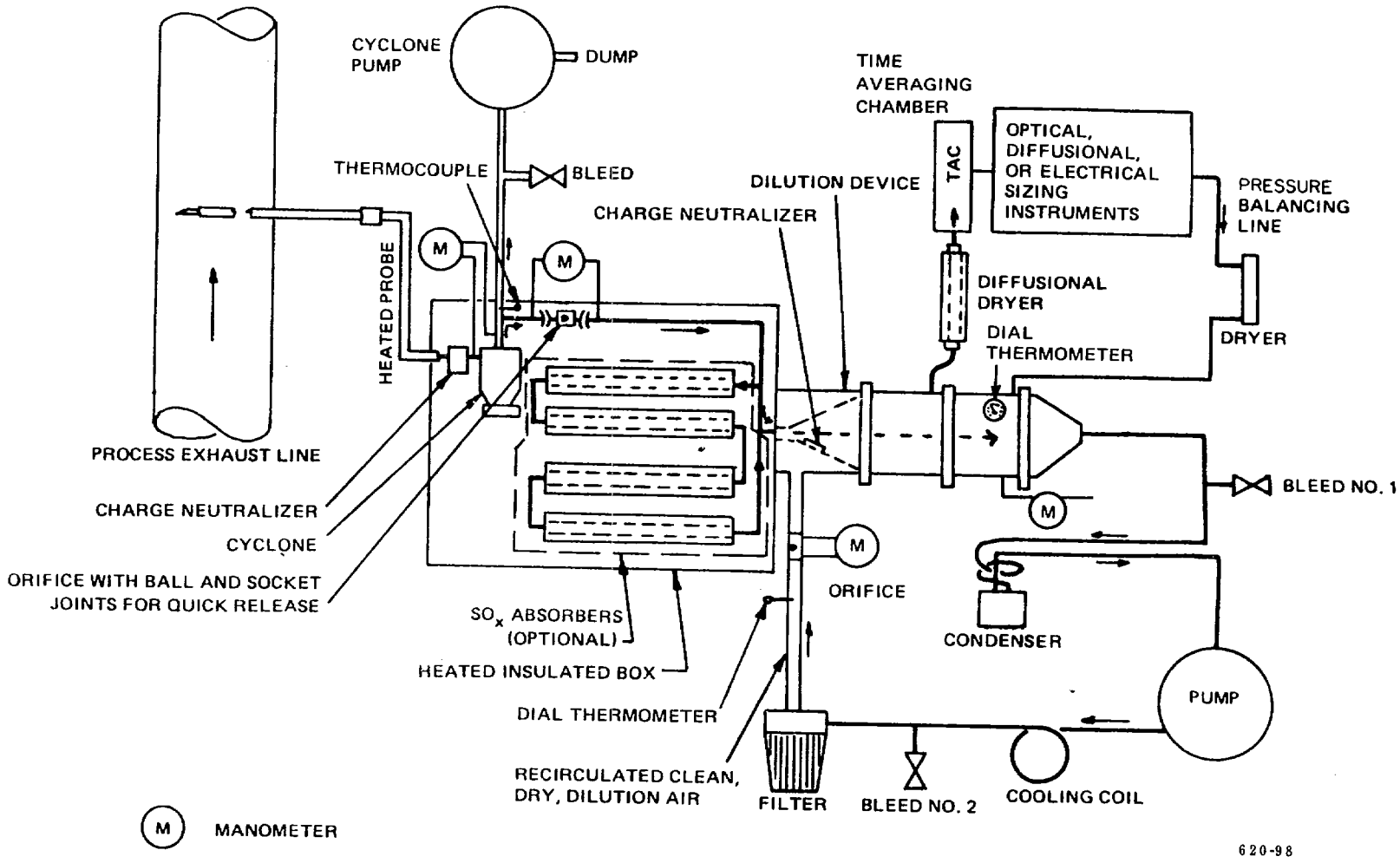

Figure 3-38. SoRI Ultrafine Particle Sample Extraction-Dilution System (SEDS).

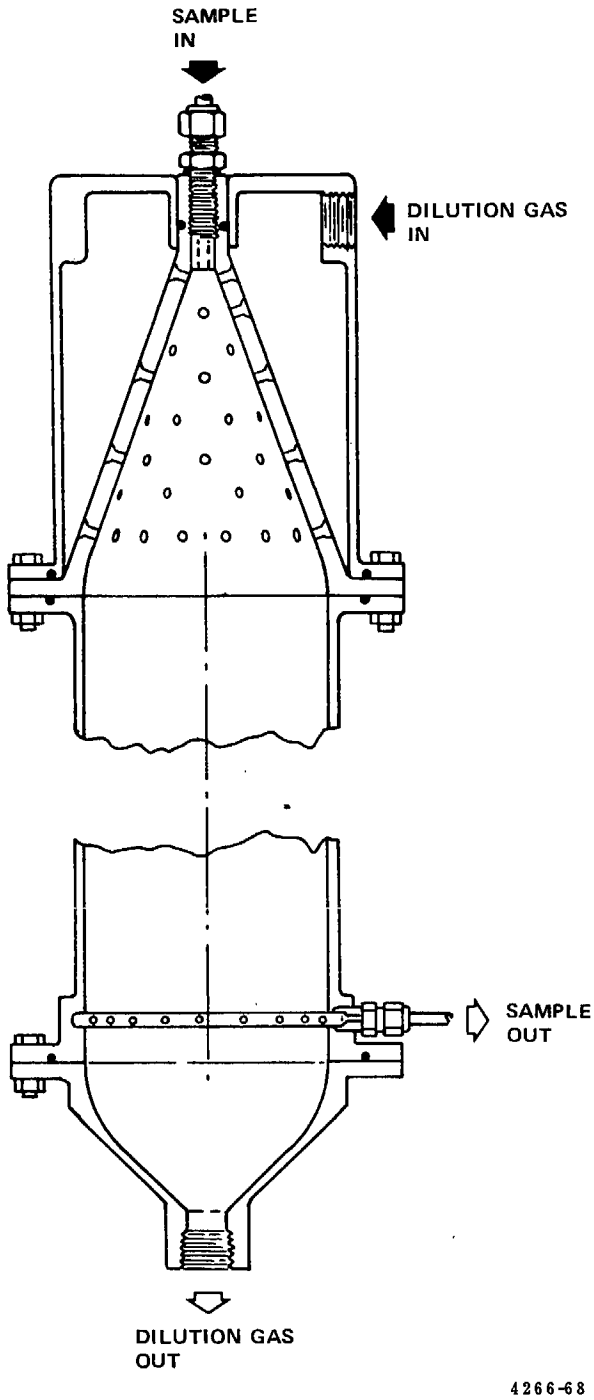

Figure 3-39. Aerosol dilution and cooling device to satisfy concentration and temperature requirements of aerosol monitoring devices.

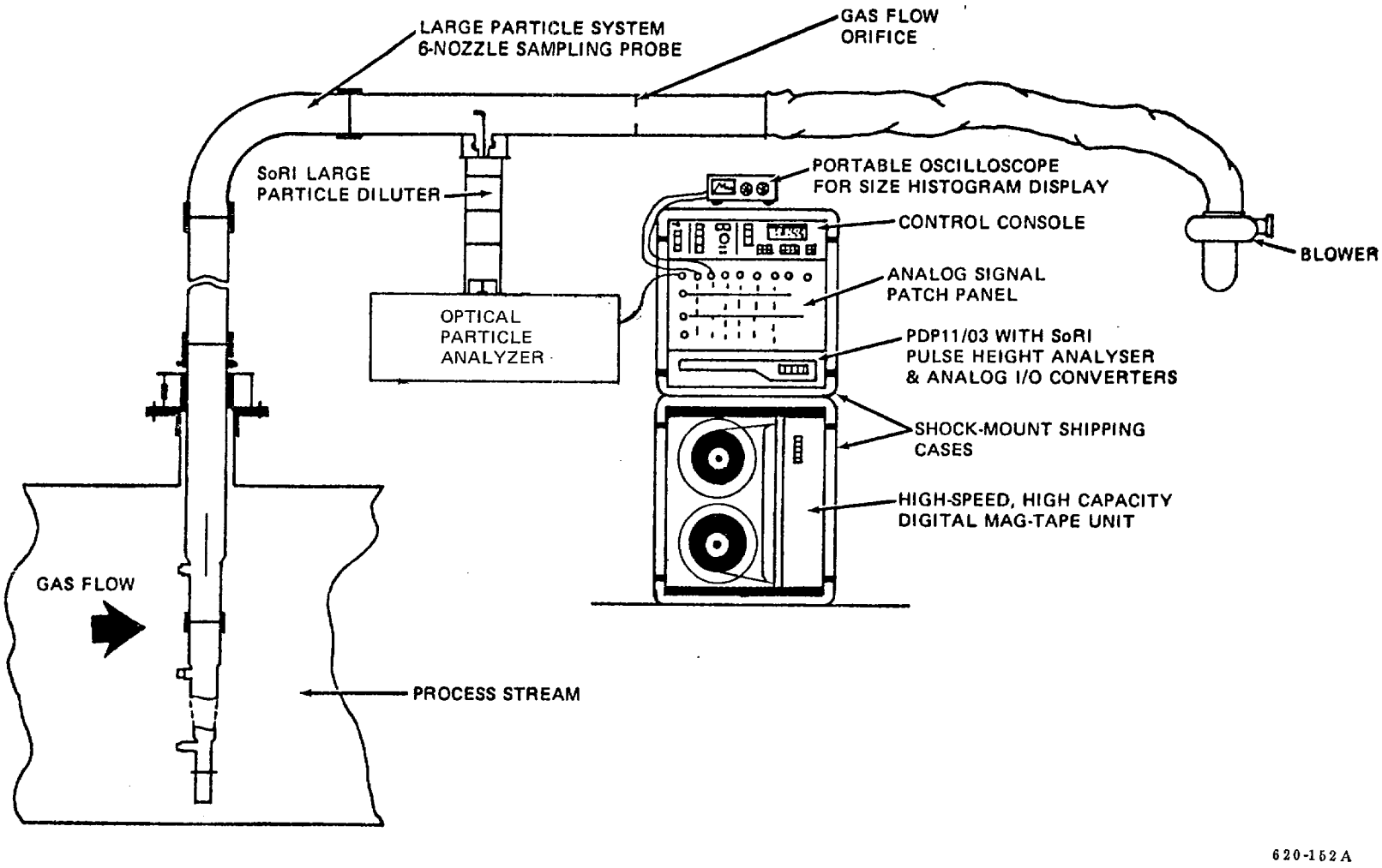

Figure 3-40. Diagram of the SoRI Large Particle Sampling System (LPSS).

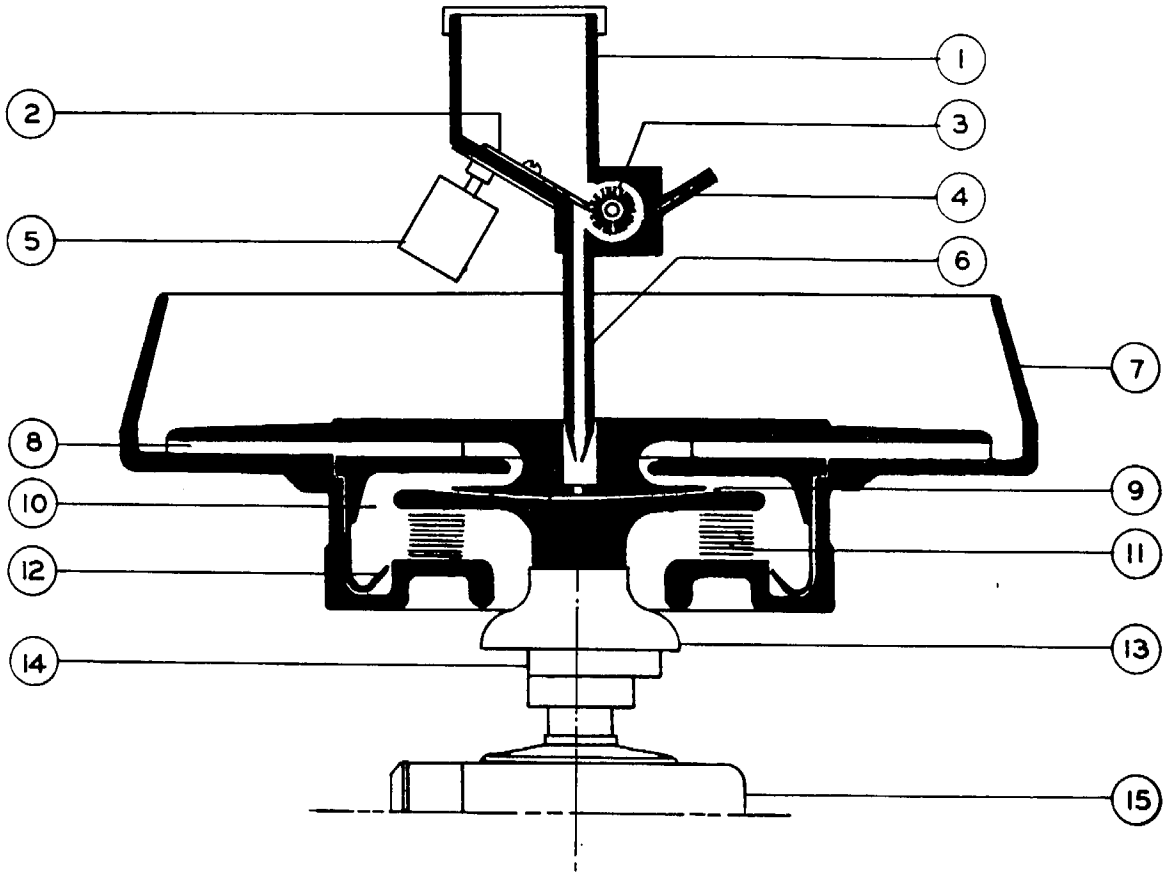

1. HOPPER
2. SPRING PLATE
3. BRUSH
4. ORIFICE TUBE
5. VIBRATOR
6. FEED NOZZLE
7. ROTOR CASTING
8. FAN VANES
9. ROTARY DUCT OPENING
10. SIFTING CHAMBER
11. SYMMETRICAL DISCS
12. CATCH BASIN
13. THROTTLE NUT
14. THROTTLE SPACER
15. MOTOR

4879-62

Figure 3-41. Operating principle for the Bahco Particle Classifier. (Source: H. W. Dietert Company)

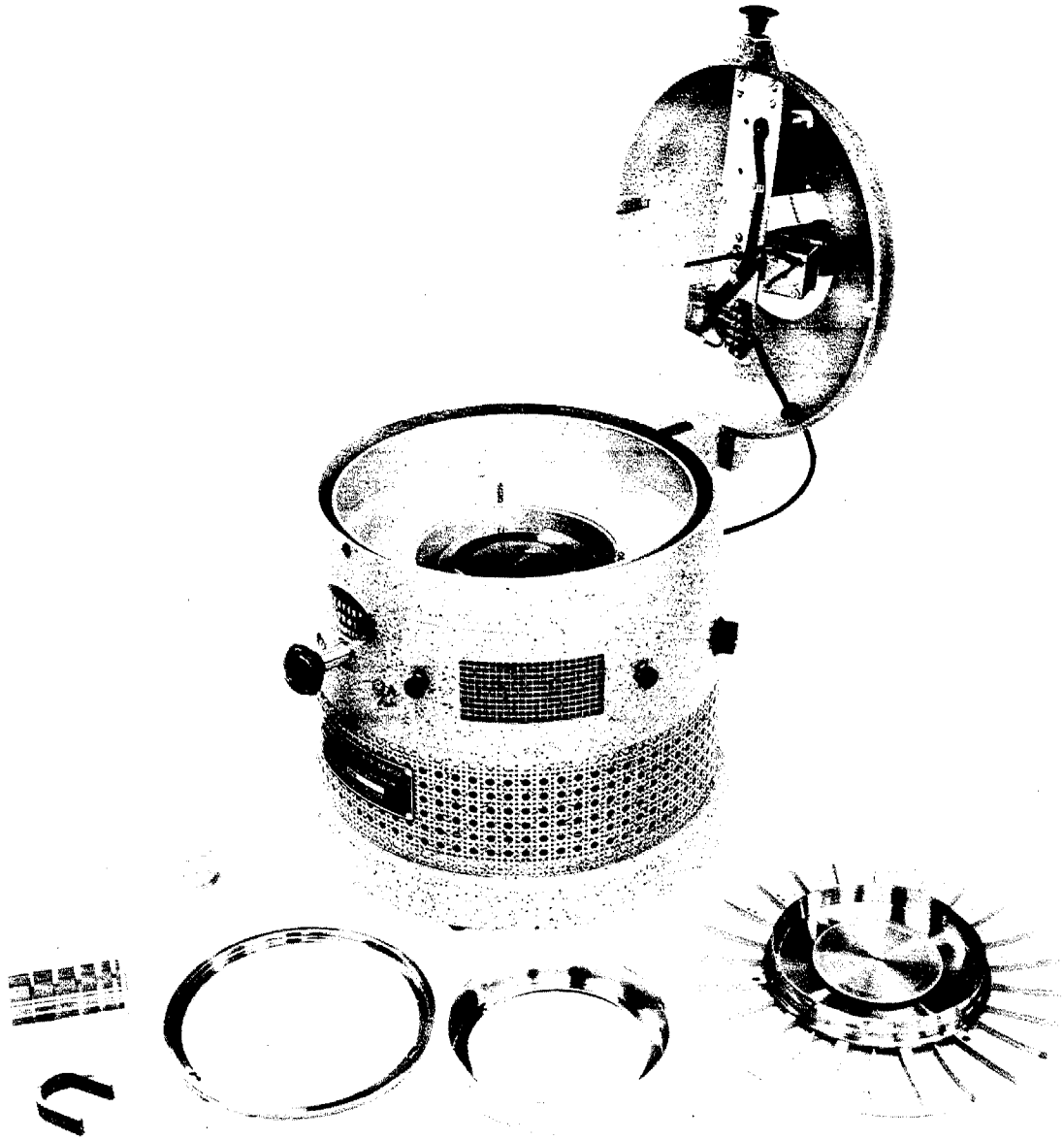

4879-61

Figure 3-42. The Bahco Particle Classifier. (Source: The Harry W. Dietert Company)

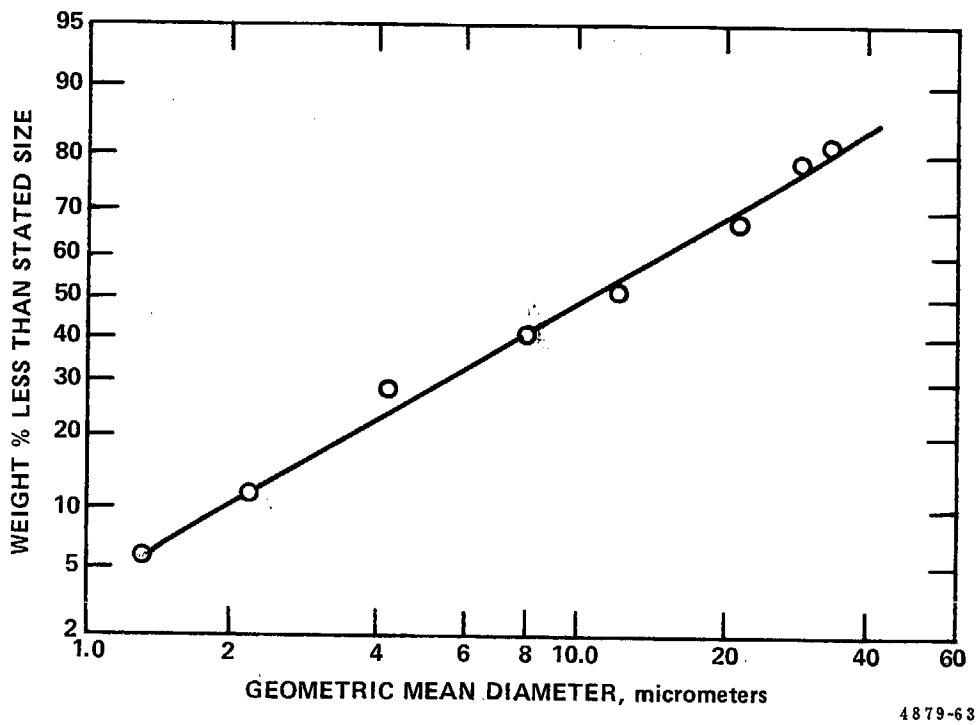

Figure 3-43. Typical cumulative size distribution of ash from a pulverized coal fired boiler as measured with the Bahco Particle Classifier.

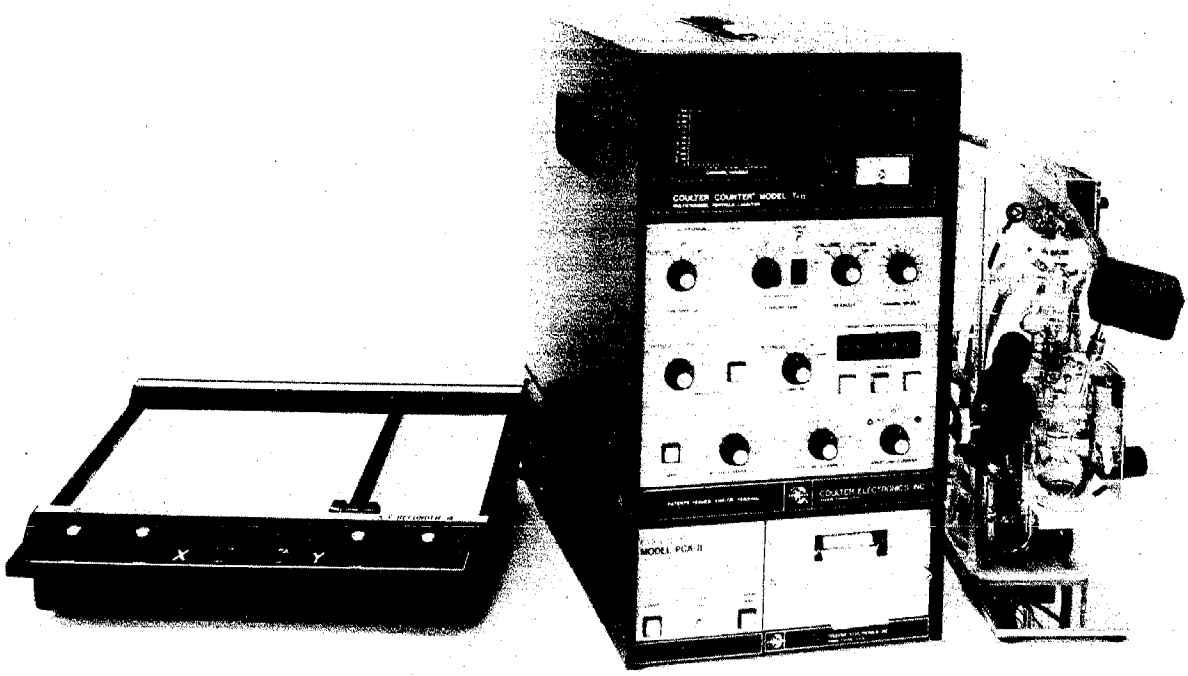

4879-64

Figure 3-44. The Coulter Counter Model TA II L. (Source: Coulter Electronics, Inc.)

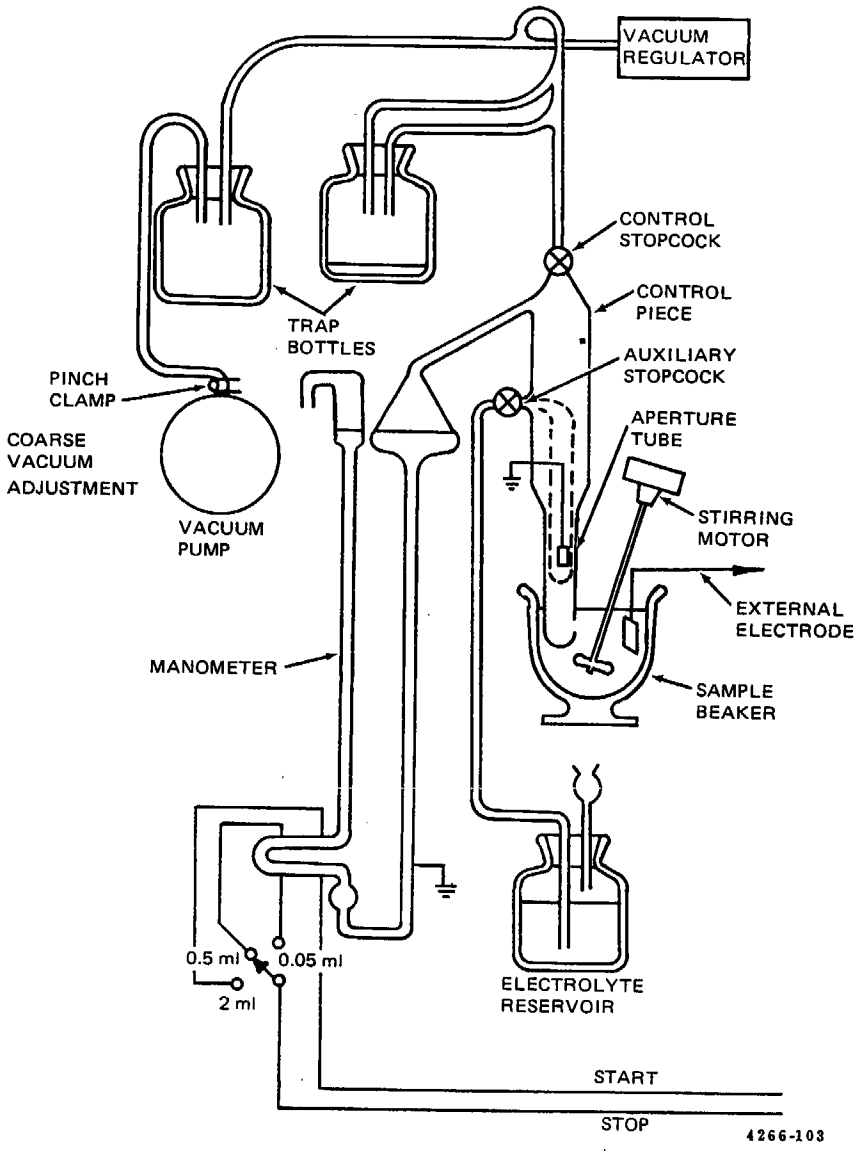

Figure 3-45. Schematic diagram of Coulter Counter Model TA II L. (Source: Coulter Electronics, Inc.)

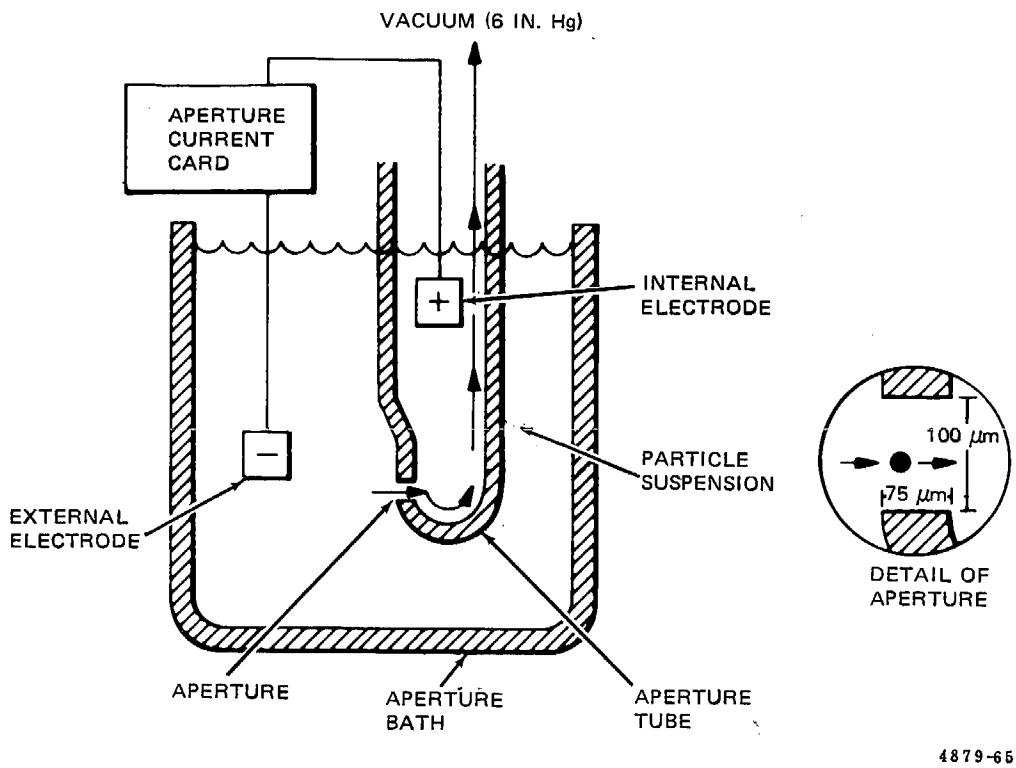

Figure 3-46. Operating principle of the Coulter Counter. (Source: Coulter Electronics, Inc.)

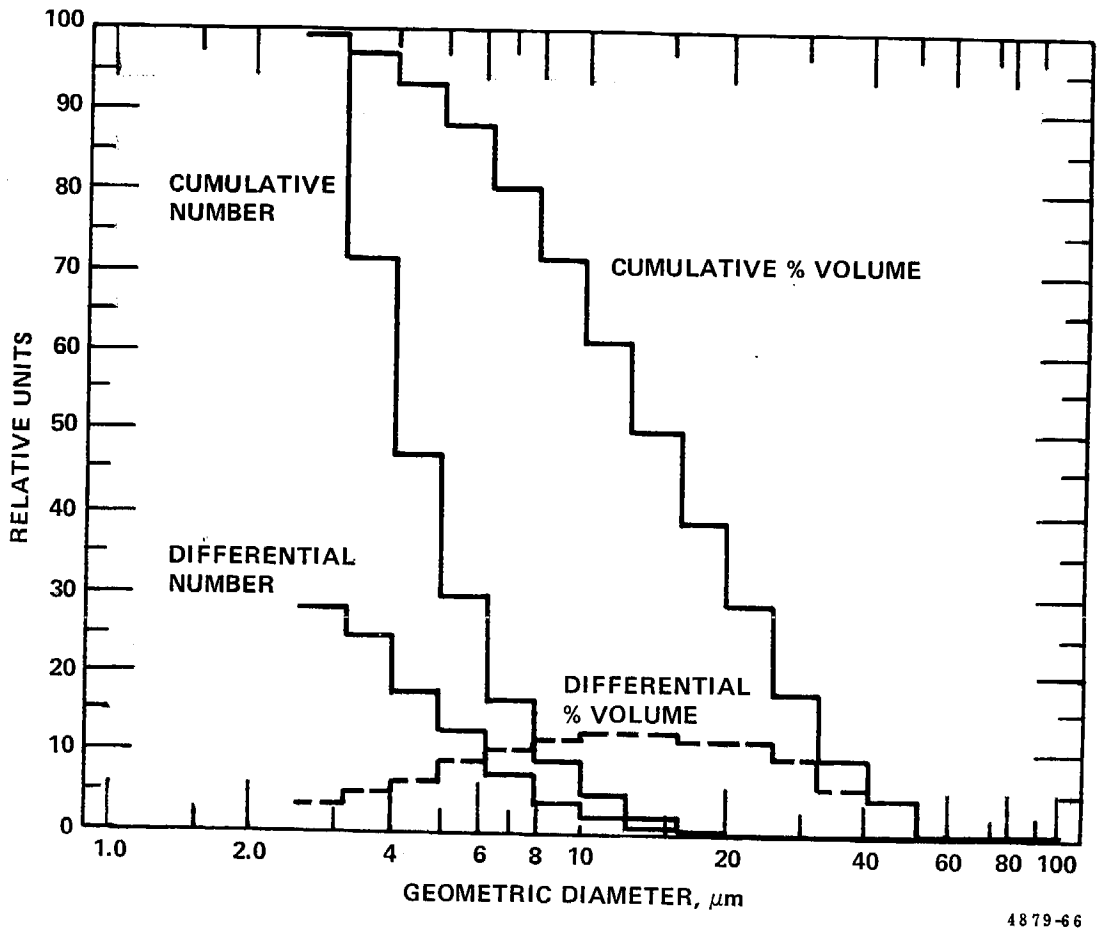

Figure 3-47. Differential and cumulative plots of the number and percent volume in each size interval of a fly ash sample obtained using the Coulter Counter Model TA II L.

Table 4-1. Typical flue gas sample conditions.

	RANGE	TYPICAL VALUE
Temperature:	170 to 450°C	150°C
Absolute Pressure:	490 to 850 mm Hg	750 mm Hg
Pressure Differential to Ambient	±75 mm Hg	-25 mm Hg
Moisture (Volume Percentage)	1 - 20%	10%
CO_2 (Volume Percentage)	8 - 15%	12%
SO_2 (Volume Percentage)	0 - 5%	0.2%
SO_3/H_2SO_4 (Volume Percentage)	0 - 0.25%	0.0005%
Particulate Mass Concentrations	≤ 20 g/m^3	Uncontrolled 5 g/m^3 Controlled 0.02 g/m^3
Concentration by Number of Particles Larger than 0.01 μm	$\leq 3 \times 10^7$/cm^3	Uncontrolled 2×10^7/cm^3 Controlled 2×10^5/cm^3

4879-111

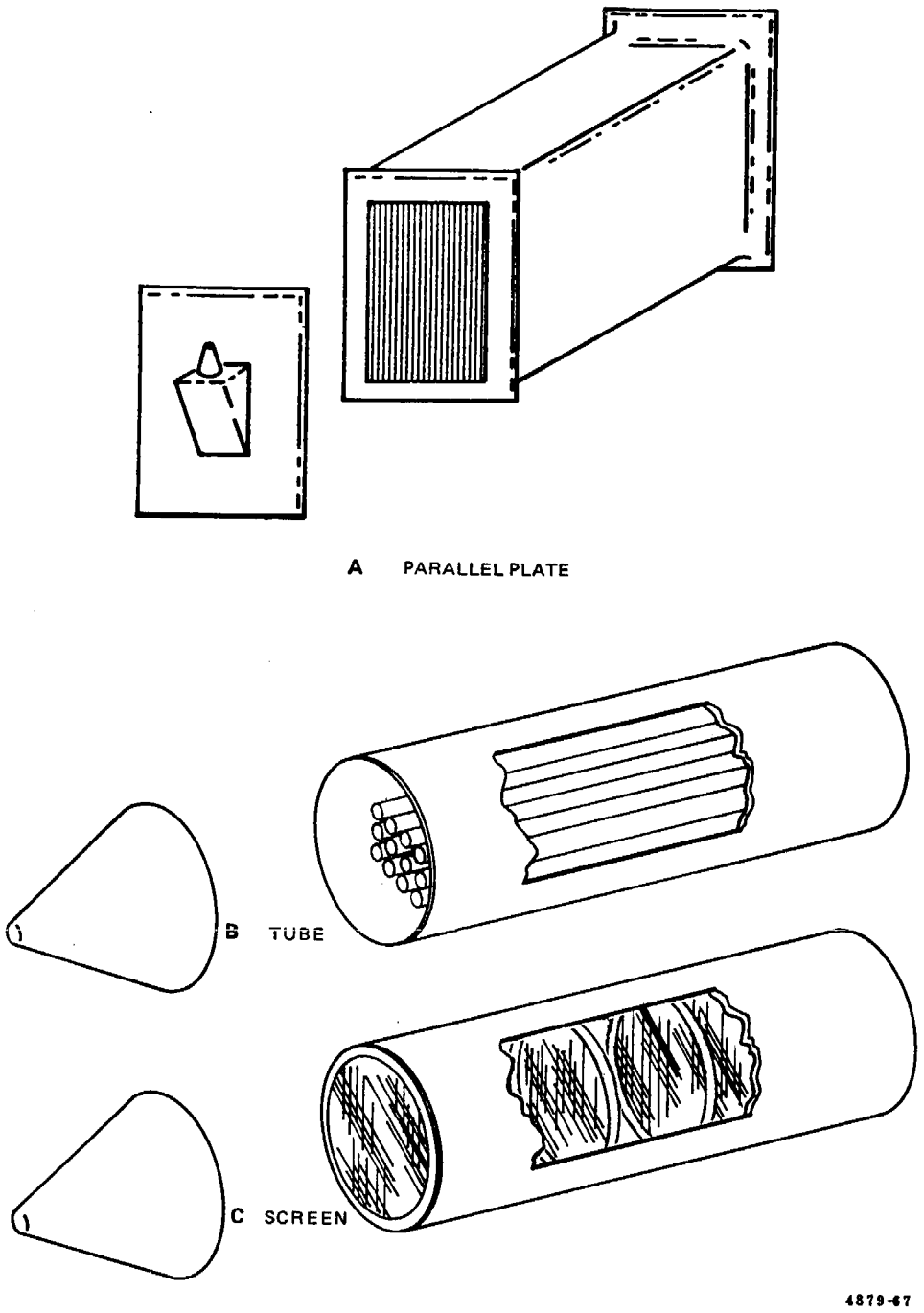

Figure 4-1. Typical diffusion battery geometries.

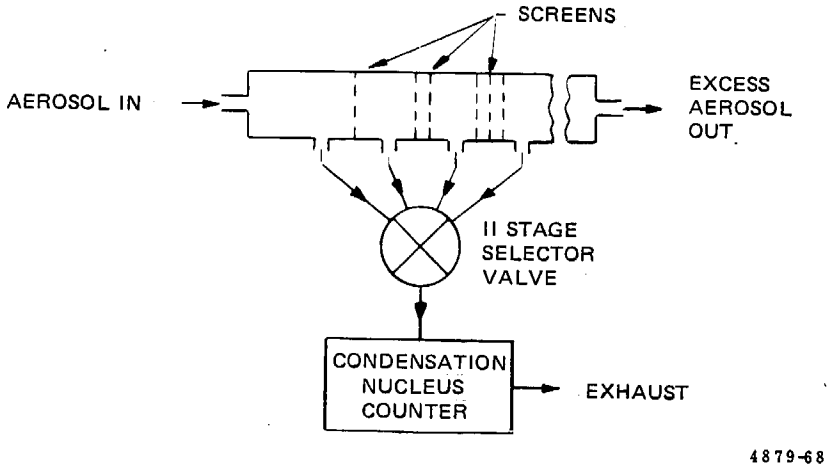

Figure 4-2. Schematic illustration of a screen type diffusion battery. (Source: TSI, Inc.)

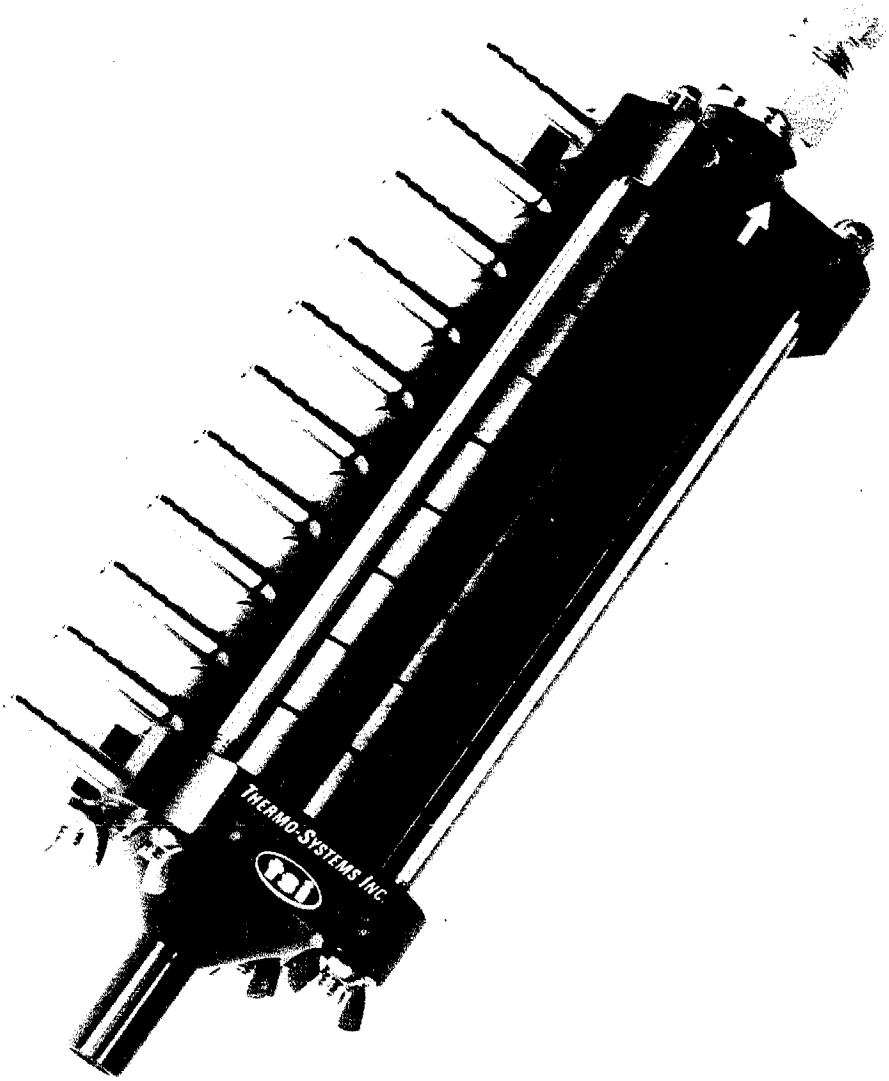

4879-69

Figure 4-3. The TSI Model 3040 Diffusion Battery. (Source: TSI, Inc.)

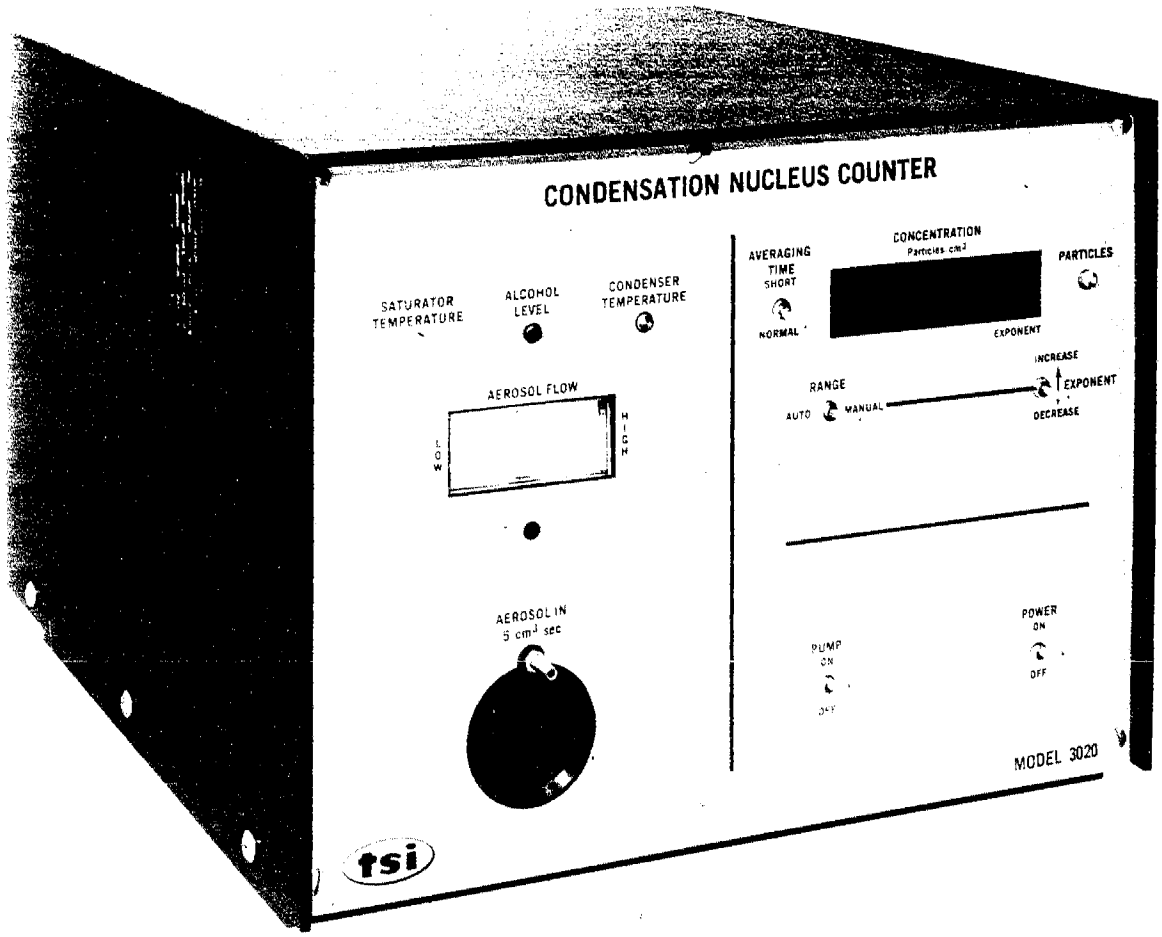

4879-70

Figure 4-4. The TSI Model 3020 Continuous Flow Condensation Nuclei Counter. (Source: TSI, Inc.)

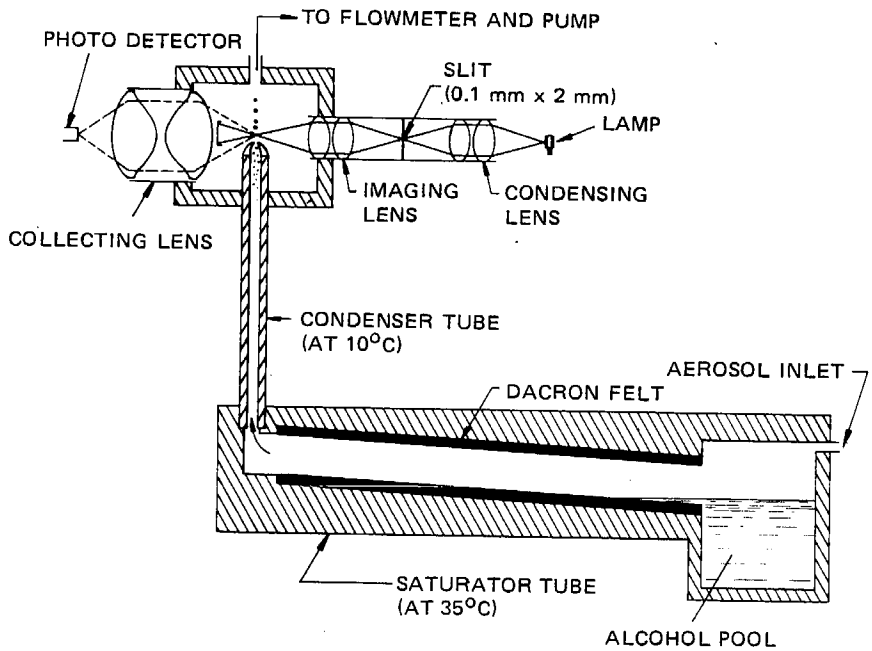

Figure 4-5. Schematic diagram of the TSI Model 3020 Continuous Flow CNC. (Source: TSI, Inc.)

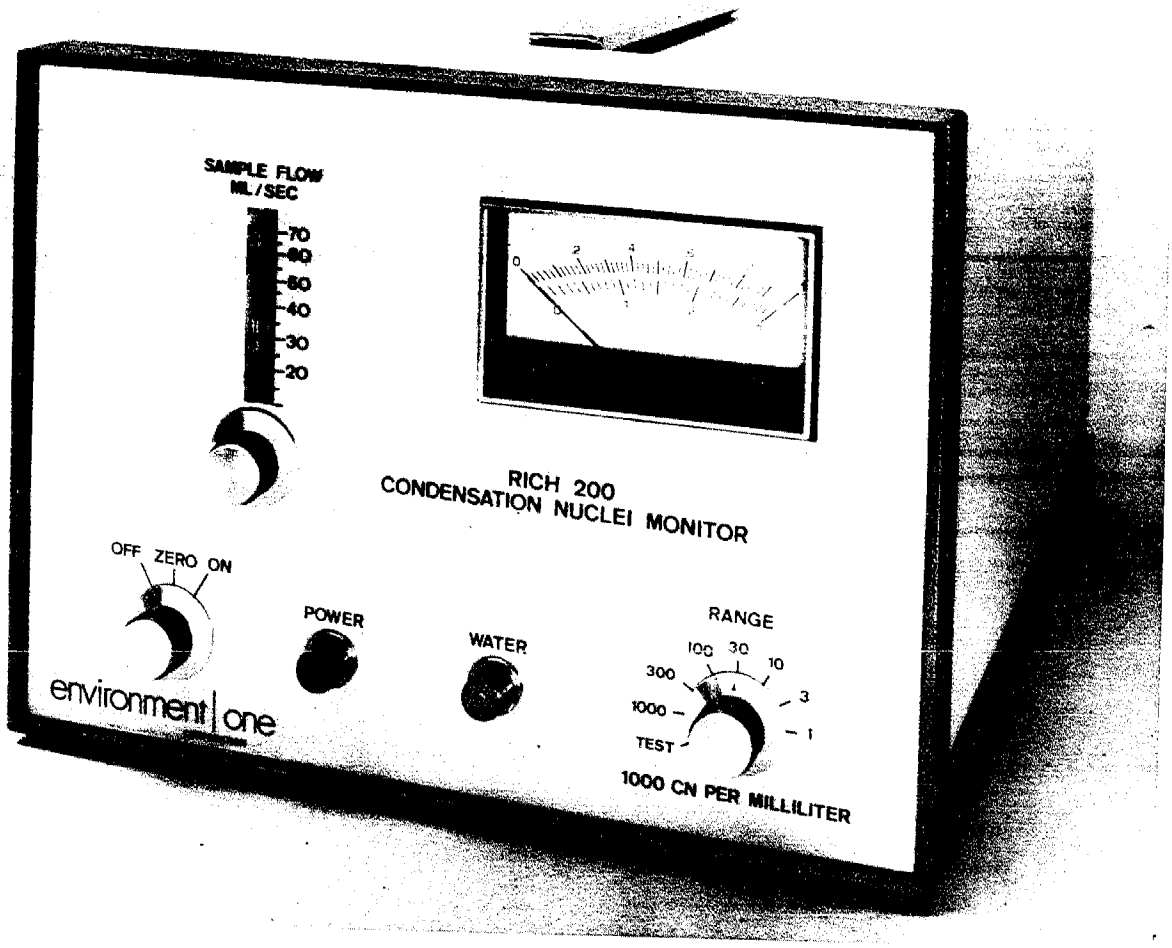

4879-72

Figure 4-6. The Rich 200 Condensation Nuclei Counter. (Source: Environmental One Corp.)

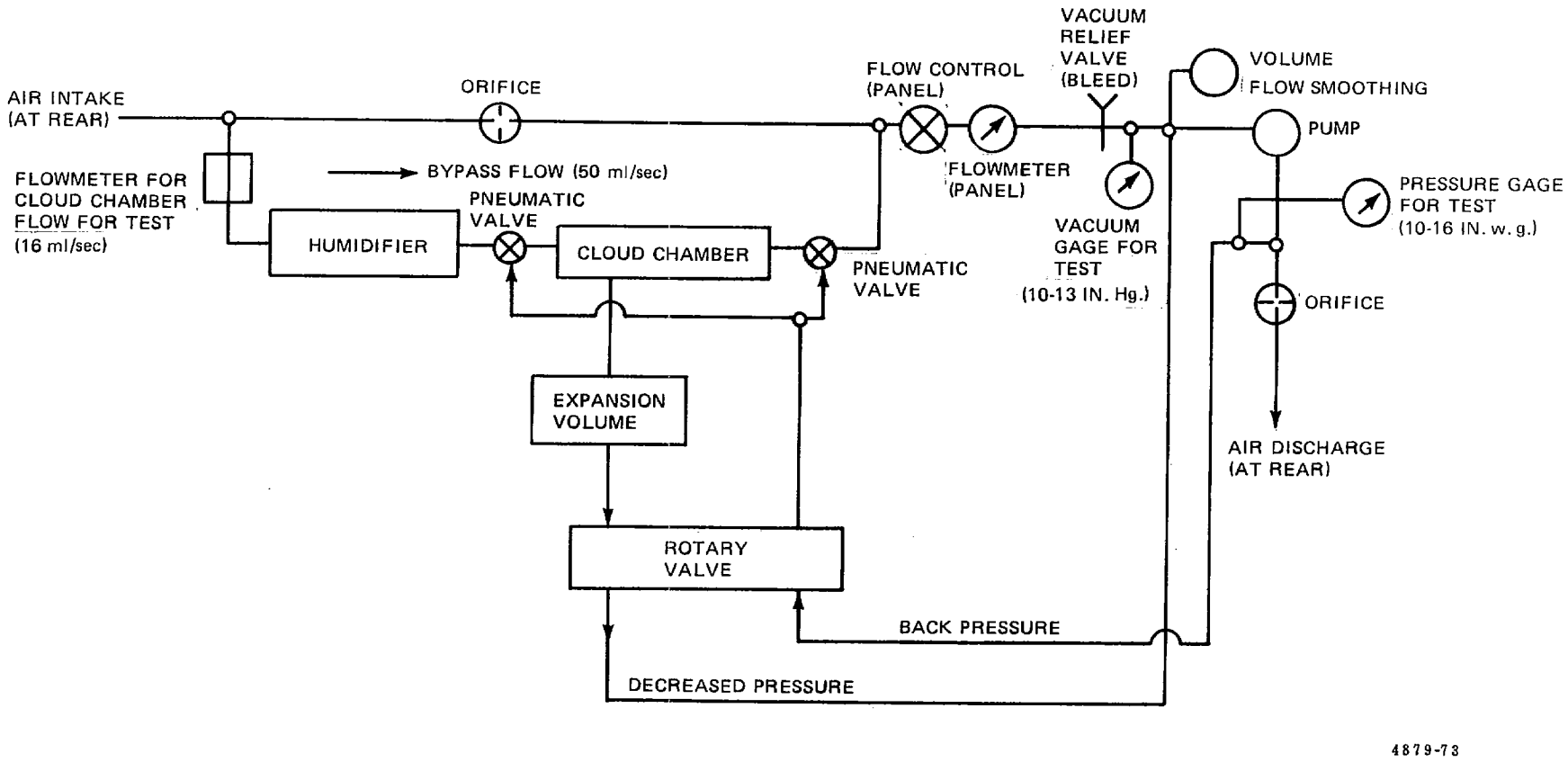

Figure 4-7. Schematic diagram of the Rich 200 CNC. (Source: Environment One Corp.)

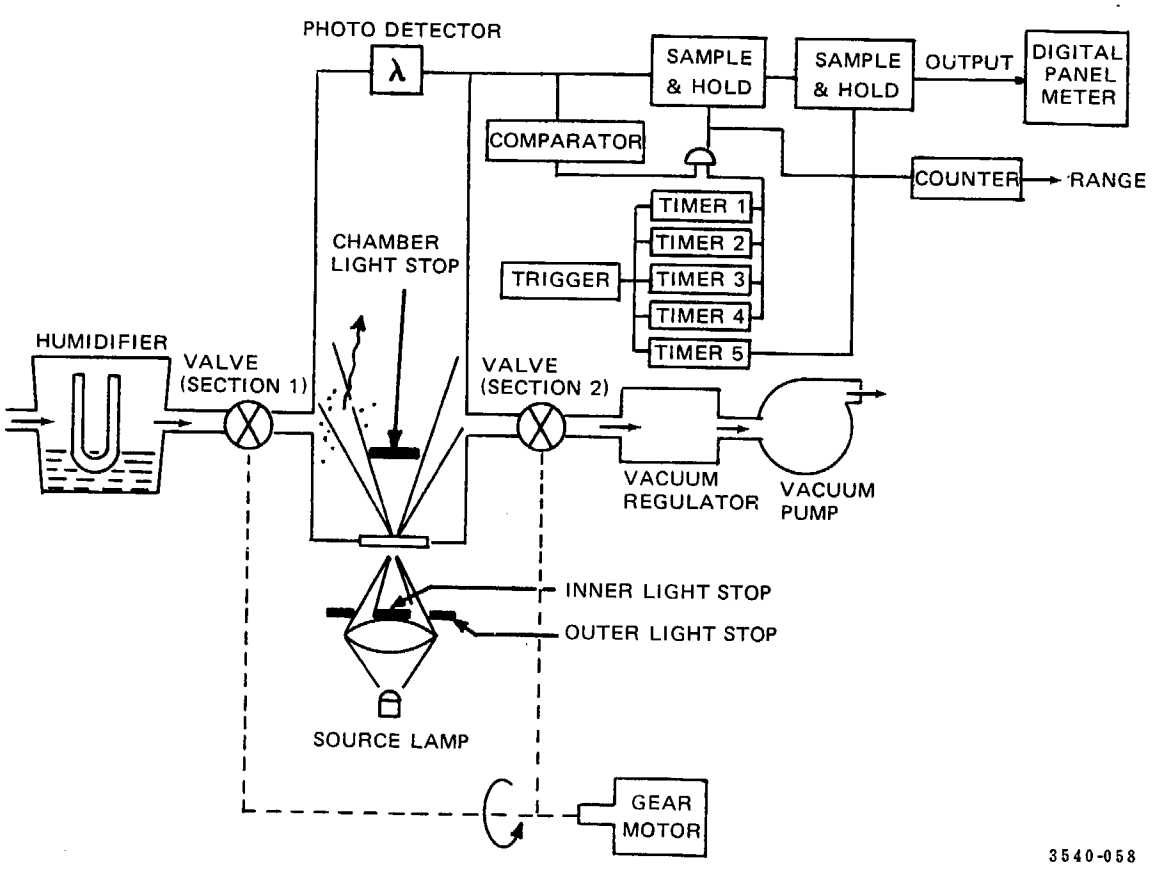

Figure 4-8. Diagram of a condensation nuclei counter. After Haberl and Fusco.[59]

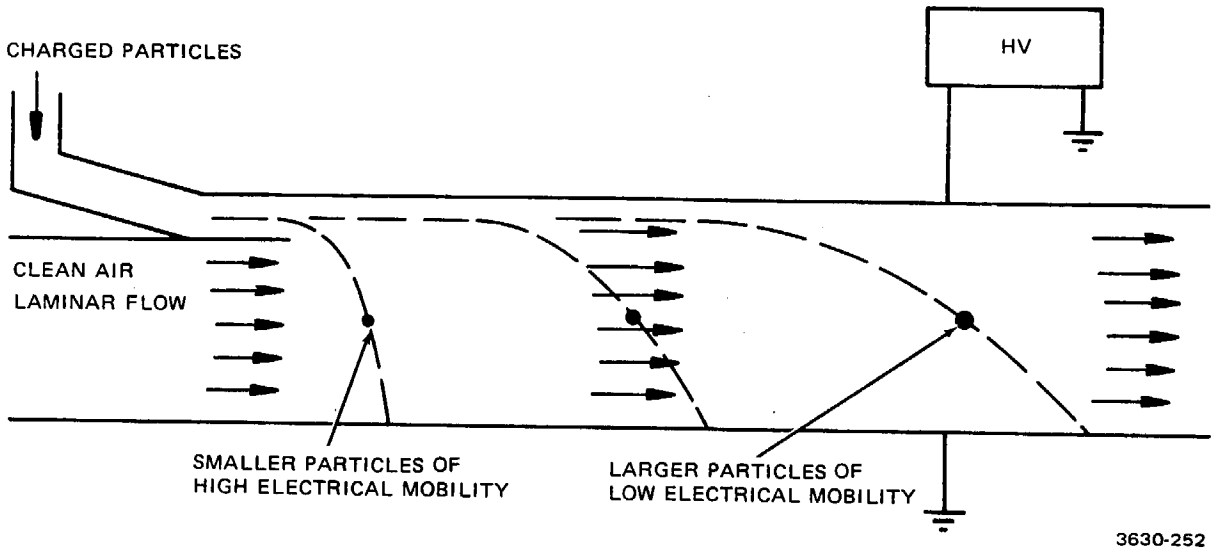

Figure 4-9. The electric mobility principle. (Source: Reference 92)

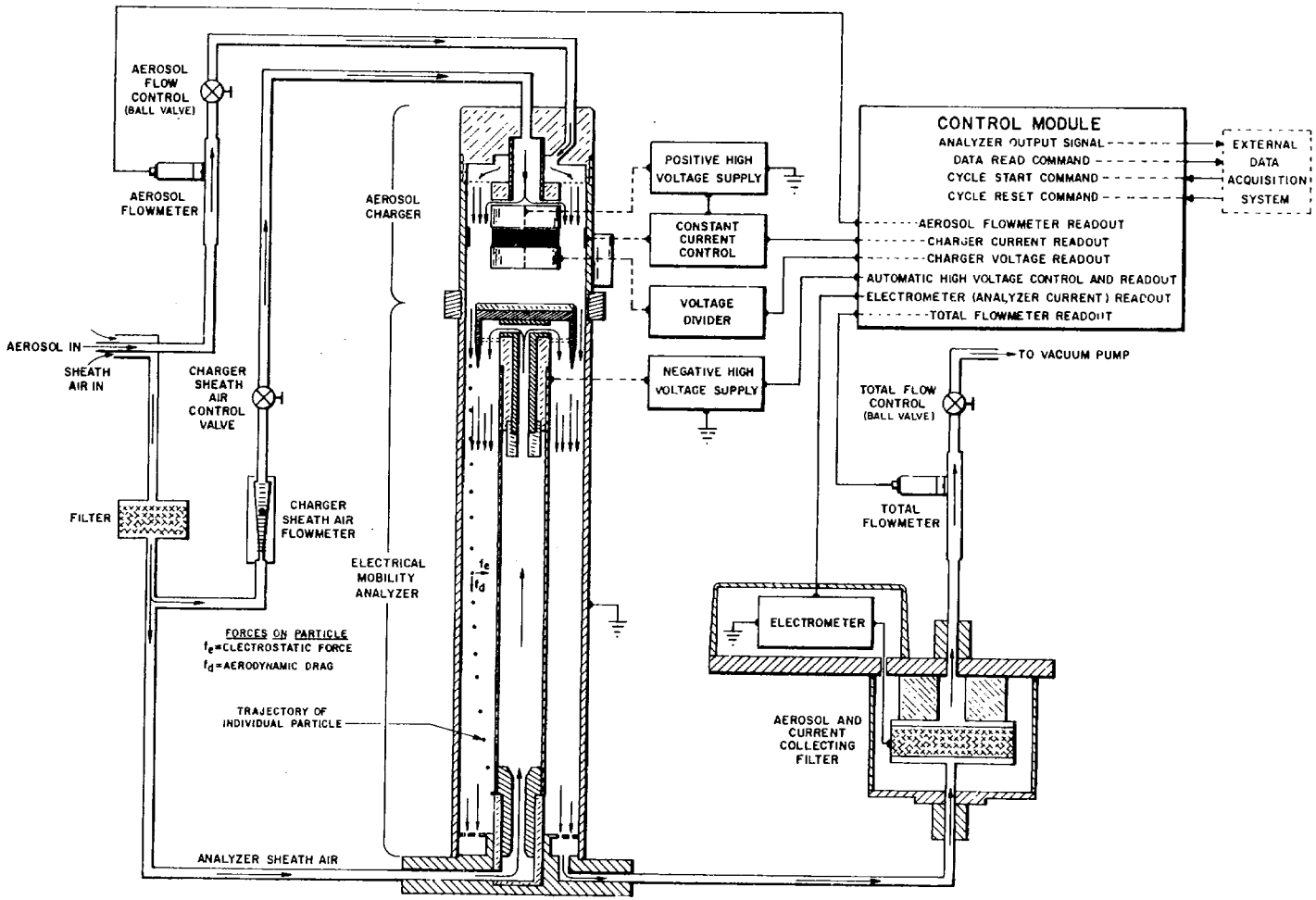

Figure 4-10. Flow schematic and electronic block diagram of the Electrical Aerosol Analyzer. After Liu, Whitby, and Pui (1974, Reference 9).

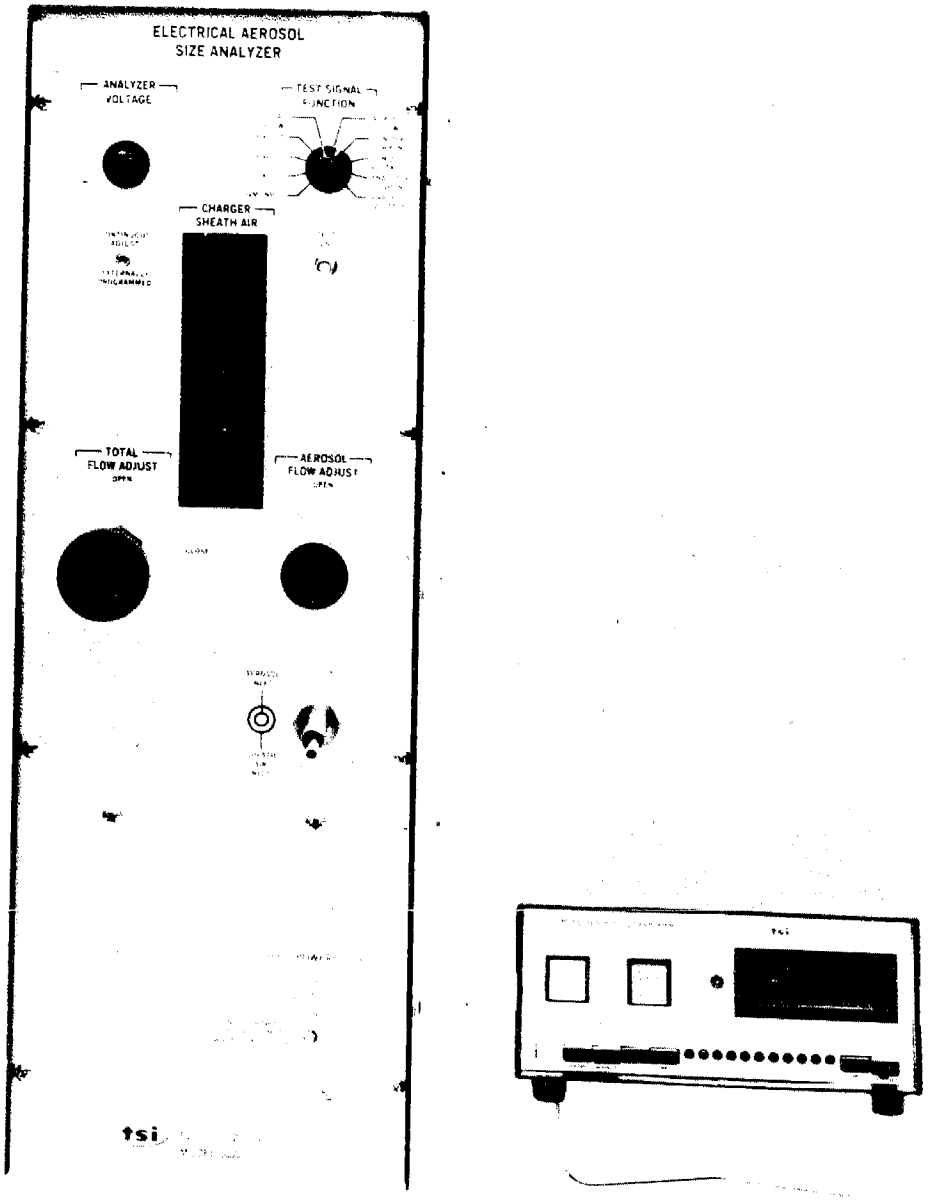

4879-74

Figure 4-11. The TSI Model 3030 Electrical Aerosol Size Analyzer. (Source: TSI Incorporated)

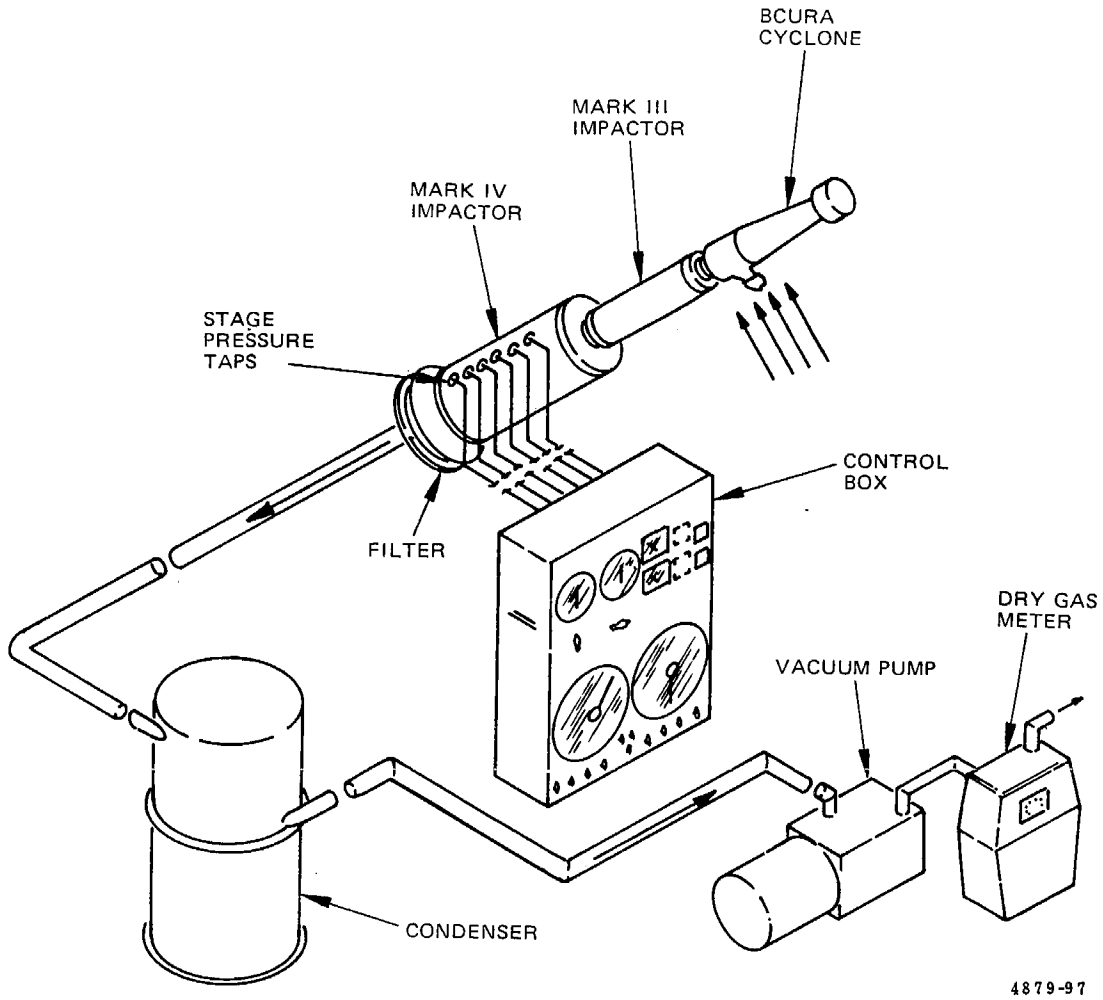

Figure 4-12. The Mark 3/4 sampling train using the Mark 4 low pressure impactor. (Source: Reference 102)

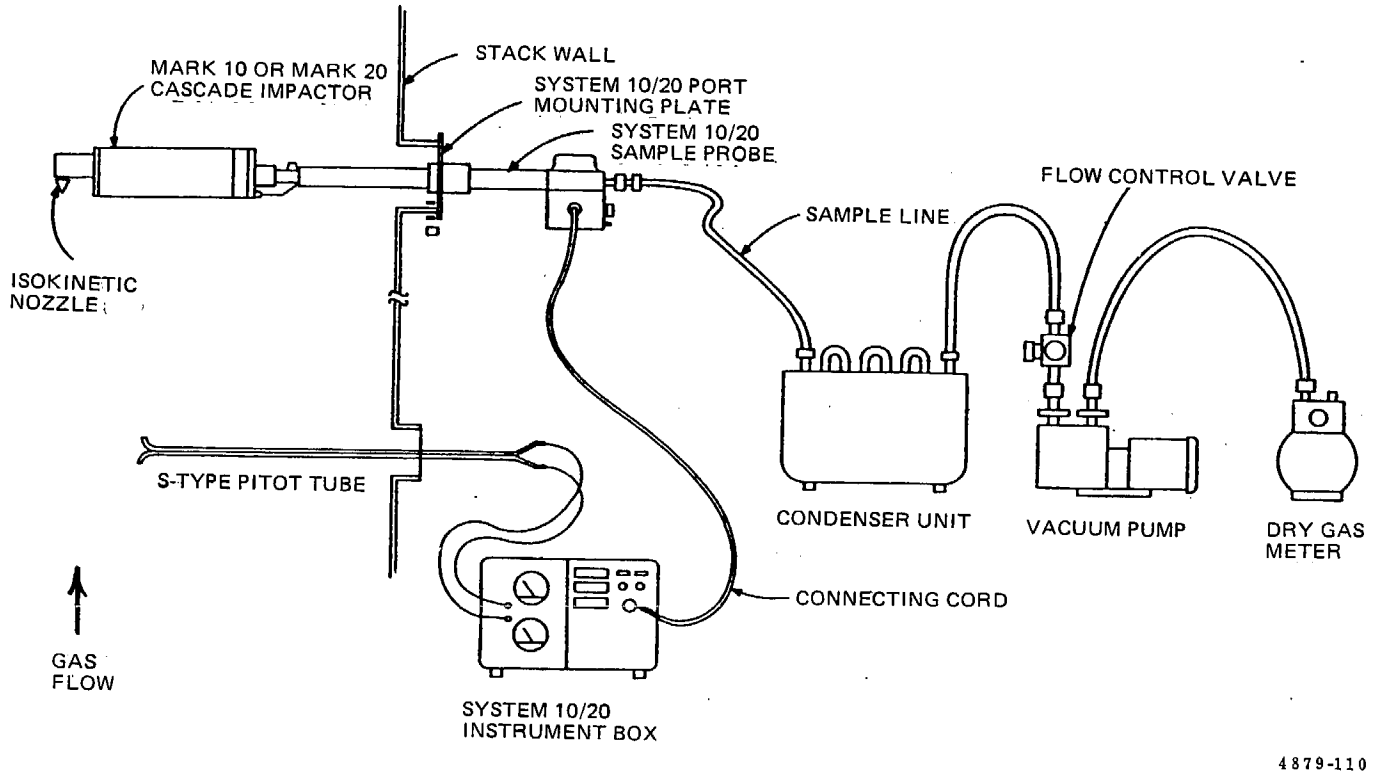

Figure 4-13. Schematic of the UW Mark 10/20 cascade impactor sampling system. (Source: Pollution Control System Corp.)

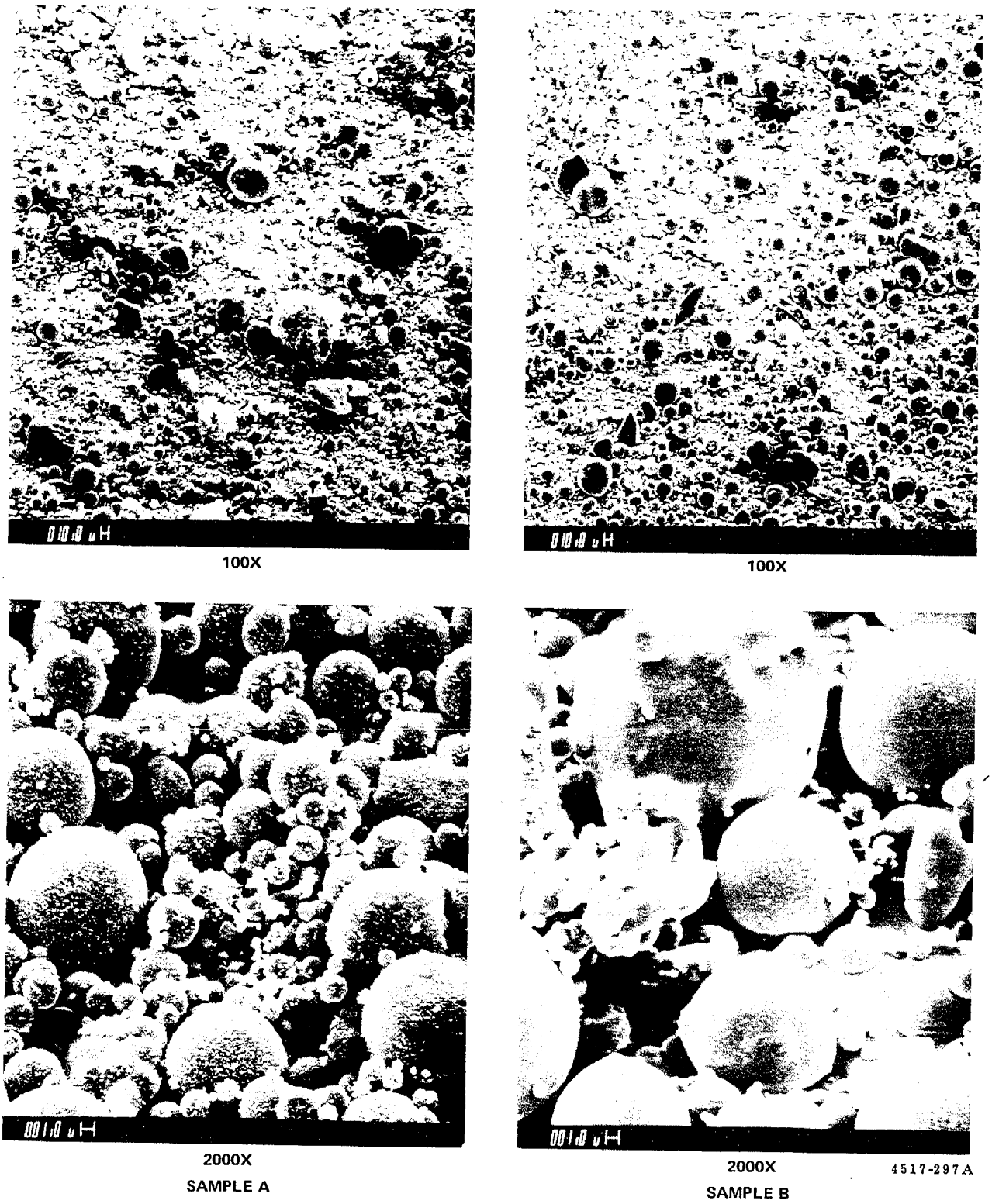

Figure 5-1. Scanning electron microscope photographs of two distinct fly ash samples. Each sample shown at 100X and 2000X magnification.

Table 6-1. Particle sizing device applications.

DEVICE	PRINCIPLE OF OPERATION	MODE OF OPERATION	SAMPLING LOCATION	SIZING RANGE, μm	INLET CONC. RANGE, g/m^3	OPERATIONAL STATUS
Impactor	Inertial	In situ	I/O	0.3 to 20	0.001 to 10.0	Routine use by skilled operator
Impactor-Low Pressure	Inertial	In situ	I/O	0.03 to 20	0.001 to 10.0	Prototype
Cyclone	Inertial	In situ/Extractive	I/O	0.3 to 20	0.01 to 100	Routine use by skilled operator
Optical counter	Light scattering	In situ	O	0.2 to 20	0.6 to 60 mg/m^3	Some commercial instruments in use
Optical counter	Light scattering	Extractive	I/O	0.3 to 10	10 $\mu g/m^3$ to 40 mg/m^3	Non-routine use by skilled operator
Diffusion battery	Brownian diffusion	Extractive	I/O	0.003 to 1.0	$\leq$ 0.5	Non-routine use by skilled operator
Mobility analyzer	Electrical mobility	Extractive	I/O	0.003 to 1.0	$\leq$ 1.0 mg/m^3	Non-routine use by skilled operator
Centrifugal classifier	Inertial	Off-line	n. a.	1 to 500	n. a.	Routine lab use
Cell counters	Electrical resistance	Off-line	n. a.	0.5 to 200	n. a.	Routine lab use
Optical microscope	Visual	Off-line	n. a.	$\geq$ 0.2	n. a.	Routine lab use
Transmission electron microscope	Electron beam attenuation	Off-line	n. a.	0.001 to 20	n. a.	Routine lab use
Scanning electron microscope	Electron beam scattering	Off-line	n. a.	0.02 to 20	n. a.	Routine lab use

n. a. = not applicable, I = Control device inlet, O = Control device outlet

4879-118

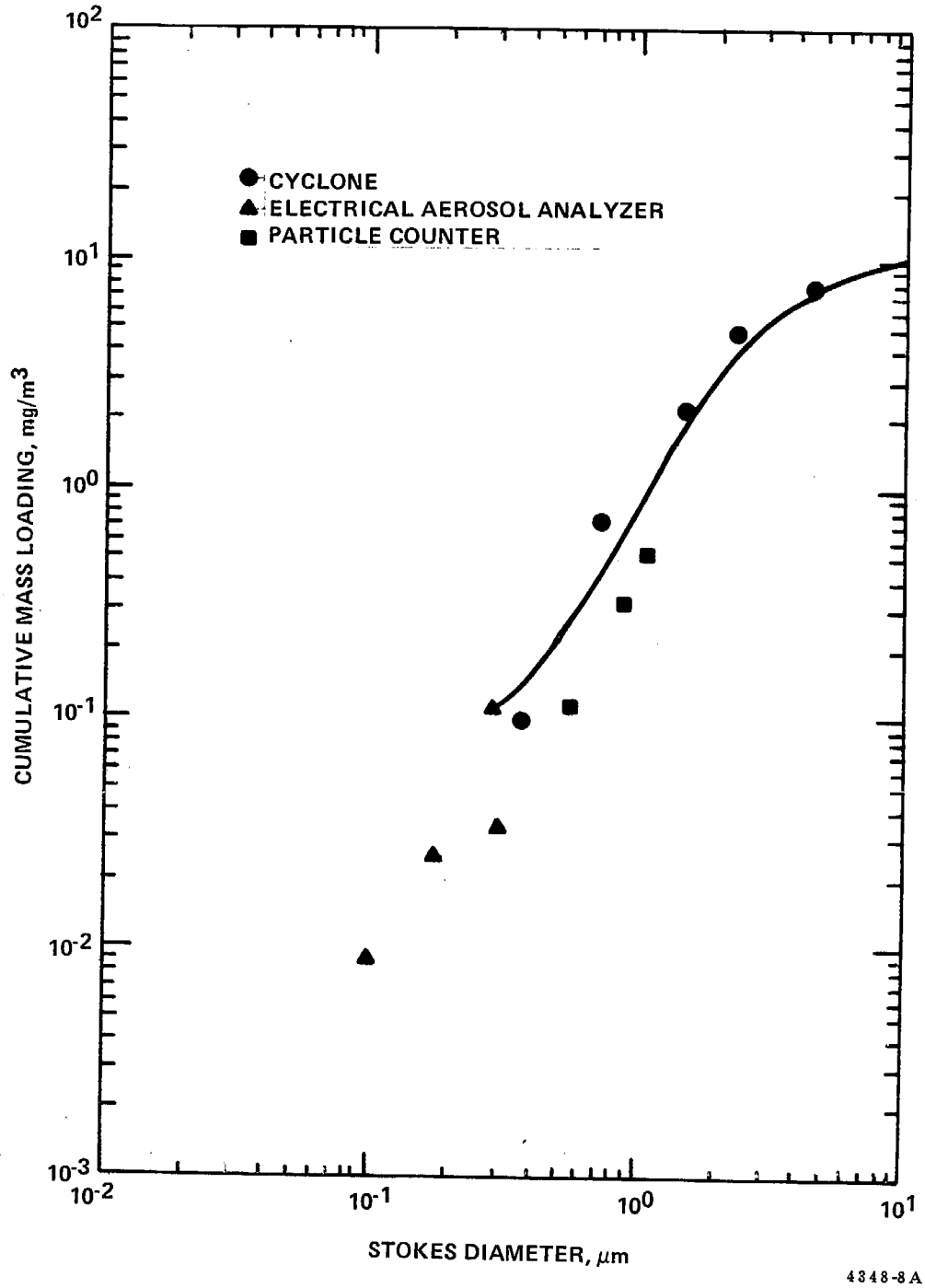

Figure 6-1. Cumulative mass concentration vs. particle size at the outlet of an electrostatic precipitator. Data obtained using a cascade impactor (solid line), a five-stage series cyclone, an electrical aerosol analyzer, and an optical particle counter. (Source: Reference 106)

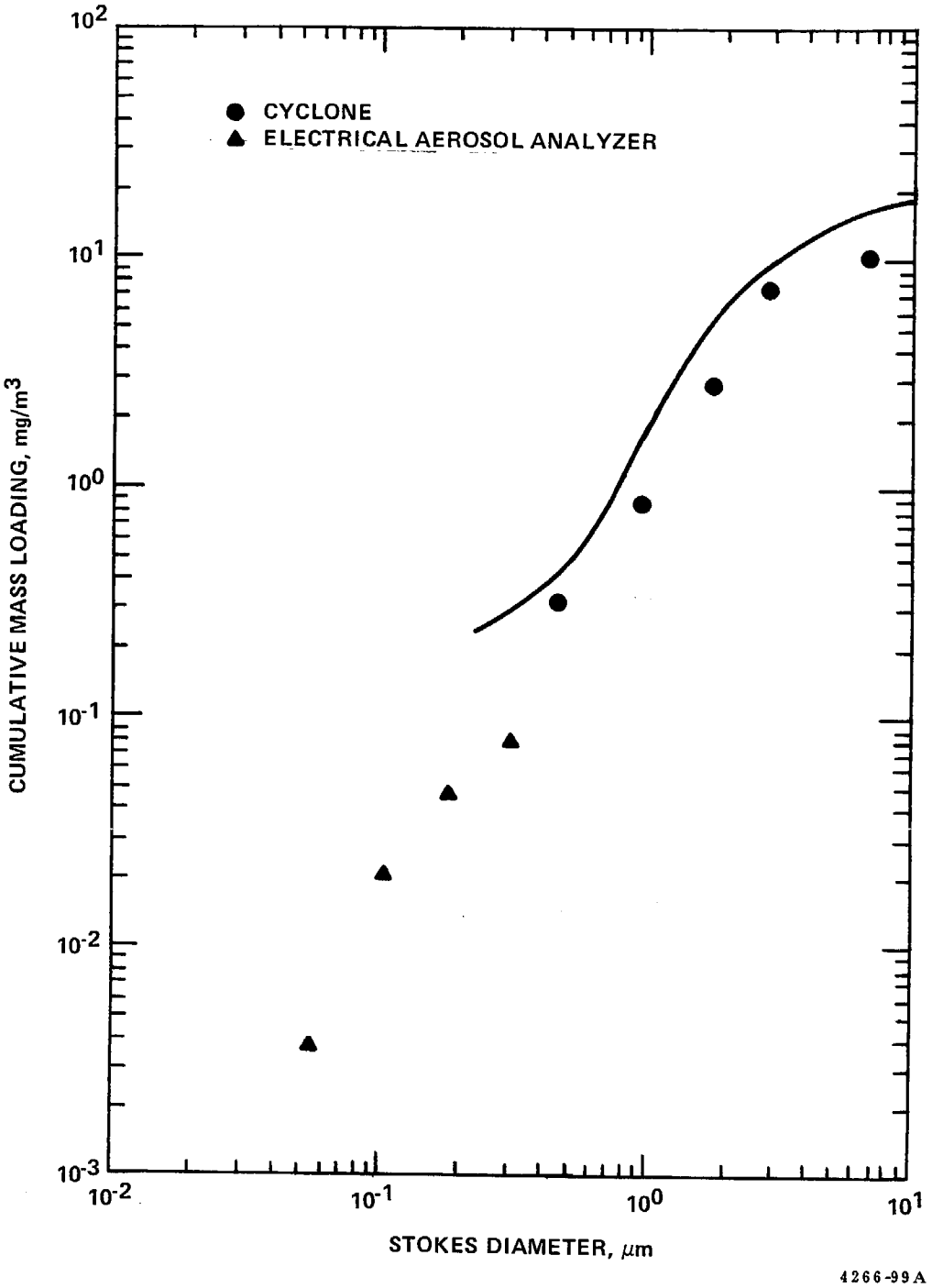

Figure 6-2. Cumulative mass concentration vs. particle size at the outlet of an electrostatic precipitator. Data obtained using a cascade impactor (solid line), a five-stage series cyclone aerosol analyzer. (Source: Reference 106)

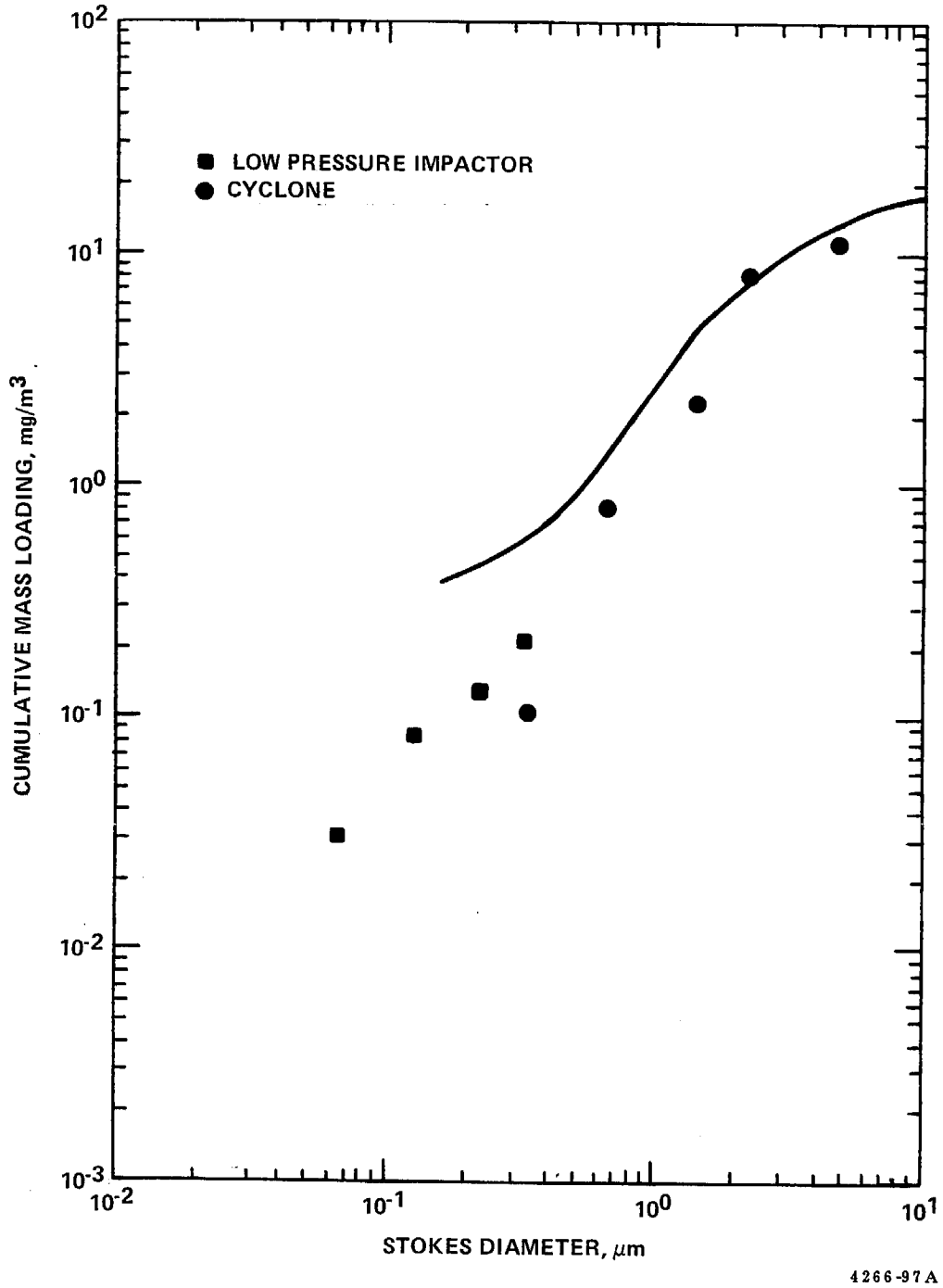

Figure 6-3. Cumulative mass concentration vs. particle size at the outlet of an electrostatic precipitator. Data obtained using a cascade impactor (solid line), a four-stage low-pressure impactor, and a five-stage series cyclone. (Source: Reference 106)